Mechanistic Studies on Metal-Catalyzed Carbon-Nitrogen Bond Forming Reactions

By Eric R. Strieter

B. S. Chemistry, University of Wisconsin-Madison, 2000

Submitted to the Department of Chemistry in Partial

Fulfillment of the Requirements for the

Degree of

Doctor of Philosophy in Organic Chemistry
at the
Massachusetts Institute of Technology

June 2005

Signature of Author:.....
Department of Chemistry
May 3, 2005

Certified by : .....
Stephen L. Buchwald
Camille and Henry Dreyfus Professor of Chemistry
Thesis Supervisor

Accepted by :.....
Robert W. Field
Chairman, Department Committee on Graduate Students

This doctoral thesis has been examined by a committee of the Department of Chemistry as follows:

Professor Barbara Imperiali.....
Chair

Professor Stephen L. Buchwald.....
Thesis Supervisor

Professor Gregory C. Fu.....

Professor Donna G. Blackmond.....

Mechanistic Studies on Metal-Catalyzed Carbon-Nitrogen Bond-Forming Reactions

By Eric R. Strieter

B. S. Chemistry, University of Wisconsin-Madison, 2000

Submitted to the Department of Chemistry in Partial

Fulfillment of the Requirements for the

Degree of

Doctor of Philosophy in Organic Chemistry

Abstract

Mechanistic studies on copper and palladium-catalyzed C-N bond forming reactions are described. To understand the mechanistic details of these processes, several principles of physical organic chemistry have been employed.

Chapter 1. We have investigated the mechanism of the copper-catalyzed *N*-arylation of amides using aryl iodides, i.e., the Goldberg reaction. The focus of the work has been directed towards amides since this reaction remains the most versatile in the presence of Cu(I)/1,2-diamine catalyst systems. The results provide insights into the role of 1,2-diamines in modulating the coordination environment around Cu(I). The catalyst is more efficient at high concentrations of 1,2-diamine and high concentrations of amide, as revealed by a nonlinear dependence of the rate on 1,2-diamine concentration. Extended premixing times between the

Cu(I) precatalyst and the amide lead to an extensive induction period which can be attenuated by replacing the Cu(I) precatalyst with a Cu(II) precatalyst. Evidence for the reduction of the Cu(II) precatalyst through the oxidation of the amide is also presented. Furthermore, we demonstrate that a 1,2-diamine ligated Cu(I)-amidate may potentially serve as the reactive species that undergoes aryl halide activation. This was established through both its chemical and kinetic competency in the stoichiometric *N*-arylation process. This behavior has important consequences for new catalyst development since these results show the significance of both the diamine and amide in modulating the overall reactivity of the system.

Chapter 2. A systematic mechanistic analysis of $Pd(OAc)_2$/ monophosphino-biaryl–catalyzed C–N bond forming reactions with aryl chlorides has been performed. The results provide insights into the relationship between the steady-state concentration of active Pd and the size and substitution pattern of the monophosphinobiaryl ligands. These insights into the nature of catalyst activation help highlight the importance of establishing a high concentration of active catalyst. The catalyst derived from the bulkiest ligand in the series, the tri-*i*-propyl ligand **13**, exhibits both accelerated rate and the increased stability required for practical application of this reaction.

Thesis Supervisor: Professor Stephen L. Buchwald

Title: Camille Dreyfus Professor of Chemistry

Acknowledgements

There have certainly been a number of people who deserve my gratitude for their assistance and support during my five years here in the Buchwald group. Everyone that I have had the pleasure of interacting with during my stay at MIT has contributed to this document in some form. Although some people may be omitted, I am truly thankful to all of you.

I would like to first thank those responsible for my becoming a scientist because they deserve special recognition. My father was the one who initially inspired my curiosity in science; it was he who infected me with his joy and passion for understanding the laws of nature and he remains as my role model to this day. As a very inexperienced freshman at the University of Wisconsin, Prof. Howard Zimmerman accepted me into his lab and it was there that I first encountered the wonders of chemical research. During the late night problem solving sessions with Prof. Hans Reich, was when I caught the organic chemistry bug; his enthusiasm for teaching chemistry was truly astounding. If it were not for Prof. Steven Burke, with whom I worked with for one year in his lab, I would not be at this stage in my life. I am forever grateful for his mentoring and support.

I have learned a tremendous amount about many different aspects of chemistry during the past five years and for that I am indebted to my advisor Steve and Donna Blackmond. Steve has provided me with several opportunities and a tremendous amount of freedom to explore chemistry even when this has not been in his interest to do so. I also appreciate his persistent questioning of results since this has allowed me to become a more critical thinker. Donna has continuously challenged me to develop more probing experiments and for that I am grateful. Her unending support, especially during her sabbatical at Harvard, provided me with a great deal of motivation, without which I could not have continued the mechanistic work described herein.

There were three people that served as my mentors when I first joined this group and thus also deserve special recognition. Dr. Utpal Singh took me under his wing and showed me the ins and outs of kinetics and reaction calorimetry, without his guidance and friendship I do not think this thesis would exist. Furthermore, without the influence of Dr. Alex Muci and Dr. Greg Hughes, both as scientists and friends, I would not have had the fortitude to make it through some difficult times. Their enthusiasm for chemistry always serves as a reminder of why I became interested in chemistry initially.

When Matt Rainka, Ed Hennessy, and I first entered this group together we were completely naïve, as most people are, to what we would experience over the next five years. Over the course of our studies, the three of us have shared many moments together (in particular over a few beverages) during both good times and bad; without this camaraderie this experience certainly would not have been as enjoyable. After all, I think we will be able to look back and indeed say that we had some "good times, good times."

The network of friends that I have established during my time in graduate school is one of the greatest rewards. For this I can never thank the following people enough (in no particular order): Joe Martinelli, Tim Barder, Liane Klingensmith, Lei Jiang, Junghyun Chae, Dirk Spielvogel, Alex Shafir, Peter Chien, Scott Ribich, Oliver Gaertzen, Ryan Kelley, Marissa Kelley, and Shana Sturla.

The support, encouragement, and unquestioning faith that my parents, Robert and Marcia Strieter, have provided me over the years are what has truly been my inspiration throughout life. Finally, I want to thank my fiancé Nicole, without whom this certainly does not mean much. She has stood by my side throughout and I promise to do the same for her.

Preface

Portions of this work have been excerpted or adapted from the following articles which were co-written by the author.

" The Role of Chelating Diamine Ligands in the Goldberg Reaction: A Kinetic Study on the Copper-Catalyzed Amidation of Aryl Iodides" Eric R. Strieter, Donna G. Blackmond, and Stephen L. Buchwald *J. Am. Chem. Soc.* **2005**, *127*, 4120-4121.

" Insights into the Origin of High Activity and Stability of Catalysts Derived from Bulky, Electron-Rich Monophosphinobiaryl Ligands in the Pd-Catalyzed C-N Bond Formation" Eric R. Strieter, Donna G. Blackmond, and Stephen L. Buchwald *J. Am. Chem. Soc.* **2003**, *125*, 13978-13980.

Table of Contents

Introduction

Mechanistic studies on catalytic reactions are typically complicated by the complexity of the multi-step reactions involved in the process. The origin of this complexity mainly resides in the various states that a catalytic species may exist, either within the catalytic cycle or external to it. To simplify matters, mechanistic investigations on a catalytic process are typically accompanied by the corresponding studies on the stoichiometric reactions that are thought to pertain to the catalytic events.[1] This method has indeed been very successful in terms of ferreting out the mechanistic details in a number of metal-catalyzed processes.

$$\frac{1}{rate} = \frac{1}{v_{max}} + \frac{K_{MM}}{v_{max}} \cdot \frac{1}{[A]} \qquad (1)$$

v_{max} = maximum rate ($M \cdot min^{-1}$)
K_{MM} = Michaelis constant (M)

The analysis of the experimental data from these catalytic processes has typically been reduced to a more straightforward means for interpreting the kinetics, such as the Lineweaver-Burk equation (eq 1).[2] This equation, which has stood the test of time since its introduction in 1934, describes the general mechanisms shown in Scheme 1. It is evident that this equation is a powerful tool for analyzing the kinetics of simple systems employing a single substrate (Scheme 1A), however, the situation becomes more complicated with reactions that use more than one substrate (Scheme 1B). The primary reason for this is that the constants v_{max} and K_{MM} now contain variables that do not remain constant over the course of the reaction. Thus, to apply the Lineweaver-Burk equation to this situation, the kinetic studies must be performed under conditions that are far removed from those of practical synthesis. For example, concentration ratios are typically distorted, such that **[B]** >> **[A]**, thus, allowing **[B]** to remain constant. To

then measure the rate dependence on [**B**], a series of Lineweaver-Burk plots each at a different concentration of [**B**] must be obtained. Moreover, initial rate measurements are often employed to avoid further complications arising from catalyst deactivation pathways. Obtaining mechanistic insight using this approach can be misleading. Recently, several studies have shown that high concentrations in one reagent may dramatically influence the chemistry of the catalytic cycle, i.e., shifting the rate-limiting step and the relative abundance of the catalytic species.[3,4,5] Additionally, the slow formation of active catalyst may give rise to anomalous measurements of rate dependencies on substrate concentrations.

Scheme 1.

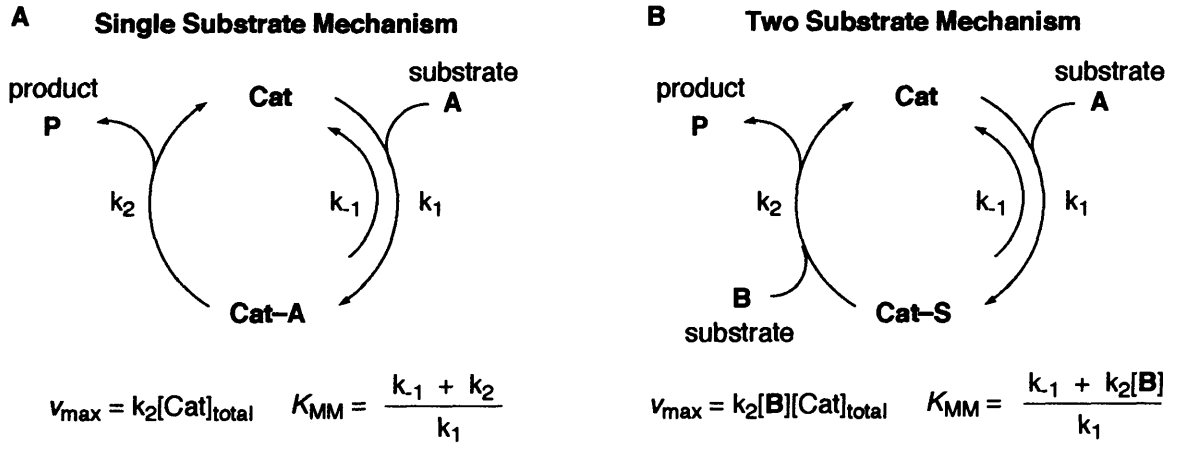

$v_{max} = k_2[Cat]_{total}$ $K_{MM} = \frac{k_{-1} + k_2}{k_1}$

$v_{max} = k_2[B][Cat]_{total}$ $K_{MM} = \frac{k_{-1} + k_2[B]}{k_1}$

The protocol that will be used here involves the method of reaction calorimetry to provide accurate concentration data over the entire course of the reaction. In each case, a large excess of one reagent over the other will not be employed. Instead, this experimental protocol will allow for the concentrations of each substrate to continuously change throughout the reaction. By taking into account the ["excess"], which is defined as the difference in initial concentrations between the two substrates (eq 2), this allows the rate expression to be dependent on a single variable (eq 3).[6] Significantly, this demonstrates that it is unnecessary to perform

reactions with high concentrations of one reagent. Thus, as long as the ["excess"] is known the kinetics of a multi-step process can be delineated.

$$[\mathbf{B}] = [\mathbf{B}]_o - [\mathbf{A}]_o + [\mathbf{A}]$$

$$[\mathbf{B}] = [\text{"excess"}] + [\mathbf{A}]$$

$$[\text{"excess"}] = [\mathbf{B}]_o - [\mathbf{A}]_o \qquad (2)$$

Applying this to the equation: $rate = \dfrac{a\,[\mathbf{A}][\mathbf{B}][\text{Cat}]_{total}}{1 + b[\mathbf{A}] + c\,[\mathbf{B}]}$

$$a = \frac{k_1 \cdot k_2}{k_{-1}} \qquad b = \frac{k_1}{k_{-1}} \qquad c = \frac{k_2}{k_{-1}}$$

We obtain:

$$rate = a' \cdot \frac{[\text{"excess"}] \cdot [\mathbf{A}] + [\mathbf{A}]^2}{1 + b' \cdot [\mathbf{A}]} \qquad (3)$$

$$a' = \frac{k_1 \cdot k_2}{k_{-1} + k_2 \cdot [\text{"excess"}]} \qquad b' = \frac{k_1 + k_2}{k_{-1} + k_2 \cdot [\text{"excess"}]}$$

The transformation of rate vs. time or concentration vs. time data to rate vs. concentration data provides an additional benefit to using the protocol described here. Reaction calorimetry provides a direct measurement of the reaction rate (eq 4), i.e., it is a differential method. Thus, to obtain concentration data as well, the fractional integral of the rate vs. time curve must be calculated (eq 5). Since a catalytic rate law exhibits a direct relationship between rate and substrate concentrations, and not rate and time, this process allows us to obtain a more

$$q = \Delta H_{rxn} \bullet V \bullet r \qquad (4)$$

Where: q = reaction heat flow

ΔH_{rxn} = heat of reaction

V = reaction volume

r = reaction rate

$$fractional\ conversion = \frac{\int_0^t q \cdot dt}{\int_0^{t_f} q \cdot dt} \qquad (5)$$

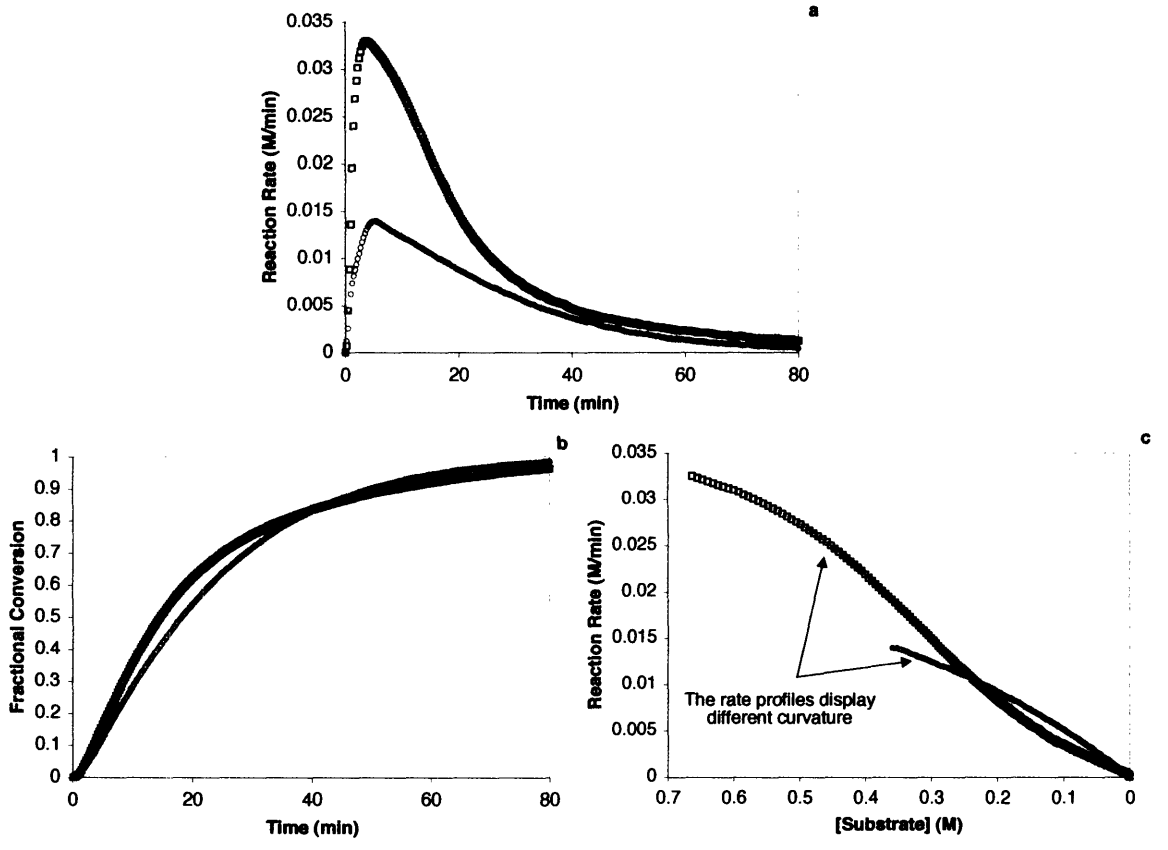

Figure 1. Comparison between reaction rate vs. time (a), conversion vs. time (b), and reaction rate as a function of [substrate] (c).

descriptive picture of the kinetic profile by looking directly at the rate expression. For comparison, Figure 1a displays a typical reaction rate vs. time profile, Figure 1b exhibits a conversion vs. time profile, and Figure 1c shows the reaction rate as a function of [substrate] for the same reactions. What can be gleaned from the temporal rate and conversion profiles (Figure 1a and 1b) is that the reaction depicted by □ exhibits a higher reaction rate than that depicted by ○. The acuteness of the difference between the direct measurement of rate and the indirect measurement of conversion is readily apparent while examining Figures 1a and 1b. In contrast, examining the reaction rate as a function of [substrate] not only provides the same information as the temporal profile but the differences in reaction rate dependencies on [substrate] can also be observed. More specifically, plotting the data in this fashion allows for the changes in the rate dependence on [substrate] to be observed over the entire course of the reaction; the change in curvature of the rate profiles is a manifestation of this behavior. Thus, when applicable, this procedure provides a more descriptive approach toward studying the kinetics of a reaction relative to the more classical approach, i.e., employing high concentrations of one reagent and measuring initial rates.

References

(1) For a discussion of this approach, see: Halpern, J. *Inorg. Chim. Acta* **1981**, *50*, 11.

(2) Lineweaver, H.; Burk, D. *J. Am. Chem. Soc.* **1934**, *56*, 658. For the introduction of Michaelis-Menten kinetics, see: Michaelis, M.; Menten, M. *Biochem. Zeitschrift* **1913**, *49*, 1333.

(3) Rosner, T.; Le Bars, J.; Pfaltz, A.; Blackmond, D. G. *J. Am. Chem. Soc.* **2001**, *123*, 1848.

(4) Rosner, T.; Pfaltz, A.; Blackmond, D. G. *J. Am. Chem. Soc.* **2001**, *123*, 4621.

(5) Singh, U. K.; Strieter, E. R.; Blackmond, D. G.; Buchwald, S. L. *J. Am. Chem. Soc.* **2002,** *124*, 14104.

(6) Eq. 2 assumes that the concentration of the intermediates [Cat-A] are small compared to the substrate concentrations.

Chapter One:

Mechanistic Studies on the Cu-Catalyzed *N*-Arylation of Amides Using Aryl Iodides

Introduction

The foundation of modern cross-coupling chemistry was built at the beginning of the twentieth century with the pioneering work of Fritz Ullmann and Irma Goldberg shown in Figure 1.[1] Their explorations into new methods for the synthesis of C-C, C-N, and C-O bonds provided the conceptual breakthrough that allowed for the use of unactivated aryl halides to supplant the electron-poor aryl halides typically required for the classical nucleophilic aromatic substitution reaction. These advancements not only expanded the scope of substrates that could be utilized in aromatic substitution reactions, it changed the way chemists thought about constructing molecules containing aryl-N and aryl-O bonds. Further testimony for this achievement is the myriad of industrial processes that utilize this methodology, i.e., in the synthesis of pharmaceuticals, agrochemicals, and in polymer chemistry.[2]

Figure 1.

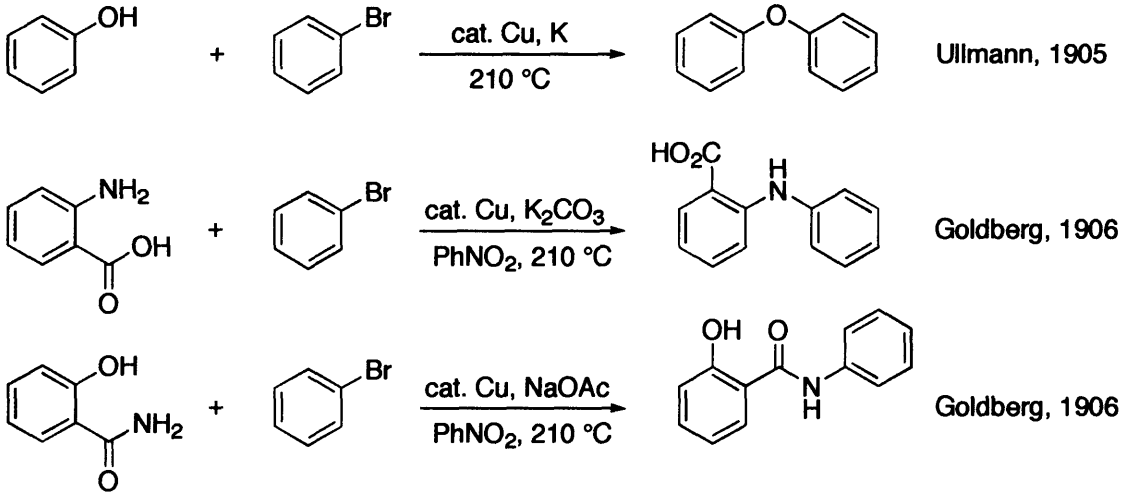

Despite the remarkable contributions of Ullmann and Goldberg, several issues typically plague the reactions that bear their names. The classic Ullmann and Goldberg protocols both require harsh reaction conditions, e.g., high temperatures, extended reaction times, and in more complicated circumstances, stoichiometric amounts of copper are required. As a result, the

reactions have been relatively undeveloped, thus hampering their utility in the synthesis of complex targets. To circumvent these issues, chemists have referred to the more recently developed palladium-catalyzed C-N bond-forming reaction as a means to generate a diverse array of arylated amines.[3] However, the palladium-catalyzed *N*-arylation also encounters some limitations. For example, substrates with functional groups containing free a N-H moiety[4] as well as amides[5] and heterocycles[4a,b] remain problematic. Since these functional groups present themselves in several therapeutically relevant compounds and Cu-catalyzed C-N bond-forming reactions have in the past been more tolerant toward these groups, the development of such processes has been revived.

The employment of chelating ligands has provided the major driving force behind the evolution of Cu-catalyzed C-N bond-forming processes. The first reports concerning the intentional use of exogenous ligands focused on 1,10-phenanthroline. For the *N*-arylation of imidazoles, the use of a catalyst system based on 1,10-phenanthroline allowed for the reaction to occur at lower temperatures, shorter reaction times, and in nonpolar solvents in comparison to the classic Ullmann conditions.[6] Also during the synthesis of triarylamines, the 1,10-phenanthroline/CuCl catalyst system was found to be the most effective, thus allowing the reactions to occur at much lower temperatures than those previously used.[7] Moreover, soluble complexes of Cu(I) and 1,10-phenanthroline, i.e., $LCu(PPh_3)Br$, and its derivatives based on neocuproine and 2,2′-bipyridine have been exploited in the synthesis of aryl amines.[8] Other chelating ligands such as ethylene glycol,[9] L-proline,[10] *N*-methyl glycine,[10] and diethylsalicylamide[11] have also proven to be quite effective in the *N*-arylation of both aliphatic and aryl amines. One of the most general catalyst systems based on a chelating ligand, which is used in the *N*-arylation of amides and heterocycles as well as cyanation and halide exchange

Figure 2.

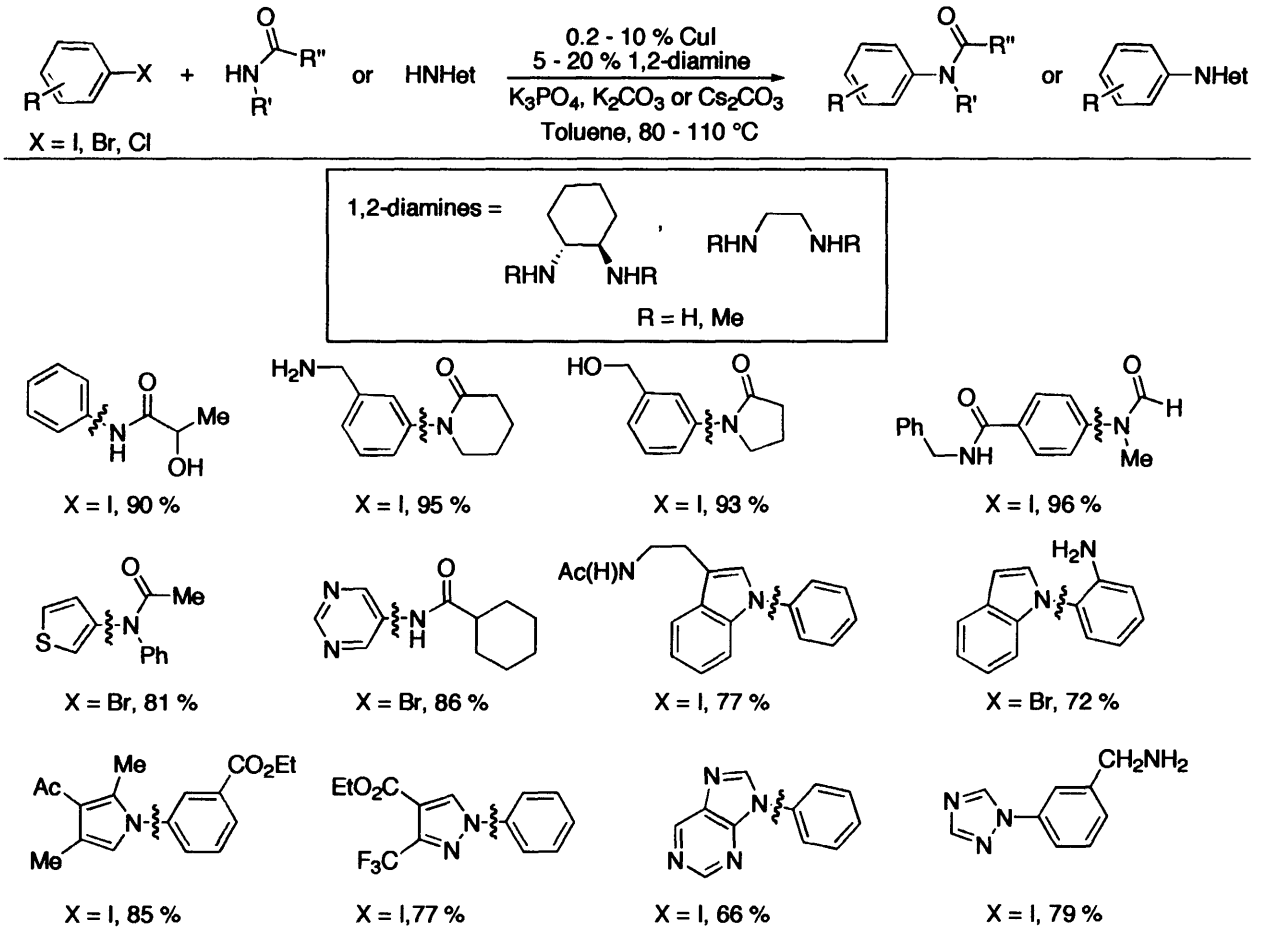

reactions, is that derived from inexpensive 1,2-diamines.[12] As shown in Figure 2, this catalyst system allows for the efficient coupling of a wide variety of substrates, specifically, those containing free N-H and O-H as well as heterocycles. Despite these achievements, most of the copper-based catalyst systems have yet to achieve the high turnover numbers that are typically obtained in the complementary palladium chemistry.[13] Moreover, reactions of less active substrates such as aryl chlorides and aryl sulfonates have thus far been relatively unsuccessful, especially in the latter case. Attempts to understand similar deficiencies in the related palladium chemistry have been investigated through a significant amount of mechanistic work; however,

analogous studies on copper-catalyzed reactions are relatively scarce.[13] This is presumably due to heterogeneity that is inherent to the use of "ligand-free" copper.

Of the few mechanistic studies that have been performed on Cu-catalyzed C-N and C-O bond-forming reactions, the major emphasis has been on the empirical observations pertaining to which catalyst system, i.e., Cu(0), Cu(I) or Cu(II), provides the fastest reaction rate. Since the earliest work by both Ullmann and Goldberg and later Adkins, several different copper sources were found to be effective for the transformation, e.g., $CuBr_2$, $CuCl_2$, $Cu(OAc)_2$, CuI, CuBr, CuCl, and even Cu(0).[1,14] Furthermore, copper sources from three different oxidation states provided nearly identical reaction rates in both *N*-and *O*-arylations, with Cu(I) salts providing slightly higher rates compared to those of Cu(0) and Cu(II). The initial hypothesis for this behavior was that a single catalytic species results from each of these precursors and the active oxidation state is Cu(I).[15] Investigations by electron paramagnetic resonance (EPR) showed that indeed the Cu(II) species decays over time while in the presence of the amine, thereby producing Cu(I).[16] This process was proposed to occur through oxidation of the ligand bound to Cu(II), either the alkoxide, phenolate, or amide. The only direct evidence for ligand oxidation occurred when tetraphenylhydrazine was isolated from the *N*-arylation of diphenylamine using $CuBr_2$ or $Cu(acac)_2$ as the precatalyst.[17] Otherwise, only circumstantial evidence has been provided for ligand oxidation, especially in the case of alkoxide and phenolate oxidation.[18] With regard to the use of Cu(0) as a precatalyst, Paine has found through SEM imaging that the surface of Cu(0) is covered with a thin layer of Cu_2O which then possibly leaches into solution upon amine coordination.[17] Taken together, these results do indeed support the primary role of Cu(I) in facilitating Ullmann-type reactions. Based on these studies alone, the identity of the active Cu(I) species, however, remains obscure.

To characterize the active Cu(I) species, several stoichiometric studies have been performed. Initial experiments have implied that a simple metathesis reaction occurs between either the CuX_2 or CuX salt and the metal alkoxide or amide, thus providing an explanation for the nearly identical reaction rates obtained with different copper salts.[15] With regard to the copper-catalyzed C-O bond-forming reaction, an additional equivalent of alkoxide is then required to form the catalytically active species which is cuprate-like, i.e., $M[Cu(OR)_2]$ where M is Na (eq 1).[18a] In contrast, with studies using phthalimide as the nucleophile, the most reactive species was generated when the Cu(I):pthalimidate ratio was >1, suggesting that a cuprate-like species is unfavorable in this case (eq 2).[19] Furthermore, both Whitesides[20] and Yamamoto[21] have shown that Cu(I) alkoxides and Cu(I) amidates can react with aryl halides when the Cu:nucleophile ratio is 1:1. Based on these results, the only consensus that can be deduced is that a Cu(I)-nucleophile complex must form prior to aryl halide activation. Even the mode of aryl halide activation has experienced a considerable amount of debate.[2] Thus, questions still remain as to the exact nature of the reactive species as well as the influence of ligands on the reactivity of Cu(I) complexes.

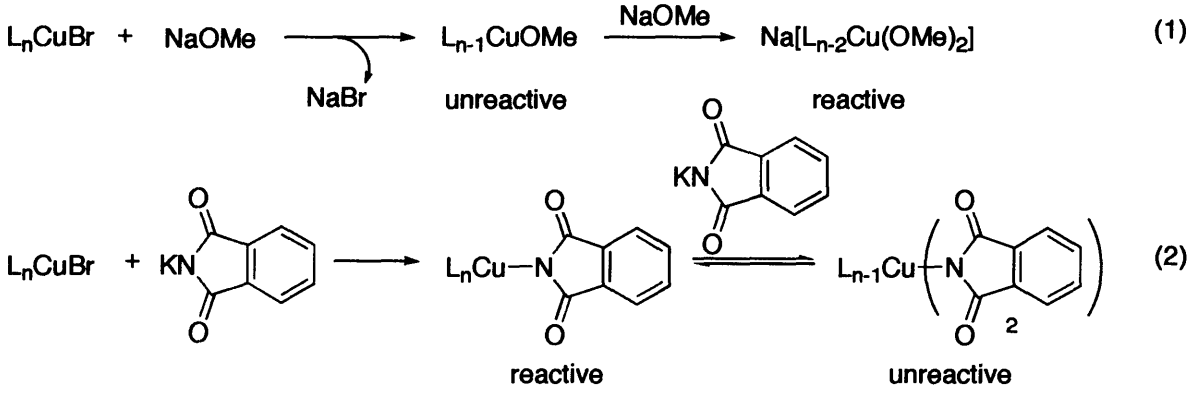

To provide a more rational basis for the development of improved copper catalysts that promote either C-C or C-heteroatom bond-forming reactions, we have investigated the mechanism of copper-catalyzed C-N bond-forming reactions. Much of this work has focused on

the *N*-arylation of amides since this reaction remains the most versatile in the presence of Cu(I)/1,2-diamine catalyst systems. The results provide insights into the role of 1,2-diamines in modulating the coordination environment around Cu(I). The catalyst is more efficient at high concentrations of 1,2-diamine and high concentrations of amide, as revealed by a nonlinear dependence of the rate on 1,2-diamine concentration. Extended premixing times between the Cu(I) precatalyst and the amide lead to an extensive induction period, an event that can be attenuated by higher 1,2-diamine concentrations or replacing the Cu(I) precatalyst with a Cu(II) precatalyst. Evidence for the reduction of the Cu(II) precatalyst through the oxidation of the amide is also presented. Furthermore, we demonstrate that a 1,2-diamine ligated Cu(I)-amidate may potentially serve as the reactive species that undergoes aryl halide activation. This was established through both its chemical and kinetic competency in the stoichiometric *N*-arylation process. This behavior has important consequences for new catalyst development since these results show the significance of both the diamine and amide in modulating the overall reactivity of the system.

Results

Kinetics Studies: 1,2-Diamine and Catalyst Effects. The *N*-arylation of 2-pyrrolidinone (**2**) with 3,5-dimethyliodobenzene (**1**) catalyzed by CuI/**3** (5/10 mol %) (eq 3) proceeds to complete conversion within 2 h at 90 °C. An Omnical SuperCRC reaction calorimeter, which is a differential scanning calorimeter, was used to acquire kinetics of the catalytic reaction in situ by monitoring the heat flow as a function of time at a constant temperature. The reaction time-course (Figure 3) displays a monotonic decrease in heat flow and a lack of an induction period.[22] On the basis of the temporal heat flow, the reaction rate (eq 4),

the fractional conversion (eq 5), and the instantaneous concentrations of the reactants/products can be calculated. Conversion measured by GC analysis was compared to conversion measured by heat flow and the agreement between the two methods validates the use of reaction calorimetry to follow the copper-catalyzed amidation of aryl iodides.

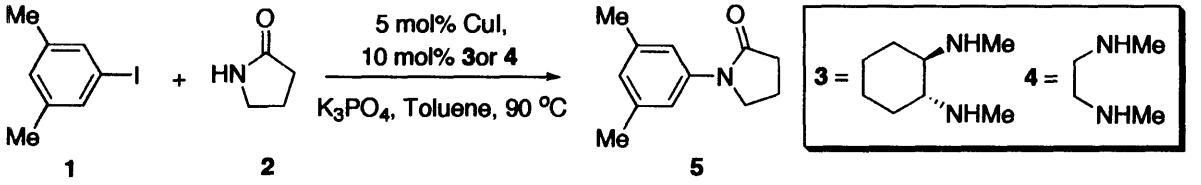

(3)

$$q = \Delta H_{rxn} \bullet V \bullet r \qquad (4)$$

Where: q = reaction heat flow

ΔH_{rxn} = heat of reaction

V = reaction volume

r = reaction rate

$$fractional\ conversion = \frac{\int_0^t q \cdot dt}{\int_0^{t_f} q \cdot dt} \qquad (5)$$

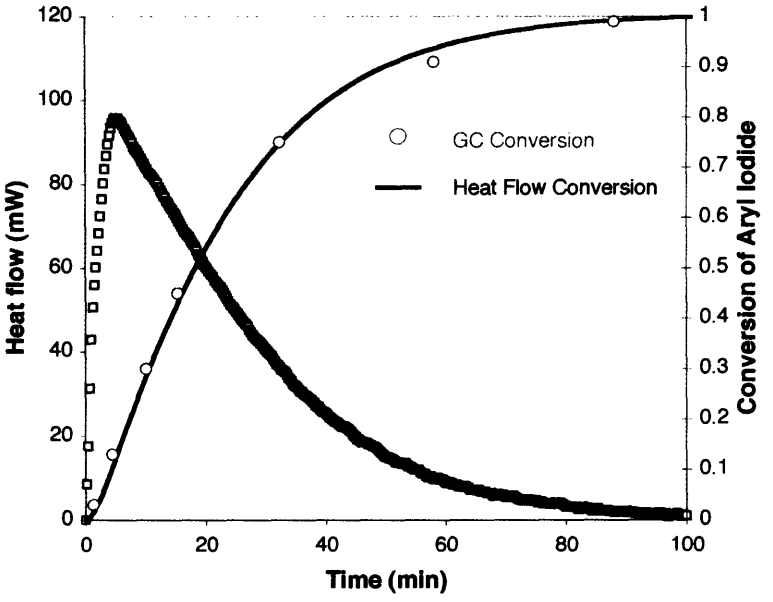

Figure 3. A representative heat flow versus time profile for the CuI/**3** catalyzed *N*-arylation of 2-pyrrolidinone with 3,5-dimethyliodobenzene and comparison of conversion data obtained from heat flow to that obtained by GC measurements. Data sampling occurred at a rate of 4 min^{-1}. Conditions: $[\mathbf{1}]_0 = 0.4$ M, $[\mathbf{2}]_0 = 0.8$ M, $[K_3PO_4]_0 = 1.0$ M, [CuI] = 0.02 M, [**3**] = 0.04 M in 2.0 mL of toluene at 90 ° C.

The initial kinetic studies focused on determining the precise role of the 1,2-diamine in this reaction. As shown in Figure 4, a nonlinear relationship between [1,2-diamine] and the reaction rate was observed over a 20-fold change in [1,2-diamine]. The data were fit using nonlinear least squares to an equation describing saturation with excellent agreement.[23] Since the nonlinear behavior observed in this case is analogous to the Michaelis-Menten kinetic model, the k_{cat} and K_{MM} parameters for each catalyst system can be obtained (Table 1). The difference in k_{cat} between the two catalyst systems represents the only statistically significant factor; the catalyst system based on **4** affords a faster k_{cat} (0.036 ± 0.002 min^{-1}) than that based on **3**, where k_{cat} = 0.025 ± 0.002 min^{-1}.

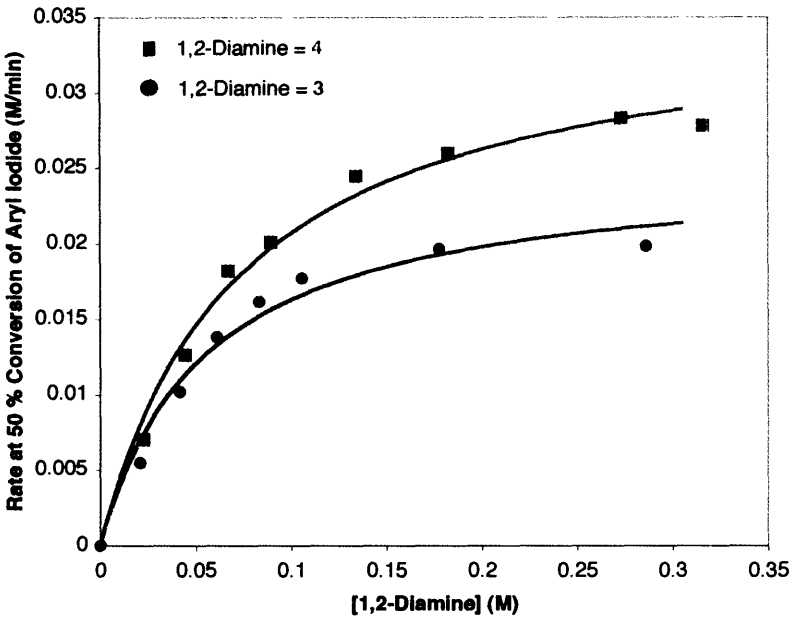

Figure 4. Reaction rate at 50% conversion of **1** vs. [**3**] in the *N*-arylation of **2** (0.8 M) with **1** (0.4 M) using [CuI] (0.02 M). The curve fit reflects a nonlinear least squares fit to a function: rate = C_1[1,2-diamine]/(C_2 + [1,2-diamine]).

Table 1. Michaelis-Menten parameters determined from nonlinear least squares fit to the reaction rate dependence on [1,2-diamine].

Catalyst	k_{cat}(min^{-1})[a]	K_m[a]	k_{cat}/K_M (min^{-1})
CuI/**3**	0.025 ± 0.002	0.05 ± 0.01	0.5 ± 0.1
CuI/**4**	0.036 ± 0.002	0.07 ± 0.01	0.49 ± 0.09

[a] Error analysis of fits was performed using SolvStat (a statistics program purchased with *Excel for Chemists*, by E. Joseph Billo).

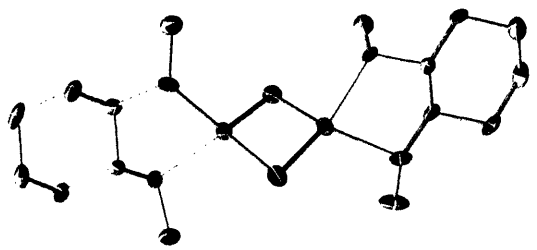

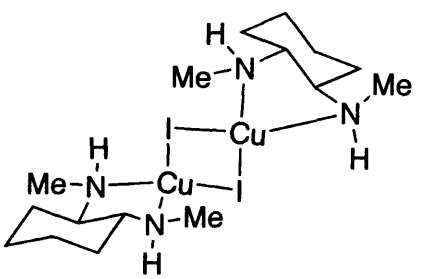

(R,R,R,R)-**6**

Prior to exploring the origins of the nonlinear rate dependence on [1,2-diamine], the possibility of this behavior arising from either catalyst solubility or catalyst deactivation had to

be determined. The observation that complete dissolution of the copper(I) salt occurs in a mixture containing CuI and **3** or **4** in a 1:1 ratio precludes an explanation for the saturation behavior based on a change in solubility of the active copper(I) species. Only upon layering a toluene solution of CuI and **3** with hexanes did a colorless precipitate form. Single-crystal X-ray diffraction analysis of these crystals revealed a dimeric complex **6** containing iodine atoms that bridge the two tetrahedrally coordinated copper(I) centers.[24,25] To examine whether catalyst deactivation could account for the saturation kinetics in [1,2-diamine] the reaction rate dependence on catalyst concentration was examined at both high and low [**3**]. If high [1,2-diamine] prevents catalyst decomposition from occurring, then a nonlinear rate dependence on [catalyst] would be expected at low [**3**], whereas, at high concentrations of [1,2-diamine] a linear rate dependence on [catalyst] would be predicted. In the event, a first-order dependence on $[copper]_{total}$ in reactions with Cu(I):**3** ratios of both 1:2 and 1:7 also rules out catalyst decomposition. This is evidenced by the overlapping rate profiles for in the plots for rate/[catalyst] versus [**1**] (Figure 5).

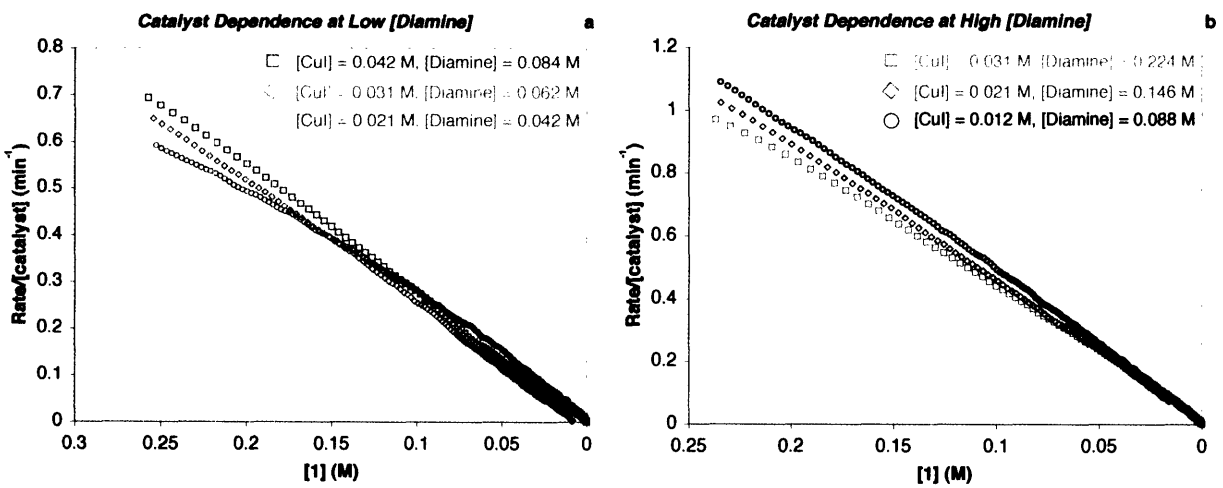

Figure 5. Dependence of the reaction rate on catalyst concentration at both (a) low [**3**] (Cu:**3** = 1:2) and (b) high [**3**] (Cu:**3** = 1:7). In both cases the reaction rate displays a first-order dependence on catalyst concentration. Conditions: [CuI] = 0.01 – 0.04 M, [**3**] = 0.04 – 0.22 M, $[\mathbf{1}]_o$ = 0.4 M, $[\mathbf{2}]_o$ = 0.8 M, $[K_3PO_4]_o$ = 1.0 M, 2 mL of toluene, 90 °C.

Kinetics Studies: Amide, Aryl Iodide, and Base Effects. The dependence of the reaction rate on the amide concentration changes as the concentration of the 1,2-diamine varies (Figure 6). At low [**3**], the reaction rate becomes inhibited at higher [amide] (Figure 6a). Not only is this reflected by the lower initial rates at higher [amide], but also the decreasing slopes of the rate curves. For example, comparing the rate profiles when $[amide]_o$ is 0.93 M to that when $[amide]_o$ is 0.6 M, indicates that at 0.93 M the initial rate is substantially lower than at 0.6 M. Also, the slope of the rate curve at 0.93 M is significantly smaller than that at 0.6 M. In contrast, at high [**3**] the reaction rate actually increases as the [amide] increases. Both the increasing slope of the rate curves as well as the higher initial reaction rates as the [amide] increases reflect this positive-order dependence on [amide]. Thus, there exists a direct correlation between the reaction rate dependence on [1,2-diamine] and the dependence on [amide]. Specifically, the positive-order rate dependence on [1,2-diamine] corresponds to the inverse dependence on [amide] at low [**3**] and the zero-order rate dependence on [1,2-diamine] corresponds to the positive-order dependence on [amide] at high [**3**].

The reaction rate exhibits a first-order dependence on aryl iodide concentration at both high and low [**3**] (Figure 7). Due to the dependence of the reaction rate on both the amide concentration and the aryl iodide concentration, the first-order dependence on [**1**] is not readily apparent. However, it is evident upon analysis of the reaction rates at different [**1**], i.e., the vertical lines in Figures 7a and 7b, that a first-order dependence on [**1**] exists. More specifically, at low [**3**] the reaction rates where the vertical lines are present correspond to 0.032 M/min, 0.021 M/min, and 0.0095 M/min, respectively. At these three points [**1**] is 0.2 M, 0.4 M, and 0.6 M, thus, the reaction rates are directly proportional to the aryl iodide concentration. This is also

the case at high [**3**], where the vertical lines represent points where the rate is: 0.042 M/min when [**1**] is 0.5 M, 0.02 M/min when [**1**] is 0.25 M, and 0.011 M/min when [**1**] is 0.125 M.

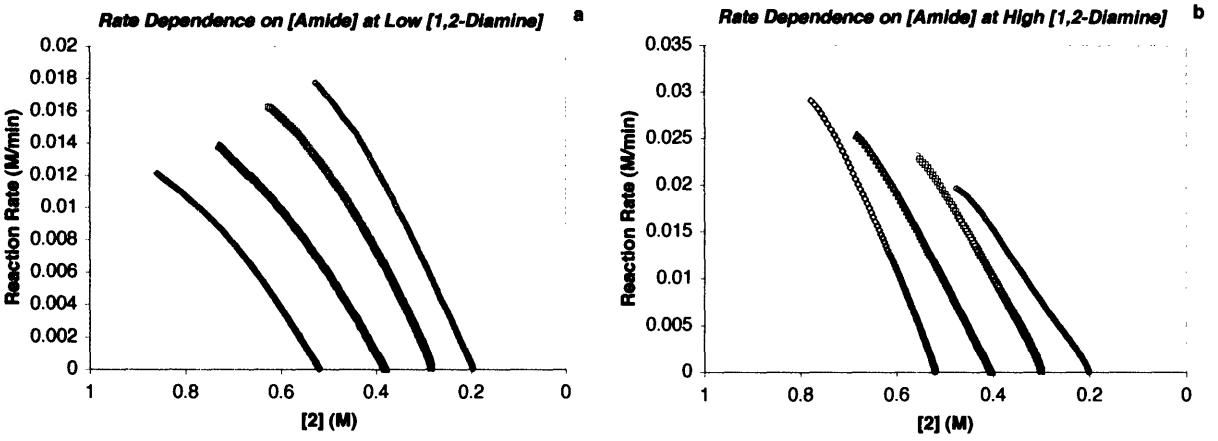

Figure 6. Dependence of the reaction rate on amide concentration ([**2**]) at both (a) low [**3**] (Cu:**3** = 1:2) and (b) high [**3**] (Cu:**3** = 1:10). Conditions: (a) [**3**] = 0.04 M and (b) [**3**] = 0.2 M, [CuI] = 0.02, $[\mathbf{1}]_o$ = 0.4 M, $[\mathbf{2}]_o$ = 0.93 M (◊), 0.8 M (Δ), 0.7 M (□), 0.6 M (O), $[K_3PO_4]_o$ = 1.0 M, 2 mL of toluene, 90 °C.

At both low and high [**3**], the reaction rate is not significantly influenced while changing the amount of K_3PO_4 by over 3-fold (Figure 8). This behavior presumably indicates that saturation of the inorganic base in a nonpolar solvent is occurring. These results further substantiate the claim that the reaction rate is not mass transfer limited, since a rate dependence on $[K_3PO_4]$ may indicate otherwise.

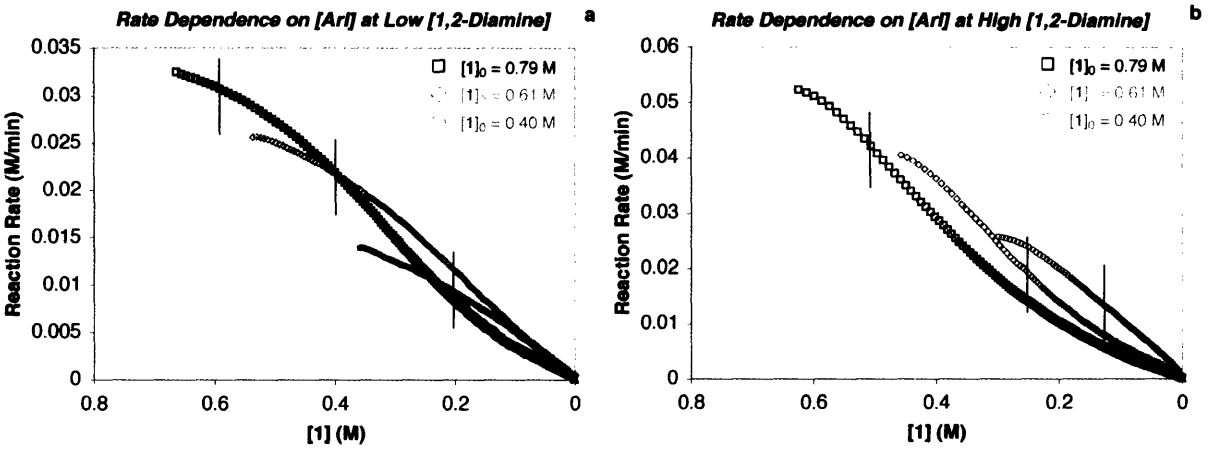

Figure 7. Dependence of the reaction rate on aryl iodide concentration ([**1**]) at both (a) low [**3**] = 0.04 M (Cu:**3** = 1:2) and (b) high [**3**] = 0.2 M (Cu:**3** = 1:10). Conditions: [CuI] = 0.02, $[\mathbf{1}]_o$ = 0.4 M (O), 0.61 M (◊), 0.79 M (□), $[\mathbf{2}]_o$ = 0.83 M, $[K_3PO_4]_o$ = 1.0 M, 2 mL of toluene, 90 °C.

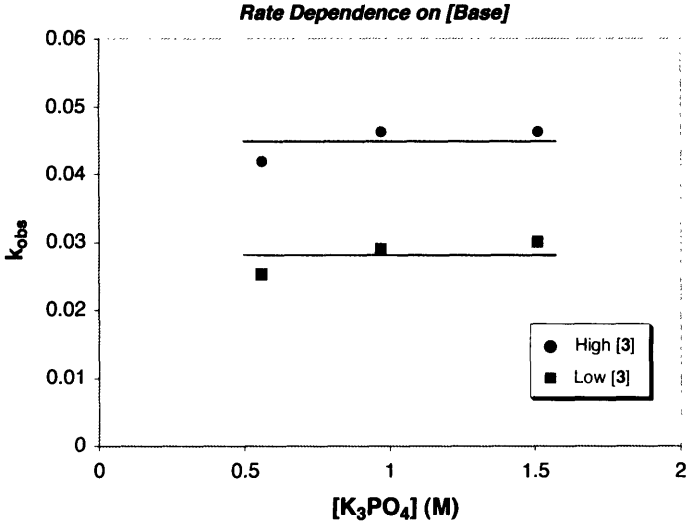

Figure 8. Dependence of the reaction rate on K_3PO_4 concentration at both (a) low [**3**] (Cu:**3** = 1:2) and (b) high [**3**] (Cu:**3** = 1:10). Conditions: (a) [**3**] = 0.04 M and (b) [**3**] = 0.2 M, [CuI] = 0.02 M, $[\mathbf{1}]_o$ = 0.4 M, $[\mathbf{2}]_o$ = 0.83 M, $[K_3PO_4]_o$ = 0.56 – 1.51 M, 2 mL of toluene, 90 °C.

Kinetics Studies: Electronic Effects. A series of *para*-substituted aryl iodides, X–C_6H_4I (X = COMe, Cl, H, Me, OMe) were used to investigate electronic effects on the catalytic turnover rate. The reaction rate exhibits a nonlinear dependence on [1,2-diamine] with each of

the aryl iodides. However, the electronic effect does not change depending on the [**3**]; at both high and low [**3**], electron-deficient analogues facilitate more rapid turnover rates (Figure 9, ρ = +0.58 ± 0.06).

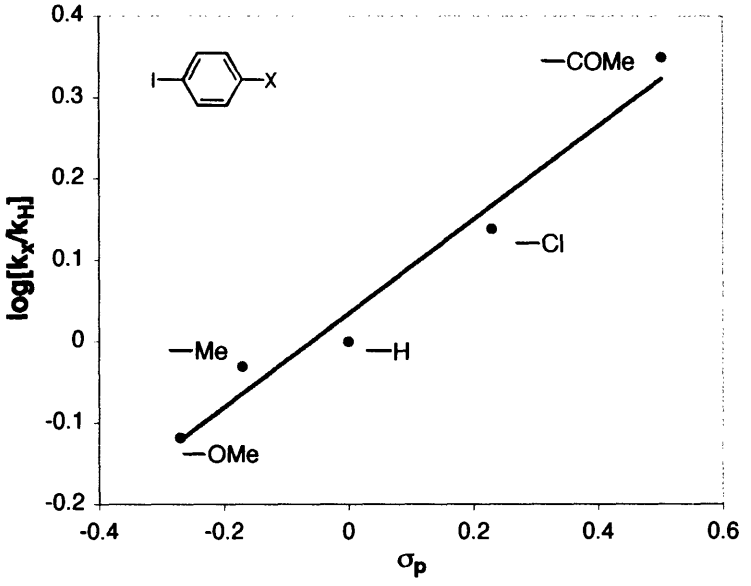

Figure 9. Hammett plot derived from the observed rate constants of the *N*-arylation of 2-pyrrolidinone (**2**) with a series of *para*-substituted aryl iodides. Conditions: [CuI] = 0.02, [**3**] = 0.2 M, [aryl iodide]$_o$ = 0.4 M, [**2**]$_o$ = 0.83 M, [K_3PO_4]$_o$ = 1.0 M, 2 mL of toluene, 90 °C.

Effects of Premixing Catalyst with the Amide and Base. To gain more insight into how the 1,2-diamine thwarts the inhibitory effect of the amide, the catalyst was allowed to premix with the amide and base prior to initiating the *N*-arylation. If higher [amide] reduces the reaction rate at low [**3**], than allowing the catalyst to premix with the amide and base in the absence of the aryl iodide should lead to an exacerbation of this inhibitory effect. This hypothesis assumes that the inactive multiply-ligated Cu(I)/amide complex is the thermodynamically preferred species relative to the 1,2-diamine-ligated Cu(I) complex. In the event, an extensive induction period lasting ca. 450 min is observed while premixing the catalyst with the amide and base for 60 min prior to the addition of the aryl iodide (Figure 10a, O). The

sigmoidal-like shape of the temporal conversion plots is evidence of this behavior. More significantly, the induction period is dependent on the time of premixing, with shorter premixing times resulting in shorter induction periods (Figure 10a). Increasing [**3**] while premixing the catalyst with the amide and base for 60 min also leads to an attenuation of the induction period (Figure 10b). These results suggest that an equilibrium process involving 1,2-diamine coordination to a multiply-ligated copper-amide species is occurring (Scheme 1, also see discussion below).

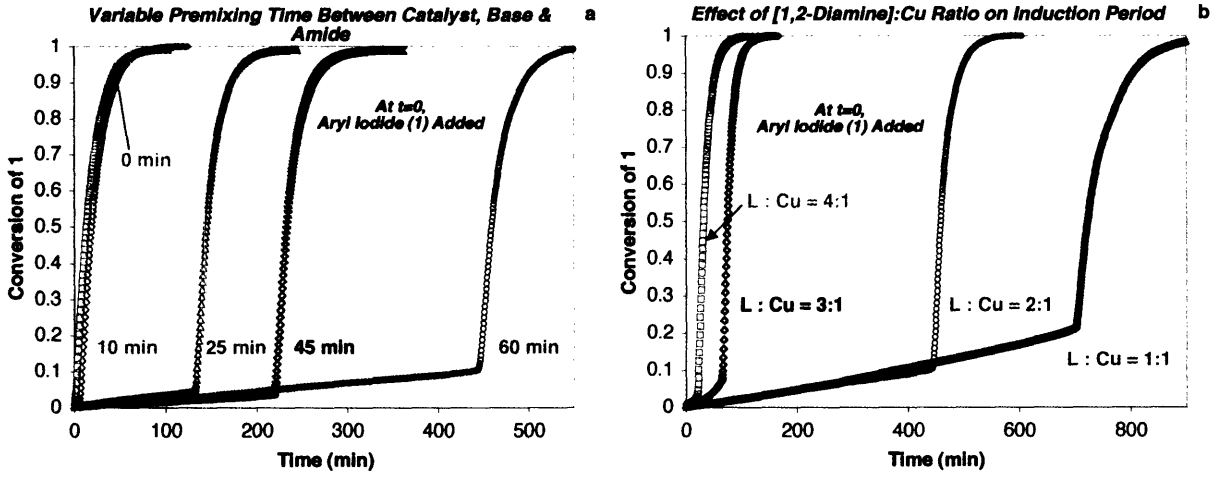

Figure 10. Effect of premixing the catalyst with amide and base prior to the addition of aryl iodide (this occurs at t = 0 min) for (a) various premixing times and (b) with different [**3**]. Conditions for (a): [CuI] = 0.04 M, [**3**] = 0.08 M, $[\mathbf{1}]_0$ = 0.8 M, $[\mathbf{2}]_0$ = 1.0 M, $[K_3PO_4]_0$ = 1.2 M, 1.5 mL of Toluene, 90 °C. Lengths of time for premixing the catalyst with the amide and base are: 0 min (□), 10 min (◊), 25 min (Δ), 45 min (**X**), 60 min (**O**). At t = 0 min, the aryl iodide (**1**) is added to the reaction mixture. Conditions for (b): [CuI] = 0.04 M, [**3**] = 0.04 M (Δ), 0.08 M (O), 0.12 M (◊), 0.16 M (□), $[\mathbf{1}]_0$ = 0.8 M, $[\mathbf{2}]_0$ = 1.0 M, $[K_3PO_4]_0$ = 1.2 M, 1.0 mL of Toluene, 80 °C. The catalyst was premixed with the amide and base for 60 min prior to the addition of aryl iodide which occurs at t = 0 min. The stirring rate for all of these experiments was set at 1100 rpm .

Scheme 1. Equilibrium for 1,2-diamine coordination to multiply-ligated copper-amide.

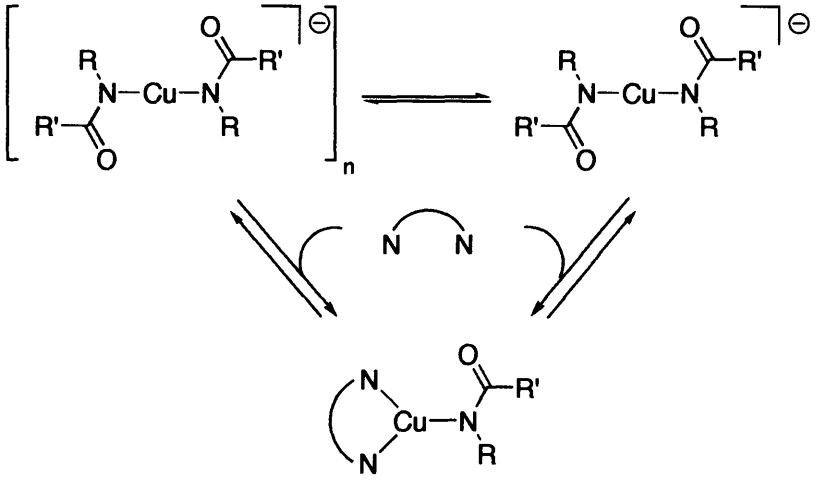

To gain further insight into the origins of the induction period as well as the dramatic rate acceleration once the induction period subsides, the Cu(I) precatalyst was replaced with a Cu(II) precatalyst in the premixing studies. On the basis of the studies described above, where 1,2-diamine ligands on Cu(I) are quite labile, we surmised that using a Cu(II) precatalyst would altogether prevent the induction period since Cu(II) has a greater affinity for chelating ligands relative to Cu(I).[26] If the reduction of Cu(II) to Cu(I) in the presence of amide and base is slow, then the concentration of Cu(I) in solution will be low enough to prevent the formation of a multiply-ligated Cu(I)/amide species. Thus, the Cu(I) that is formed from the reduction will mostly reside as the 1,2-diamine bound species. To test this hypothesis, the $CuBr_2$/**3** catalyst system was premixed with **2** and K_3PO_4 for 60 min at 80 °C prior to the introduction of the aryl iodide. As shown in Figure 11, the Cu(II)/**3** precatalyst does indeed prevent an induction period from occurring in relation to the Cu(I)/**3** catalyst system. Comparing the rates of *N*-arylation between the Cu(I) and Cu(II) catalyst systems once the induction period subsides, indicates that:

1) premixing the Cu(II) precatalyst provides a nearly identical rate for the *N*-arylation to that of the Cu(I) catalyst after the induction period is over, and 2) unlike the rate of *N*-arylation with the Cu(I) catalyst, the Cu(II) system is dramatically influenced by the premixing process (Table 2).[27] It is important to note that the values for k_{obs} in Table 2 were obtained from the rate of the *N*-arylation after the induction period is complete. The effect of the premixing process on the Cu(II) system also reveals that the reduction of Cu(II) to the active Cu(I) species occurs at a slower rate relative to that of the *N*-arylation process. This is evidenced by: 1) the lack of an induction period while not premixing the Cu(II) precatalyst, 2) the linear decay of the rate versus concentration while not premixing, and 3) the 4-fold increase in reaction rate upon premixing.

The Cu(II) catalyst system was allowed to premix with the amide and base for various amounts of time to obtain more qualitative information regarding the reduction of Cu(II) to Cu(I). As shown in Figure 12, premixing the Cu(II)/**3** catalyst system with the amide and base for longer periods of time leads to increasing reactions rates as predicted by the experiments in Table 2. Premixing times longer than 60 min, however, produce an induction period similar to that observed during the Cu(I)/amide/base premixing experiments (data not shown). To correlate the increasing reaction rates observed during the Cu(II) premixing studies in Figure 10 with the reduction of Cu(II) to Cu(I), EPR spectroscopy was employed to monitor the decay of Cu(II). As shown in Figure 13, the initial EPR spectrum of a solution containing the $CuBr_2$/**3** precatalyst, **2** and K_3PO_4 in toluene (the solution was mixed for 1 min at 80 °C prior to obtaining the EPR spectrum at 23 °C) consists of a 4-line pattern resulting from the hyperfine coupling to one Cu nucleus ($I = 3/2$). [28] The deviation from a simple 1:1:1:1 quartet pattern results from the decreasing line widths at higher field; a characteristic of Cu(II) species in a tetragonal environment with four strongly bound equatorial ligands and two weakly bound axial ligands.[29]

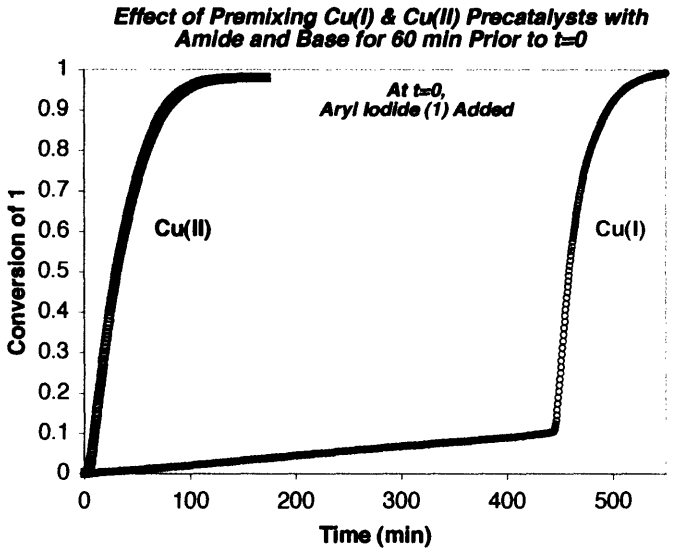

Figure 11. Comparison between Cu(I) (O) and Cu(II) (□) precatalysts while premixing the catalyst with amide and base prior to the addition of aryl iodide (this occurs at t = 0 min). Conditions: $[\mathbf{1}]_0$ = 0.8 M, $[\mathbf{2}]_0$ = 1.0 M, $[K_3PO_4]_0$ = 1.2 M, (□) [CuBr2] = 0.04 M, [**3**] = 0.08 M, (O) [CuI] = 0.04 M, [**3**] =0.08 M, 1.0 mL of Toluene, 80 °C.

Table 2. Comparison of reaction rates between Cu(I)/1,2-Diamine and Cu(II)/1,2-Diamine catalyst systems once the induction period is complete.

Catalyst	Premix w/ Amide + K_3PO_4[a]	k_{obs} (min^{-1})[b,c]
CuI/ **3**	Yes	$4.92 \pm 0.02 \times 10^{-2}$
$CuBr_2$/ **3**	Yes	$4.41 \pm 0.03 \times 10^{-2}$
$CuBr_2$/ **3**	No[d]	$1.15 \pm 0.01 \times 10^{-2}$

[a] Catalyst premixed with **2** and K_3PO_4 in 1.5 mL of Toluene at 80 °C for 60 min prior to the addition of **1**. [b] Error analysis perfomed by LINEST (a statistical analysis program affliated with Excel). [c] Values for k_{obs} obtained from the reaction once the induciton period is complete. [d] Catalyst and K_3PO_4 in 1.5 mL of Toluene equilibrated at 80 °C for 60 min prior to the simultaneous addition of **1** and **2**.

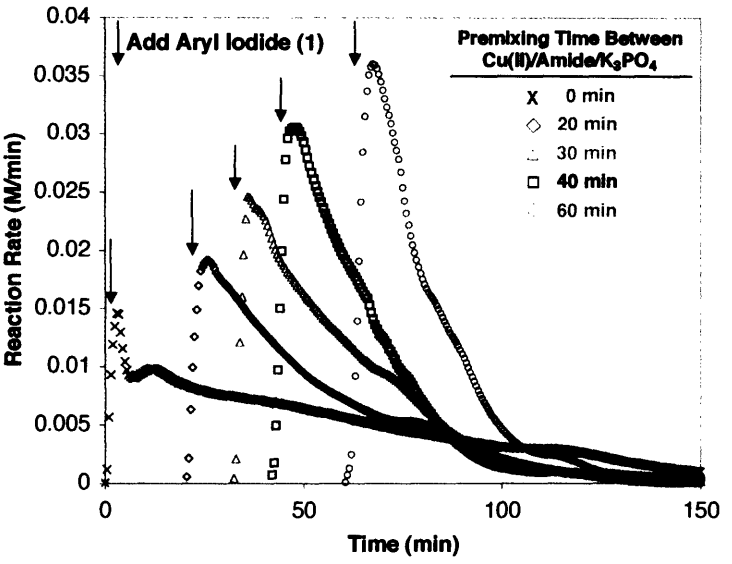

Figure 12. Effect of Cu(II)/Amide/K_3PO_4 premixing times on the rate of *N*-arylation. At t = 0, **2** (1.0 M) is added to a solution of [$CuBr_2$] = 0.04 M, [**3**] =0.08 M, [K_3PO_4] = 1.2 M, in 1.0 mL of Toluene, at 80 °C. Once the desired premixing time has occurred, **1** (0.8 M) is added to the reaction mixture.

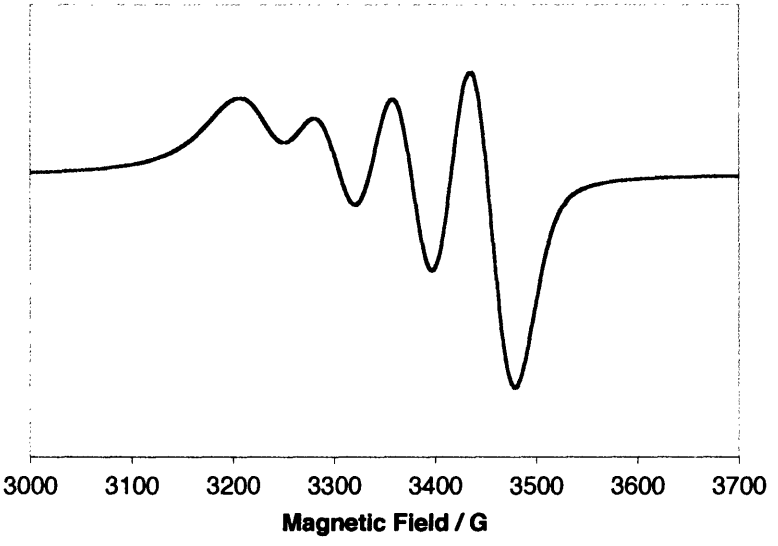

Figure 13. EPR spectrum of a solution containing $CuBr_2$ (0.02 M), **3** (0.08 M), **2** (0.8 M) and K_3PO_4 (1.0 M) in 0.4 mL of Toluene at 23 °C.

The g-factor was estimated as $g = 2.10 \pm 0.01$ from the magnetic field at the spectral center. The hyperfine coupling constant, i.e., $a(Cu^{II})$, could not be accurately determined by simulation using the SimFonia® software due to the changing line widths. However, similar Cu(II)-amine complexes in solution exhibit $a(Cu^{II})$ values between 70 – 90 G and line widths between 50 – 20 G.[30] To further probe the coordination environment of the Cu(II) species in Figure 13, the EPR intensity was monitored as a function of 1,2-diamine:Cu. The maximum signal intensity was obtained at a **3**:Cu ratio of 2:1, suggesting that two 1,2-diamine ligands reside at the metal center. Moreover, **7**, which was obtained from a mixture of $CuBr_2$ and **3** in MeOH in 87 % (eq 6), exhibits an identical EPR spectrum to that in Figure 13 while in a toluene solution containing **2** (0.6 M).[31] Observation of the EPR intensity of **7** over a 90 min period while mixing with **2** and K_3PO_4 in a toluene solution at 80 °C does indeed indicate that there is decay in the [Cu(II)] with

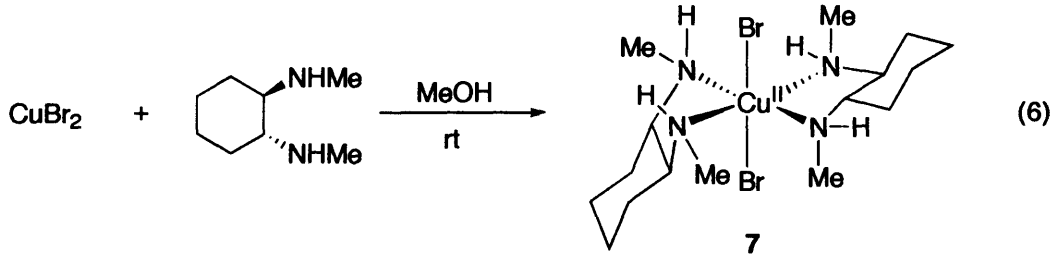

(6)

extended mixing times (Figure 14). It is important to note that the initial point in Figure 14 was obtained 1 min after adding **2** to a mixture of **7** and K_3PO_4 in Toluene at 80 °C due to the poor solubility of **7** in the absence of **2**. Since Cu(I) is diamagnetic and thus unobservable by EPR, the decay in the Cu(II) EPR intensity presumably corresponds to the formation of Cu(I), however, oligomeric Cu(II) species often do not result in an EPR signal. Nonetheless, these data correlate with the increasing reaction rates observed at longer mixing times between Cu(II)/**3**, **2**, and K_3PO_4 (Figure 12 and Table 2).

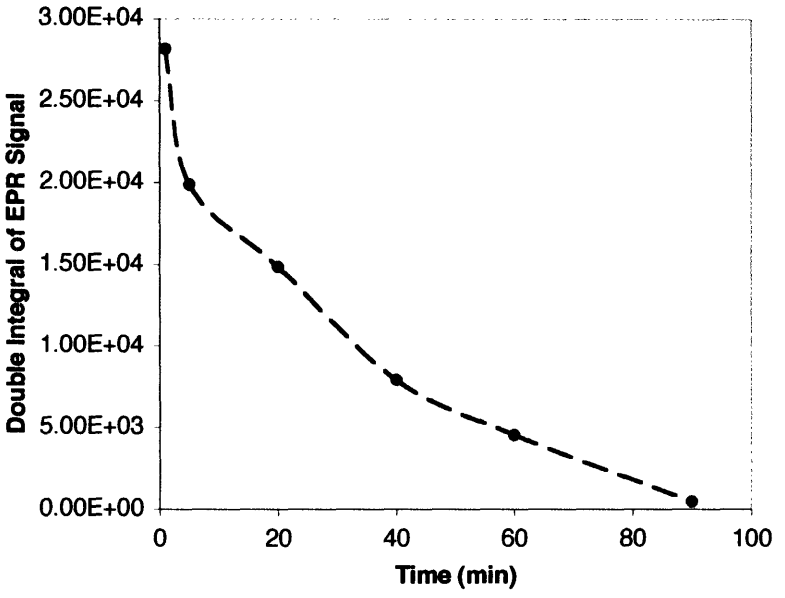

Figure 14. Decay of EPR signal (23 °C) for **7** (0.02 M) as a function of mixing time with **2** (0.6 M) and K_3PO_4 (0.9 M) in 2 mL of Toluene at 80 °C.

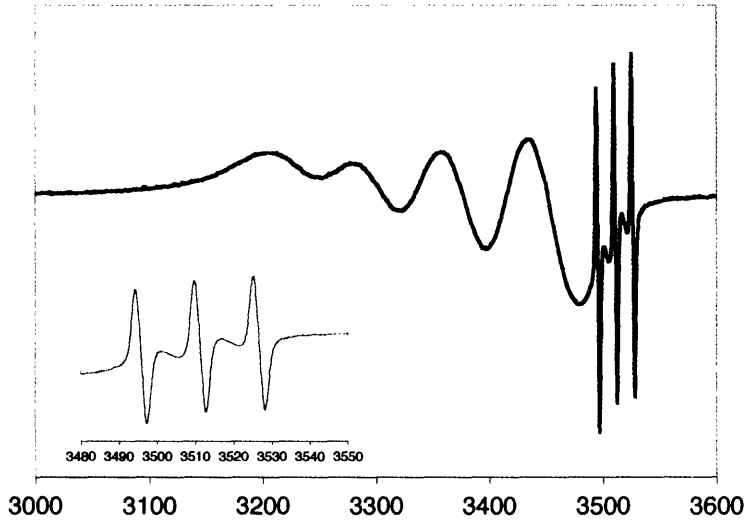

Figure 15. EPR spectrum of a mixture containing **7** (0.02 M), **2** (0.6 M) and K_3PO_4 (0.9 M) in 2 mL of Toluene after 90 min at 80 °C. The inset provides a closer look at the 1:1:1 triplet at g = 2.006, a_N = 15.4 G.

The appearance of an organic radical is observed at extended mixing times between the Cu(II)/1,2-diamine complex, amide, and base. After mixing **7** with **2** and K_3PO_4 in toluene at 80

°C for 90 min a 1:1:1 triplet is observed in the region of the *g* factor associated with the free electron (Figure 15 and inset). The splitting pattern of the organic radical is consistent with an *N*-centered radical due to spin $I = 1$ for ^{14}N nuclei.[32,33] Further analysis of the EPR spectrum affords a hyperfine coupling constant of $a_N = 15.4$ G and a *g*-factor of 2.006. Since the premixing studies between the Cu(II) precatalyst and amide certainly indicate that there exists a direct correlation between the loss of Cu(II) and the generation of the *N*-centered radical, the origin of this free radical is most likely the amide. To examine further the potential oxidation of the amide, ^{15}N-2-pyrrolidinone (^{15}N-**2**) was employed. In this case, after mixing the Cu(II) precatalyst with ^{15}N-**2** in the presence of K_3PO_4 at 80 °C for 90 min, a singlet with a *g*-factor of 2.007 was observed in place of the 1:1:1 triplet obtained with ^{14}N-**2**. Since a doublet would be expected on the basis of the spin $I = 1/2$ for ^{15}N nuclei, it truly is unclear whether the *N*-centered radical resides on the 1,2-diamine ligand or the amide.

Synthesis and Characterization of Cu(I) Amidates. The Cu(I) amidate **8** was obtained from the reaction between dry, oxygen-free **2** and halide free mesitylcopper[34] at room temperature in toluene under a nitrogen atmosphere (eq 7).[35] Cu(I) amidate **8** is soluble in both toluene and 1,4-dioxane and less soluble in diethyl ether, THF, and hexanes. The Cu(I) amidate **8**, was obtained as a white solid upon removal of toluene under vacuum and washing with hexanes.

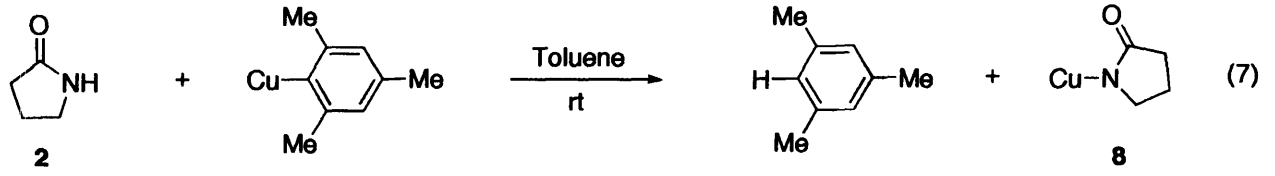

(7)

The Cu(I) amidate **8** is hydrolyzed on contact with water and rapidly oxidized by air. The ratio of amidate to Cu(I) was analyzed for the composition of 2-pyrrolidinone by gas chromatography through the hydrolysis of **8** upon addition of concentrated HCl to a solution of **8** in toluene; the Cu content was analyzed by iodometric titration. These analyses indicate that the ratio of amidate:Cu is approximately 1:1.[36]

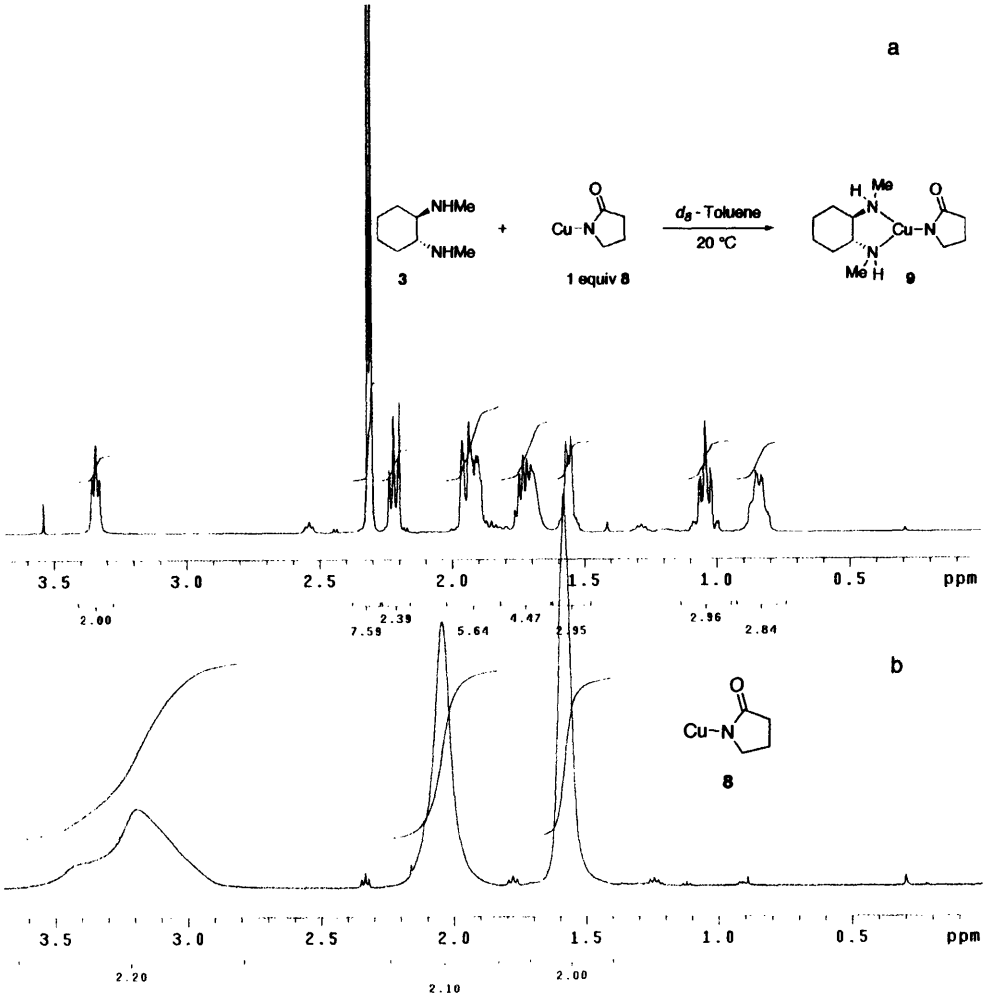

Figure 16. ^{1}H NMR spectra of a solution containing a) **8** and **3** and b) just **8** in d_8 – toluene at 20 °C.

The solution structure of **8** is dependent on whether the chelating 1,2-diamine is present. In accordance with the solution behavior of Cu(I) alkoxides,[20,37] Cu(I) amides,[35] and CuCN,[38] **8**

exists as a rapidly exchanging oligomeric species as evidenced by the broadened resonances in the room temperature ^{1}H NMR spectrum (Figure 16b). However, upon addition of **3** to a solution of **8** in toluene the resonances are sharpened in the ^{1}H NMR spectrum (Figure 16a), which is consistent with an "average" structure where the 2-pyrrolidinoate moieties are no longer rapidly exchanging with other oligomeric forms. This suggests that a single species results from the addition of **3** to **8**. Since the N-H protons from **3** remain, the complex that forms is most consistent with **9**, which is a three-coordinate 1,2-diamine bound Cu(I) amidate (eq 8).

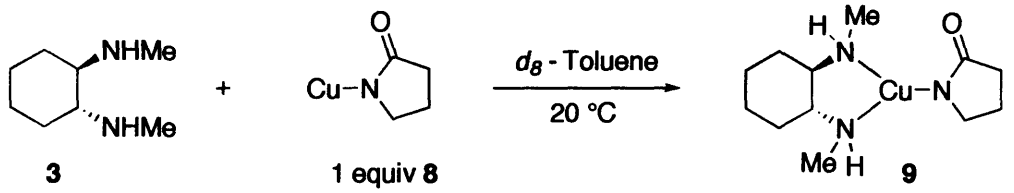

(8)

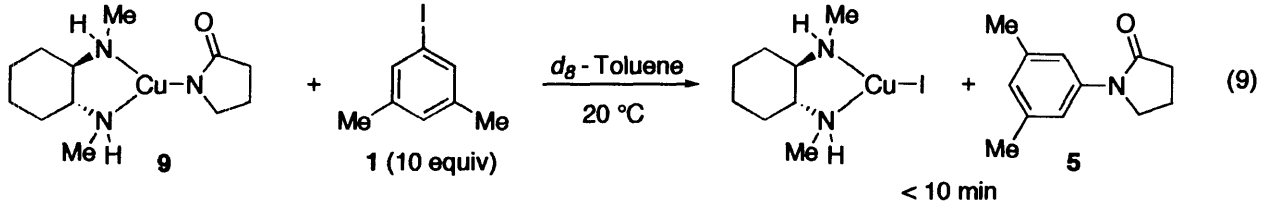

(9)

Kinetics Studies: *N*-Arylation of Cu(I) Amidate with Aryl Iodides. To characterize the kinetic competency of the Cu(I) amidate as a potential intermediate during the catalytic *N*-arylation process, the kinetics of the *N*-arylation of **9** were investigated by ^{1}H NMR. The addition of 10 equiv of aryl iodide **1** to the solution of **9** shown in Figure 16a results in complete conversion of **9** to the corresponding *N*-arylated 2-pyrrolidinone **5** in < 10 min at 20 °C (eq 9).[39] Further kinetic analysis, which assumes a second-order overall process based on eq 10 – 13 , does indeed indicate that the reaction is first-order with respect to both [**1**] and [**9**]. It is important to note that the reaction rate for aryl iodide activation is independent of [**3**] at ratios of **3**:Cu(I) amidate >1. As shown in Figure 17, the plot of $1/[\mathbf{9}]_t - 1/[\mathbf{9}]_0$ versus time furnishes a

linear plot with slope equal to k_{app} for the *N*-arylation of **9** over 3 half-lives. Comparing $\Delta G^{\ddagger}$ (obtained from the second-order rate constant, i.e., k_{app}) for the Cu(I) amidate **8** based on ligand **3**, i.e., **9**, to that based on ligand **4** reveals a nearly identical activation energy; 19.4 kcal•mol^{-1} for the former and 19.5 kcal•mol^{-1} for the latter, respectively.

$$\text{Rate} = k_{app}[\mathbf{1}][\mathbf{9}] \tag{10}$$

Where [**9**] = [(1,2-diamine)Cu(I)Amidate] and [**1**] = [Aryl Iodide]

$$\text{When } [\mathbf{9}] = [\mathbf{1}], \text{ Rate} = k_{app}[\mathbf{9}]^2 \tag{11}$$

$$\frac{d[\mathbf{9}]}{dt} = -k[\mathbf{9}]^2 \implies \int_0^t \frac{1}{[\mathbf{9}]^2}\, d[\mathbf{9}] = -k\int_0^t dt \tag{12}$$

$$\frac{1}{[\mathbf{9}]_t} - \frac{1}{[\mathbf{9}]_o} = kt \tag{13}$$

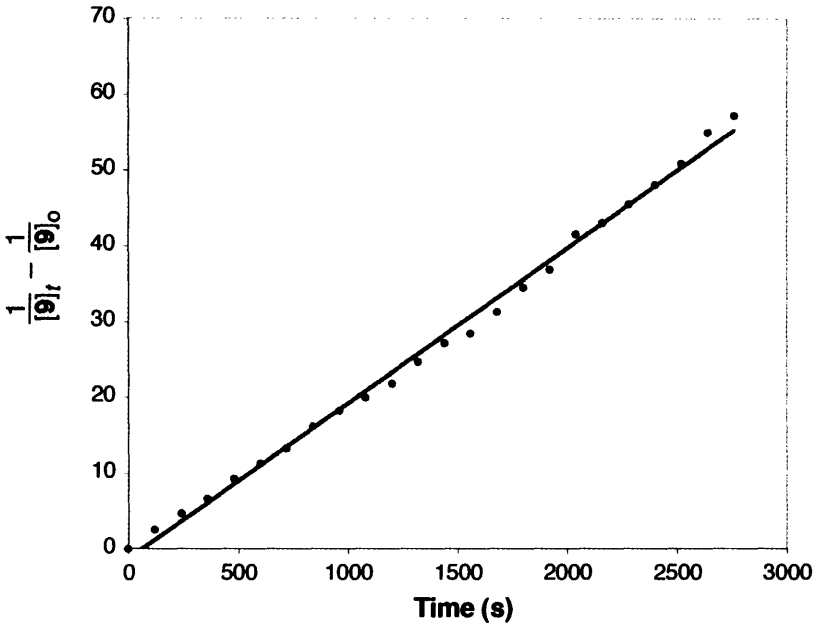

Figure 17. Linear relationship between $1/[\mathbf{9}]_t - 1/[\mathbf{9}]_o$ and time (s) for the *N*-arylation of **9** (52 mM) with **1** (52 mM) in 1 mL of d_8 – toluene at 20 °C; $k_{app} = 2.04 \times 10^{-2}\ M^{-1} \bullet s^{-1}$.

The activation parameters for the stoichiometric *N*-arylation process allowed for further characterization of the aryl iodide activation step. Measuring the second-order rate constant, k_{app}, over a 30 °C temperature range, i.e., 0 – 30 °C, provided a linear Eyring plot (Figure 18). Table 3 provides the activation parameters. The $\Delta H^{\ddagger}$ was measured as 5.5 ± 0.5 kcal•mol^{-1} and the $\Delta S^{\ddagger}$ was measured as –46.6 ± 1.7 eu.

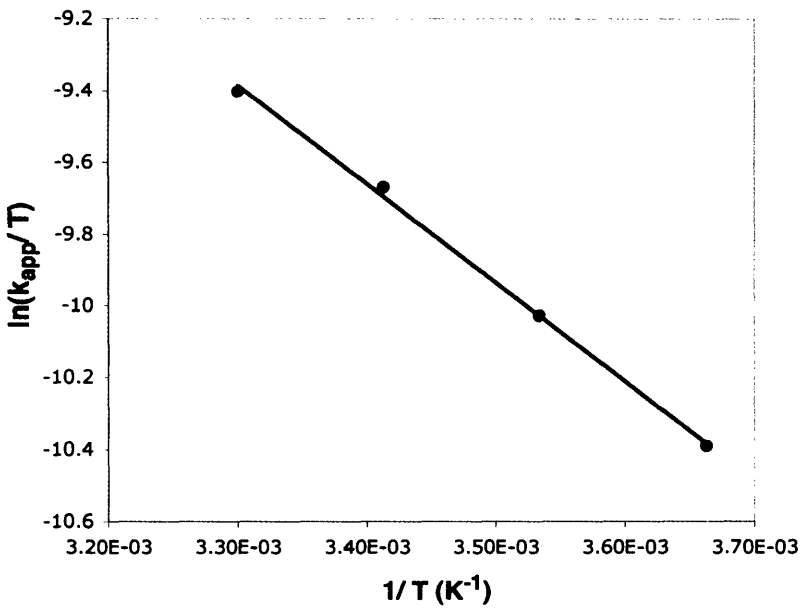

Figure 18. Eyring plot for the *N*-arylation of **9** (52 mM) with **1** (52 mM) in 1 mL of toluene from 0 – 30 °C.

Table 3. Activation Parameters for the Stoichiometric *N*-Arylation of (1,2-Diamine)Cu(I) Amidate (**9**).

$\Delta H^{\ddagger}$	$\Delta S^{\ddagger}$	$\Delta G^{\ddagger}$ at 20 °C
5.5 ± 0.5 kcal•mol $^{-1}$	– 46.6 ± 1.7 eu	19.5 ± 0.6 kcal•mol^{-1}

A series of *para*-substituted aryl iodides, X–C_6H_4I (X = OMe, H, Cl, COMe, CN) were used to investigate electronic effect on the *N*-arylation of **9**. As shown in Figure 19, a linear Hammett plot is obtained, which indicates that electron-deficient aryl iodides enhance the rate at which the aryl iodide activation occurs ($\rho = +0.55 \pm 0.05$). This result is similar to that obtained from the catalytic process.

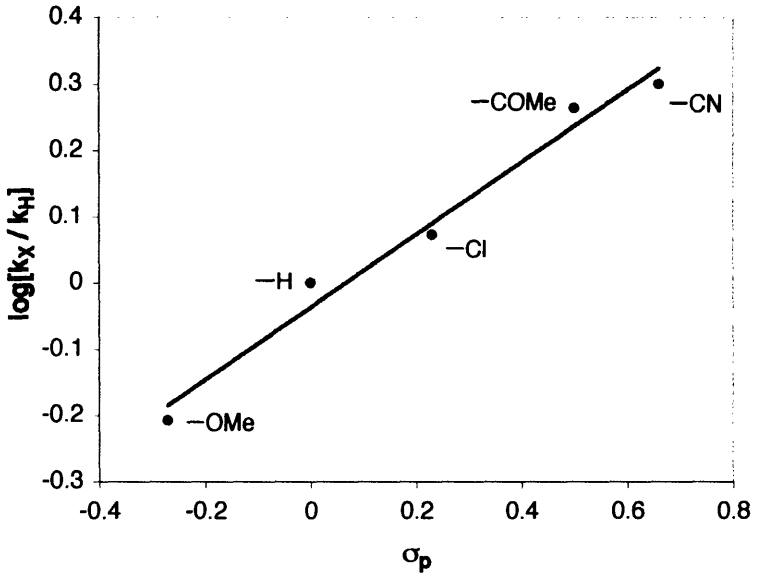

Figure 19. Hammett plot derived from the second-order rate constant, k_{app}, obtained from the *N*-arylation of (1,2-diamine)Cu(I) amidate (**9**) with a series of *para*-substituted aryl iodides. Conditions: [**9**] = 52 mM, [aryl iodide] = 52 mM, 1 mL of toluene, 20 °C.

Discussion

Scheme 2. Simplified Catalytic Cycle Displaying the Two-Stage Cu(I)-Catalyzed *N*-Arylation Process.

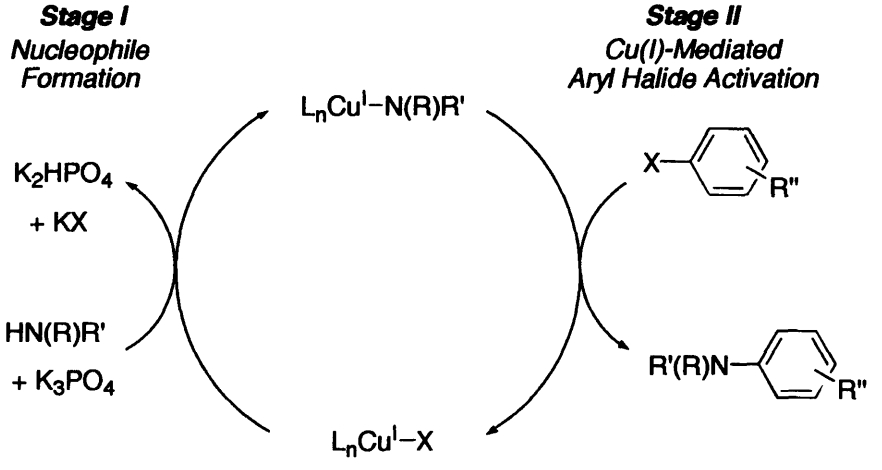

Catalytic Mechanism: Overview. The Cu(I)-catalyzed C-N bond-forming reaction between *N*-nucleophiles and aryl halides proceeds by a Cu(I)-mediated nucleophilic aromatic substitution type mechanism in which the aryl halide activation and the nucleophile formation

occur in two independent, sequential stages (Scheme 2). Consistent with this proposal, Cu(I) amidates promote the kinetically competent stoichiometric *N*-arylation. To our knowledge, this is the first time a discrete Cu(I) amidate has been characterized both chemically and kinetically in the context of the catalytic reaction.[40]

Kinetic studies on the catalytic *N*-arylation of amides using the Cu(I)/1,2-diamine catalyst system reveal a positive-order rate dependence on aryl iodide concentration under conditions where the rate dependence on [amide] and [1,2-diamine] are changing, i.e., the studies carried out at high and low [1,2-diamine]. These results suggest that the Cu(I)-mediated aryl halide activation step (Stage II, Scheme 2) occurs, under all circumstances, on or before the turnover limiting process. Moreover, the linear Hammett plot obtained under the changing dependencies on [amide] and [1,2-diamine] further substantiate this proposal.

Evidence pinpointing a single mechanism for the Cu(I)-mediated aryl halide activation step (Stage II, Scheme 2) is relatively scarce. Previous research concerning the mechanism of the Ullmann C-N bond-forming reaction has suggested that the aryl halide activation step occurs through an oxidative addition process where the redox chemistry takes place between either a Cu(III)/Cu(I) couple or a sequential electron-transfer process involving all three oxidation states of copper, i.e., Cu(I), Cu(II) and Cu(II) (Scheme 3).[2] Additionally, there are two plausible mechanisms for the inner-sphere electron transfer involving the Cu(II)/Cu(I) couple. The first involves a radical anion intermediate which forms without atom-transfer to Cu(II) prior to C-N bond formation, i.e., a $S_{RN}1$-type mechanism,[41] while the second involves an aryl radical which forms upon oxidation of Cu(I) to Cu(II) with concurrent atom-transfer (Scheme 3). All of these postulates originate from the pioneering work of Kochi,[42] Whitesides,[43] Johnson,[44] and Cohen[45] through their mechanistic investigations on alkyl radical additions to Cu(II), Ullmann C-C

coupling, halogen-exchange, and organocuprate nucleophilic substitutions. A consensus on a single pathway for the Cu(I)-mediated activation and subsequent reactions of alkyl and aryl halides with copper in its various oxidation states, however, has not been established.

Scheme 3. Mechanisms for the Cu(I)-Mediated Aryl Halide Activation Step.

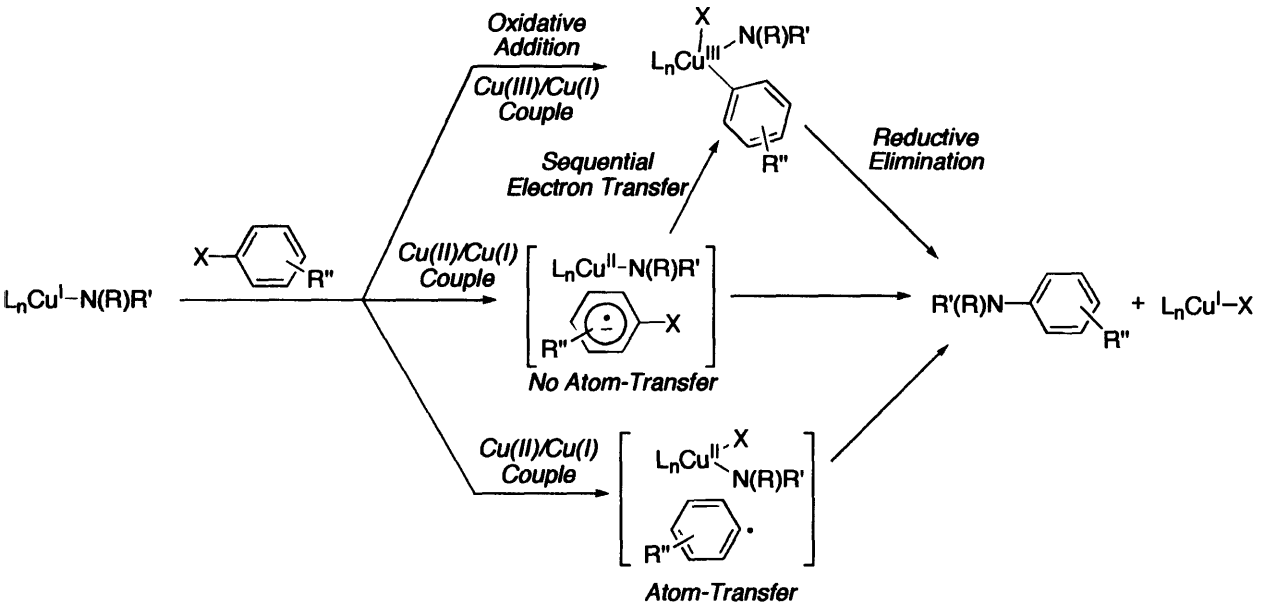

With regard to the mode of aryl halide activation during the Cu(I)-mediated C-N bond-forming reaction, the situation is not much different from that described above. Hida and coworkers have provided the most substantial evidence supporting a single pathway for aryl halide activation during C-N bond-forming reaction.[46] More specifically, while studying the Ullmann condensation reaction of haloanthraquinone derivatives with 2-aminoethanol the initial Cu(I) species was oxidized to a Cu(II) species with the concomitant formation of a 1-bromoanthraquinone radical anion, which was observed by EPR spectroscopy (Scheme 4). Indeed, this result supports an aryl halide activation process involving a Cu(II)/Cu(I) redox couple, but unfortunately due to the rate of subsequent steps the intermediacy of a Cu(III) species could not be established. Nonetheless, this was the first time the formation of an organic radical

was observed as a result of the oxidation of Cu(I) to Cu(II). In contrast, Bethell has suggested that a Cu(III) intermediate is formed during the coupling reaction between 1-halogenoanthraquinones and primary amines (Scheme 5).[47] This proposal was based on the

Scheme 4. Observation of a Radical Anion during the Cu(I)-Mediated Aryl Halide Activation.

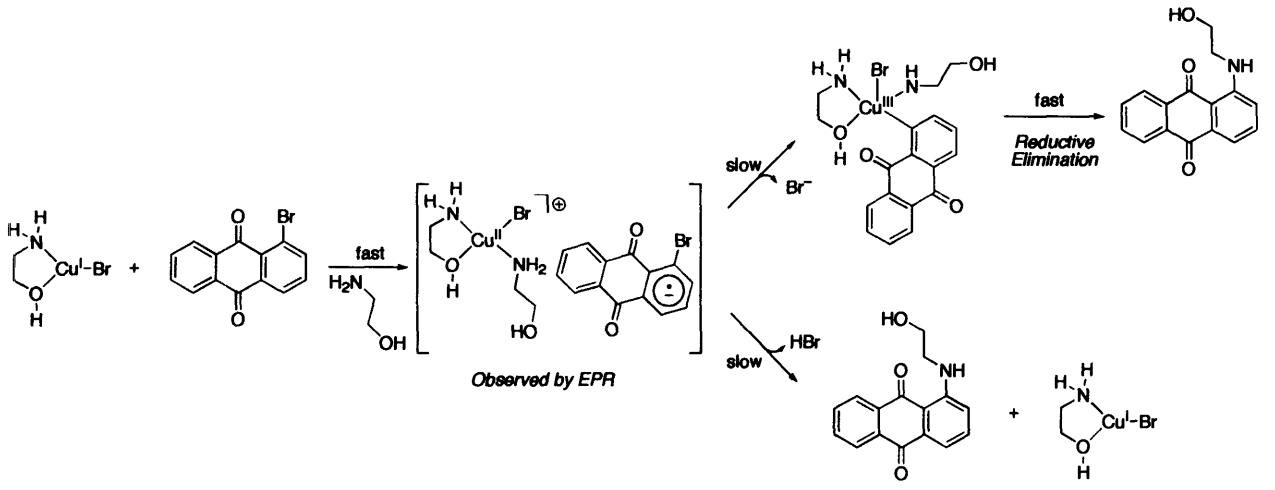

Scheme 5. The Partitioning of a Common Intermediate during the Cu(I)-Mediated Aryl Halide Activation.

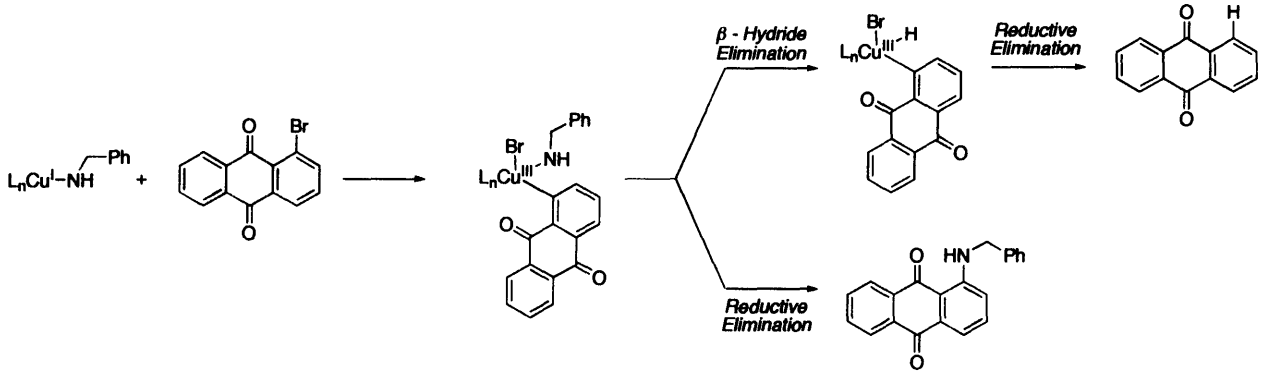

following observations: 1) the reactivity order for the 1-halogenoanthraquinones follows I > Br >> Cl, while the ratio of products, i.e., amination: hydrodehalogenated, is independent of which 1-halogenoanthraquinone is used, and 2) the presence of a product isotope effect in the absence of a kinetic isotope effect. The product isotope effect was thought to occur through a β-hydride

elimination pathway as shown in Scheme 5. These observations can also be explained, however, on the basis of Hida's results which demonstrate that the Cu(II)-radical anion complex can serve as a common intermediate during the partitioning into amination and hydrodehalogenated products. Specifically, the product isotope effect in Bethell's studies can arise from the preference for α-hydride over α-deuteride abstraction from the α-position of the amine. This would generate a more stable highly substituted radical, over α-deuteride abstraction.

Considering the present mechanistic studies on the stoichiometric *N*-arylation of the Cu (I) amidate, a well-defined pathway for aryl iodide activation cannot be resolved. However, the activation parameters in addition to the ρ – value ($\rho = +0.55 \pm 0.05$) are consistent with an aryl iodide activation process similar to that demonstrated in Hida's work (Scheme 6). In this case, the rate-determining step is the generation of the Cu(II)-radical anion species. The relatively low $\Delta H^{\ddagger}$, which is 5.5 ± 0.5 kcal•mol^{-1}, is congruent with a process involving very little bond cleavage in the transition state of the rate-determining step. Furthermore, the large negative value obtained for $\Delta S^{\ddagger}$, which was measured to be –46.6 ± 1.7 eu, suggests that a bimolecular process occurs. Taken together, these data are consistent with a route involving aryl iodide coordination to the Cu(I) amidate, a process facilitated by electron-donating groups in the *para*-position of the aryl iodide,[48] followed by a single-electron transfer from Cu(I) to the aryl iodide generating a Cu(II) species in addition to a radical anion without considerable changes in bonding. Electron-deficient groups in the para-position of the aryl iodide facilitate the latter process.

Scheme 6. Proposed Mechanism for the Cu(I) Amidate Promoted Aryl Iodide Activation.

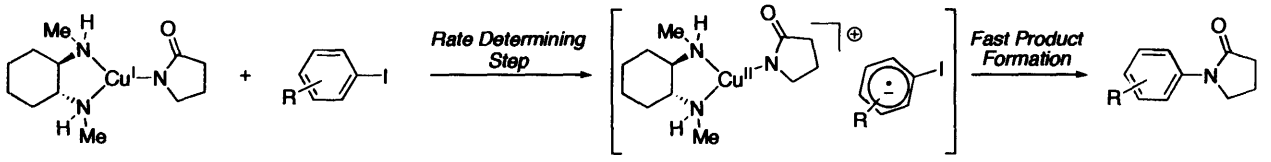

It has been assumed during this evaluation that the 1,2-diamine, like the amino alcohol substrate used in Hida's work, facilitates aryl halide activation by stabilizing the Cu(II) oxidation state, i.e., shifting the redox potential of the Cu(II)/Cu(I) couple cathodically.[49] This principle has been applied to a number of recently developed Cu(I)-based catalysts. For example, Meyerstein and coworkers while developing catalysts for the Ullmann synthesis of phenols have also employed this premise.[50] Specifically, while using the Cu(I)-catalyst **10**, they observed a cathodic shift in redox potential for the Cu(II)/Cu(I) couple relative to the Cu(II)/Cu(I) aqueous couple. The increased activity of catalysts such as **10** was thus associated with these findings. Since this principle seems to be consistent for the Cu(I)-catalyzed *N*-arylations as well, it is imperative for the future development of catalysts to focus on those ligands that indeed favor the cathodic shift in Cu(II)/Cu(I) couple. This is especially relevant on the basis that aryl halide activation serves as the turnover-limiting step in this chemistry (Stage II, Scheme 3). In addition, determining the role of the ligand in the other catalytic steps will also facilitate the development of more active catalysts.

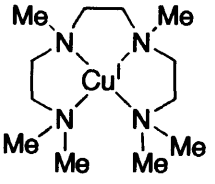

10

Scheme 7. Proposed Mechanism for the Cu(I)-Catalyzed *N*-Arylation of Amides.

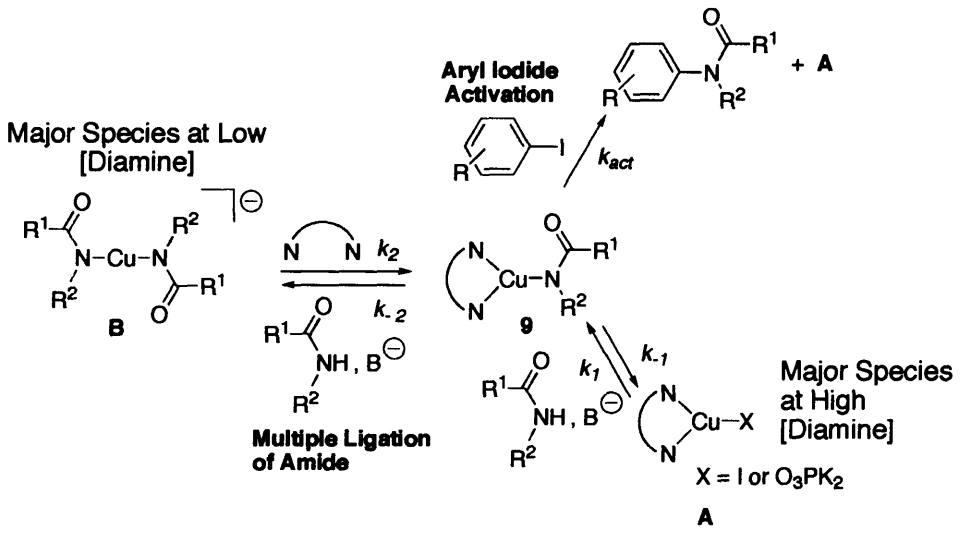

Catalytic Mechanism: Controlling the Resting State of the Catalyst with the 1,2-Diamine Ligand. The kinetic results on the catalytic system provide specific insights into the mechanism of the Cu(I)-catalyzed *N*-arylation of amides with aryl iodides. The nonlinear rate dependence on [1,2-diamine] (Figure 4) implicates a complex process involving multiple equilibria. Specifically, in the absence of saturation in [**3**] due to the increase in solubility of copper as well as catalyst decomposition, the other alternative resides in the prevention of multiple ligation of the amide at high [**3**], which would lead to an inactive copper species. This proposal is supported by the observation that there exists a direct correlation between the reaction rate dependence on [**3**] and that on [amide]. More specifically, at low [**3**] the reaction rate is inhibited by increasing [amide], while at high [**3**] the reaction rate increases with increasing [amide] (Figure 6). The mechanism shown in Scheme 7 proposes that the intermediate Cu(I) amidate (**9**) is formed either through amide coordination to **A** followed by

deprotonation or through 1,2-diamine association and subsequent amide dissociation from **B**. Once formed, **9** reacts with the aryl iodide, affording the desired *N*-arylated amide.

The corresponding rate expression for the mechanism in Scheme 7 is given by eq 20. The derivation of eq 20 is provided in eq 14 – 19. Quasi-equilibria are assumed for $K_1 = k_1 / k_{-1}$ and $K_2 = k_2 / k_{-2}$ on the basis that aryl iodide activation serves as the turnover-limiting step at both high and low [**3**]. Overall, eq 20 is consistent with the kinetic data shown in Figure 4, showing saturation kinetics in [**3**] with all other concentrations held constant.

$$\text{rate} = k_{act}[\text{Cu-amidate}][\text{ArI}] \tag{14}$$

$$[\text{Cu}]_{total} = [\text{Cuprate}] + [\text{Diamine-Cu}] + [\text{Cu-amidate}] \tag{15}$$

$$K_1 = \frac{[\text{Cu-amidate}]}{[\text{Diamine-Cu}][\text{Amide}]} \Longrightarrow [\text{Diamine-Cu}] = \frac{[\text{Cu-amidate}]}{K_1\,[\text{Amide}]} \tag{16}$$

$$K_2 = \frac{[\text{Cu-amidate}][\text{Amide}]}{[\text{Cuprate}][\text{Diamine}]} \Longrightarrow [\text{Cuprate}] = \frac{[\text{Cu-amidate}][\text{Amide}]}{K_2[\text{Diamine}]} \tag{17}$$

$$[\text{Cu}]_t = \frac{[\text{Cu-amidate}][\text{Amide}]}{K_2[\text{Diamine}]} + \frac{[\text{Cu-amidate}]}{K_1\,[\text{Amide}]} + [\text{Cu-amidate}] \tag{18}$$

$$[\text{Cu}]_t = [\text{Cu-amidate}]\left(\frac{K_1[\text{Amide}]^2 + K_2[\text{Diamine}] + K_1K_2[\text{Amide}][\text{Diamine}]}{K_1K_2[\text{Diamine}][\text{Amide}]}\right) \tag{19}$$

$$\textit{rate} = \frac{k_{act}K_1K_2[\text{Cu}]_t[\text{ArI}][\text{Diamine}][\text{Amide}]}{K_1[\text{Amide}]^2 + K_2[\text{Diamine}] + K_1K_2[\text{Amide}][\text{Diamine}]} \tag{20}$$

Evaluating the kinetic dependence on [amide] provides additional support for the kinetic model in the form of limiting cases of the rate expression given in eq 20. Specifically, the first-

order rate dependence on 1,2-diamine concentration at low [**3**] suggests that under these conditions the resting state of the catalyst is the multiply amide-ligated species **B** (Scheme 7). Increasing the concentrations of the 1,2-diamine **3** or **4** drives the reaction back to intermediate **9** in equilibrium with **A**. Thus, increasing concentrations of 1,2-diamine increases the reaction rate, while increasing amide concentrations should suppress it. This results in the limiting case of the rate expression of eq 20 shown in eqs 21 and 22. The straight-line relationship between the function rate/[ArI] and 1/[Amide] provided by eq 22 is borne out in Figure 20, where three experiments performed at different [amide] converge into the same straight-line relationship with slope equal to K'. These data confirm the inverse dependence on [amide] at low [**3**]. By contrast, under conditions of high [**3**], Figure 21 reveals that a straight-line relationship is observed between the function rate/[Amide] versus [ArI], suggesting the limiting form of eq 20 shown in eqs 23 and 24. This implies that, under high [**3**], the situation holds where K_1 [Amide] << 1 and the resting state of the catalyst shifts to species **A** (Scheme 7), affording first-order kinetics in both [ArI] and [Amide] and zero-order kinetics in added [**3**]. The difference between the catalyst system based on **4** (Figure 4) which provides a larger k_{cat} using the Michaelis-Menten model for saturation (Table 1) and that based on **3**, thus, resides in the value of k_{act} K_1 $[Cu]_t$. Since there does not exist a difference in k_{act} between the two catalyst systems as evidenced by the nearly identical k_{app} and $\Delta G^{\ddagger}$ obtained from the stoichiometric *N*-arylation of Cu(I) amidates based on **3** and **4**, the value for K_1 must be the discriminating factor between the two.

***At Low [1,2-Diamine]*:**

$$rate = \frac{k_{act}K_2[Cu]_t[ArI][Diamine]}{[Amide]} \quad (21)$$

$$\text{or} \quad \frac{rate}{[ArI]} = K' \cdot \frac{1}{[Amide]} \quad \text{Where } K' = k_{act}K_2[Cu]_t[Diamine] \quad (22)$$

***At High [1,2-Diamine]*:**

$$rate = \frac{k_{act}K_1[Cu]_t[ArI][Amide]}{1 + K_1[Amide]} \quad (23)$$

$$\text{or} \quad \frac{rate}{[Amide]} = K'' \cdot [ArI] \quad \text{Where } K'' = k_{act}K_1[Cu]_t \quad (24)$$

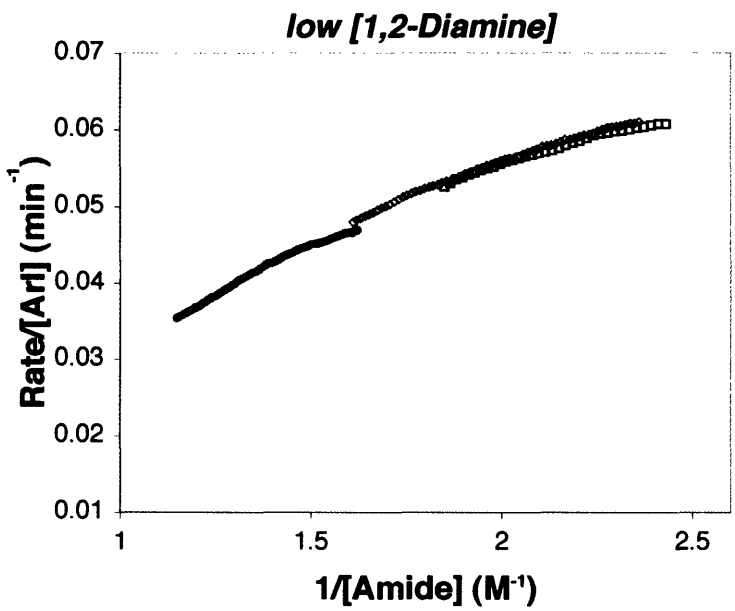

Figure 20. Reaction rate dependence on [amide] at low [**3**]. The linear relationship between rate/[ArI] and 1/[Amide] is shown based on eq 22. Conditions: low [**3**] (10 mol % **3**, 5 mol % CuI) $[\mathbf{1}]_o = 0.4$ M, (o) $[\mathbf{2}]_o = 0.9$ M, (◊) $[\mathbf{2}]_o = 0.7$ M, (□) $[\mathbf{2}]_o = 0.6$ M.

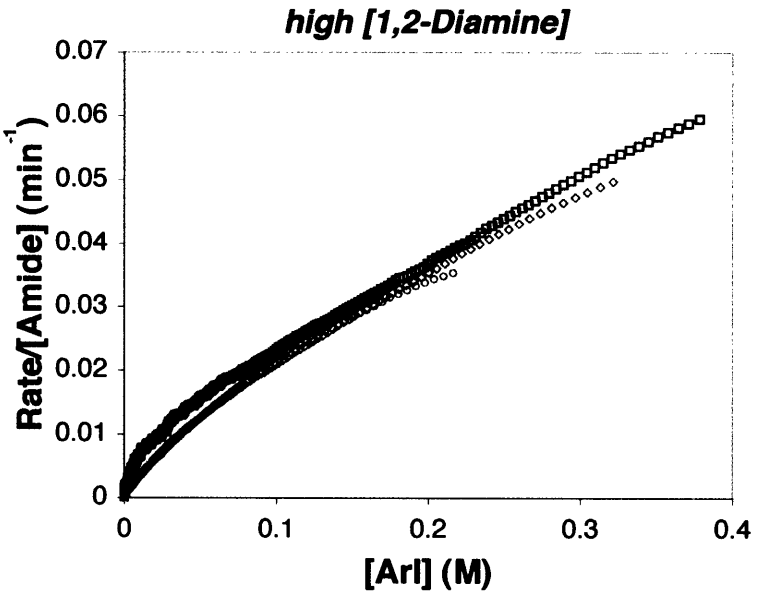

Figure 21. Reaction rate dependence on [amide] at high [**3**]. The linear relationship between rate/[Amide] and [ArI] is shown based on eq 24. Conditions: high [**3**] (70 mol % **3**, 5 mol % CuI). Reaction conditions: (o) $[\mathbf{2}]_o = 0.9$ M, $[\mathbf{1}]_o = 0.4$ M, (◊) $[\mathbf{2}]_o = 1.0$ M, $[\mathbf{1}]_o = 0.6$ M, (□) $[\mathbf{2}]_o = 0.7$, $[\mathbf{1}]_o = 0.6$ M.

$$\frac{K'}{K''} = \frac{k_{act}K_2[Cu]_t[Diamine]}{k_{act}K_1[Cu]_t} = \frac{K_2[Diamine]}{K_1} \qquad (25)$$

$$\frac{K_2}{K_1} = \frac{K'}{K'' \cdot [Diamine]} \qquad (26)$$

To establish a relationship between the catalytic reaction mechanism in Scheme 7 and the stoichiometric *N*-arylation of the Cu(I) amidate, the kinetic data from the stoichiometric process was extrapolated to 90 °C. Using the Eyring plot shown in Figure 18, a value for k_{app} at 90 °C is calculated to be 0.14 ± 0.02 $M^{-1} \cdot s^{-1}$. Applying this value for k_{app} to eqs 22 and 24 (both of which are based on the catalytic process) in place of k_{act} affords the equilibrium constants K_1 and K_2 ($K_1 = 5.64 \pm 0.96 \times 10^1$ and $K_2 = 2.29 \pm 0.39 \times 10^2$). Thus, the ratio of K_2/K_1 is 4.07 ± 0.98. Comparing this value to the ratio of K_2/K_1, which is 2.89 ± 0.72, obtained from the slope of the

straight-line relationships in Figures 20 and 21 (eq 26) exemplifies the consistency between the catalytic and stoichiometric *N*-arylation reactions. Although this correlation provides further evidence of the intermediacy of the 1,2-diamine ligated-Cu(I) amidate in the catalytic reaction, the thermodynamic data obtained from K_1 and K_2, i.e., the standard free energy of formation ($\Delta G°_{363}$) for the Cu(I) amidate **9** from **B** and the $\Delta G°_{363}$ for the formation of **9** from **A** (Scheme 7), do not conform to the kinetic studies on the catalytic reaction. For example, $\Delta G°_{363}$ for the Cu(I) amidate **9** from **B**, which is based on K_2, is -3.92 ± 0.11 kcal•mol^{-1} and the $\Delta G°_{363}$ for the formation of **9** from **A**, which is based on K_1, is -2.91 ± 0.11 kcal•mol^{-1}. Both of these results indicate that **9** resides at a lower point along the potential energy surface than either **B** or **A** (Figure 22). While in contrast, the kinetic studies on the catalytic reaction suggest that both **B** and **A** are lower in energy than **9** since the results indicate that the former two species serve as the catalyst resting state under either low or high [1,2-diamine] (Figure 23).

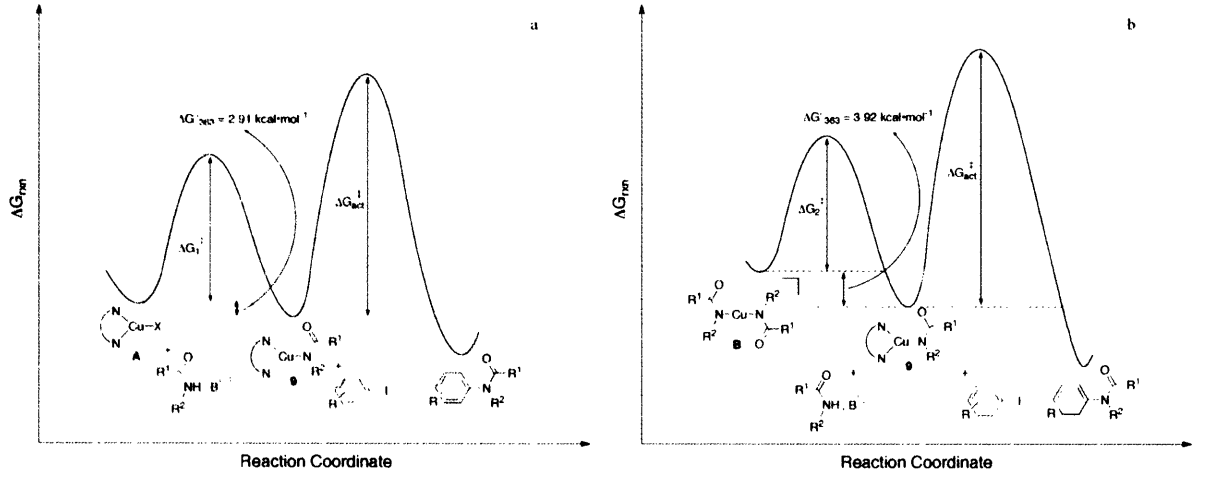

Figure 22. Reaction coordinate diagrams for the *N*-arylation of Cu(I) amidate **9** from **A** (a) and **B** (b), based on the application of the stoichiometric *N*-arylation of **9** to the kinetic model from the catalytic system.

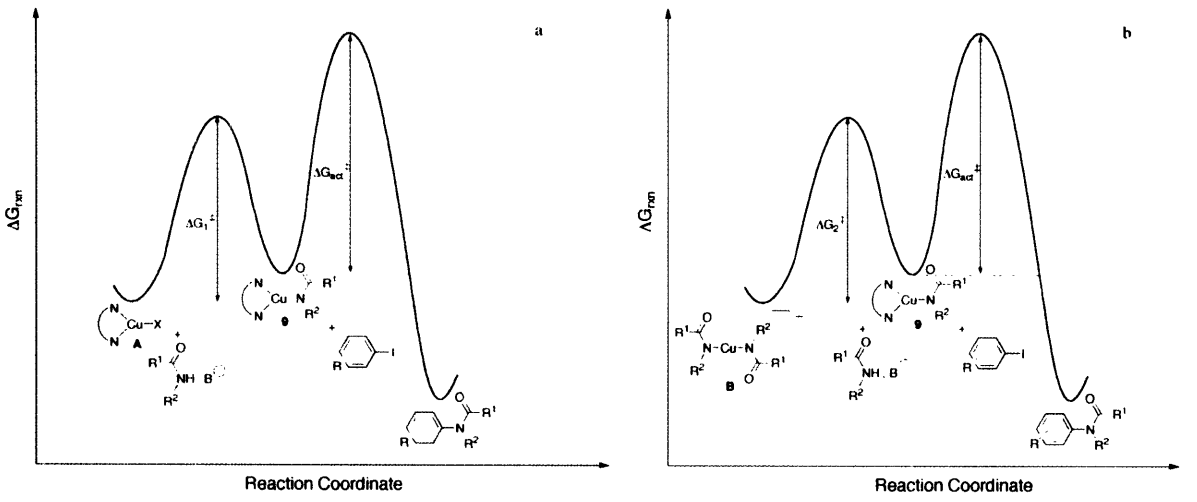

Figure 23. Reaction coordinate diagrams for the *N*-arylation of Cu(I) amidate **9** from **A** (a) and **B** (b), based on the kinetics of the catalytic system.

Although the origins of the discrepancy between the thermodynamic data obtained from the stoichiometric *N*-arylation of Cu(I) amidate **9** and the kinetics on the catalytic system are unknown, the results from the catalytic system are consistent with what would be predicted on the basis of hard soft acid base theory (HSAB).[51] Typically, the soft Cu(I) ion prefers softer ligands such as amides and heterocycles relative to amines and 1,2-diamines, which are harder ligands. Validation of the HSAB theory in the context of Cu(I) was recently provided by Kebarle's studies on the dissociation free energies $\Delta G°$ for the reactions $CuL_2^+ = Cu^+ + 2L$ based on the measured free energies for exchange reactions $CuA_2^+ + 2B = CuB_2^+ + 2A$.[52] Specifically, Kebarle demonstrated that 12.6 kcal•mol^{-1} is required for the dissociation of MeCONHMe relative to the 5.9 kcal•mol^{-1} required for the dissociation of NH_3. The absolute hardness η of a series of amides have not been established, however, it is expected that they exhibit similar characteristics to $HCONH_2$ and DMF, which have η values of 6.1 and 5.8, respectively. Indeed, comparing these η values to those obtained from various amines, e.g., NH_3 (η = 8.2), CH_3NH_2 (η

= 7.2), and $(CH_3)_3N$ ($\eta = 6.3$), provided a correlation between absolute hardness η and the relative binding affinities of various ligands to Cu(I).

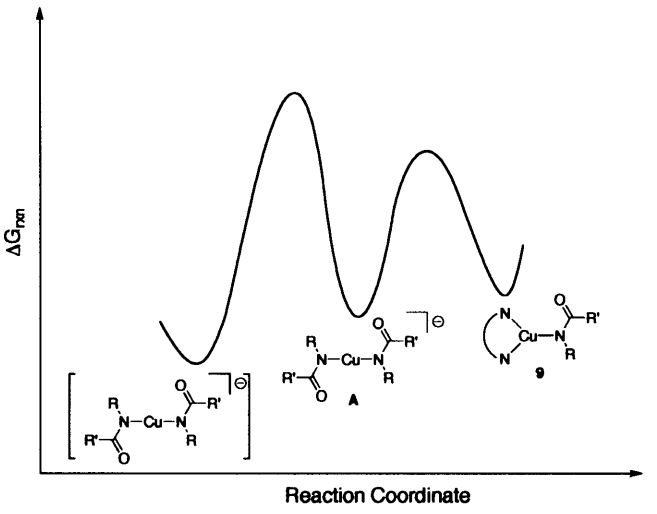

Figure 22. Reaction coordinate diagram demonstrating the kinetic versus thermodynamic control over copper speciation.

Insights into the Origin of the Induction Period. Attempts to glean further information regarding the speciation of Cu(I) in the catalytic reaction revolved around the presence of an induction period. In response to the evidence in support of the kinetic model, it was proposed that premixing the Cu(I)/**3** catalyst system at low [**3**] with the amide and base prior to the introduction of the aryl halide would result in an oligomer of the cuprate species (Scheme 1) which was more thermodynamically stable than either the monomeric cuprate species **A** or the Cu(I) amidate **9**. A description of this process is shown in the reaction coordinate diagram in Figure 24. The 1,2-diamine-ligated Cu(I) amidate is initially formed due to its lower activation barrier for formation, however, over time the Cu speciation begins to change due to the thermodynamic stability of a multiply-ligated cuprate-like species. According to this hypothesis, allowing the Cu(I)-catalyst to incubate with the amide and base for extended periods of time

should favor the formation of the latter species and induce an induction period. As indicated in Figure 10a, an induction period that is dependent on the amount of premixing time between the catalyst, amide, and base is indeed observed; where longer premixing times lengthen the induction period. The reversibility of these events was then established by observing that an increase in [**3**] results in shorter induction periods even at extended premixing times (Figure 10b). At a **3**:Cu ratio of 4:1 the reaction has little, if any, induction period. These observations are also consistent with the proposed role of the 1,2-diamine in preventing multiple ligation of the amide. It is important to point out that the induction periods deviate slightly from the sigmoidal shape that would be expected from a typical induction period. Although, it is not well understand what brings about this obscure behavior, e.g., this could be attributed to the physical and not the chemical characteristics of the oligomerized cuprate species, a similar phenomenon has been previously observed.

Both Hida and Bethell have also detected an extensive induction period during their mechanistic investigations into the *N*-arylation of amines with haloanthraquinone derivatives.[46,47,53] While in the case of Bethell's work where the induction period is a result of the formation of Cu(II) from an oxygenated solution of Cu(I) and amine, Hida has alternatively suggested that the induction period is terminated by the presence of Cu(II). The latter proposal is based on the observation that the addition of $CuBr_2$ to the Cu(I) catalyst system increases the activity of the catalyst. Similar to the Cu(I)/**3** catalyst system presented here, increasing the amount of amino alcohol, which is the substrate in Hida's work, also leads to an attenuation of the induction period. However, the effect of the increasing [amino alcohol] on the induction period was attributed to the formation of Cu(II), which was observed by EPR with increasing intensity upon increasing [amino alcohol]. This led to the proposal that Cu(II) promotes the *N*-

arylation of 2-amino ethanol through the reaction in eq 27, where a Cu(I) haloanthraquinone complex reacts with a Cu(II) amino alcohol species providing the *N*-arylated product. In the present work, however, no EPR signal corresponding to the presence of a Cu(II) species was observed during the induction period even at high [1,2-diamine].

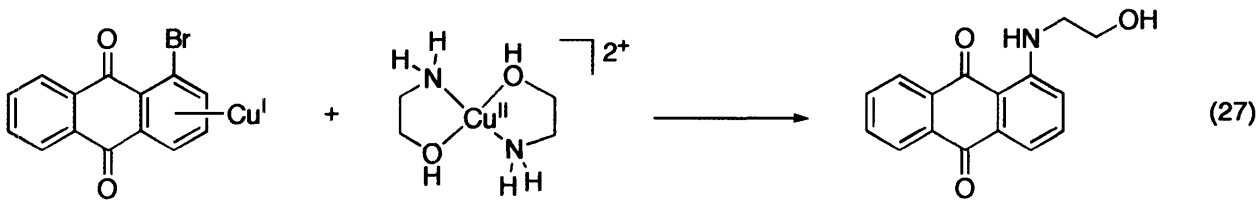

(27)

Similar to Hida's work, an induction period was not observed while premixing the Cu(II)/**3** catalyst system with the amide and base prior to the introduction of the aryl iodide (Figure 11 and Table 2). Furthermore, the addition of $CuBr_2$ to the Cu(I)/**3** catalyst system while maintaining a constant total concentration of copper also reduces the length of the induction period. Thus, the question still remains as to what role the Cu(II) serves in preventing the induction period. Turning to the variable premixing time studies between the Cu(II)/**3** precatalyst with the amide and base (Figure 12) as well as the decrease in Cu(II) signal intensity, as measured by EPR, with extended mixing times with the amide and base (Figure 14) it is evident that Cu(II) is not an active catalytic species. Instead, mixing the amide and base with Cu(II) results in the reduction of Cu(II) to Cu(I) through the formation of an amide or diamine radical (Figure 15 and Scheme 8). This process is supported by the observation of a ^{14}N-centered radical by EPR. A similar ^{14}N-centered radical was also observed during the reduction of Cu(II) to Cu(I) in a bis-(–)-ephedrine Cu(II) complex.[54] Thus, it is unlikely that the concentration of Cu(II) builds up during the course of the induction period, since the results presented here indicate that Cu(II) is reduced to Cu(I) under the reaction conditions. However, if a low

concentration of Cu(II) is maintained through the disproportionation of Cu(I) during the induction period or during the process of premixing the Cu(I)/**3** catalyst system with the amide and base, the Cu(II) may prevent the formation of the oligomeric species which may cause the induction period to occur. This possibility is evidenced by the absence of an induction period while allowing the Cu(II)/**3** catalyst system to premix with the amide and base prior to the addition of the aryl iodide to the reaction mixture. Since Cu(II) exhibits a greater affinity toward chelating ligands as indicated by the differences in equilibrum constants for the disproportionation reaction of Cu(I), i.e., 2Cu(I) = Cu(II) + Cu(0), based on metal complexes with ethylenediamine ($K = 10^5$), pentane-1,5-diamine ($K = 3 \times 10^{-2}$), and ammonia ($K = 2 \times 10^{-2}$), multiple ligation of the amide to the precatalyst may be avoided.[26] Although Cu(II) may not have a direct role in the induction periods observed with the Cu(I)/**3** catalyst system, the use of Cu(II) instead of Cu(I) is important in the sense that Cu(II) has the ability to control the amount of Cu(I) that is generated, thus avoiding the potential formation of oligomeric Cu(I) species. This is especially pertinent with *N*-based substrates that are more nucleophilic toward Cu(I).

Scheme 8. Reduction of Cu(II)/1,2-Diamine Complex to Cu(I)/1,2-Diamine in the Presence of Amide and Base.

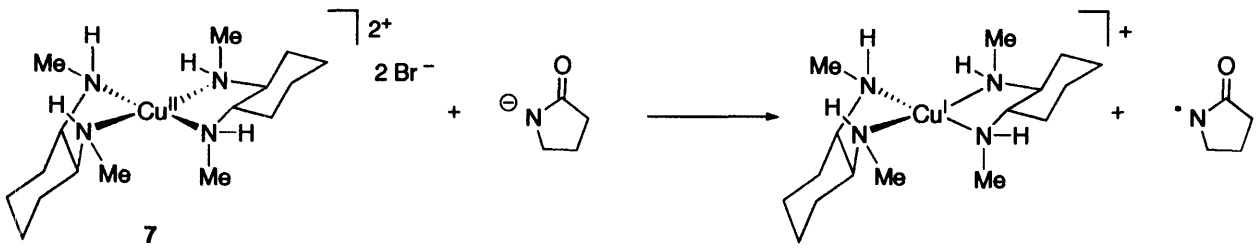

7

Summary

The Cu(I)/1,2-diamine catalyst system has been applied to a variety of *N*-arylation reactions as well as halogen-exchange reactions and this mechanistic study on the *N*-arylation of 2-pyrrolidinone with aryl iodides provides insights into the factors that control catalyst activity. We have, for the first time, complemented the kinetic study of a Cu(I)-catalyzed Goldberg reaction with the direct *N*-arylation of a Cu(I) amidate. Such data facilitated the elucidation of the detailed mechanism of Cu(I)-nucleophile formation and also revealed the intricacies involved in multiple ligation of the *N*-based nucleophile to the Cu(I) catalyst. In particular, the nonlinear rate dependence on the [1,2-diamine] highlighted the role of the 1,2-diamine in establishing a high concentration of active catalyst throughout the course of the reaction. Furthermore, initial insights into the mechanism of aryl iodide activation were gleaned. This study also sheds light on the role of Cu(II) in the catalytic system. The preference for Cu(II) to bind to chelating ligands such as 1,2-diamines in relation to amides provides an additional pathway for avoiding the formation of an inactive multiply-ligated Cu(I) species.

Experimental Section

Reagents: Copper(I) iodide (fine grey powder) was purchased from Strem Chemicals and stored in an amber vial in a dessicator. Racemic *trans*-1,2-cyclohexanediamine was purchased from Aldrich. The quality of the inorganic base K_3PO_4 is quite important. Reproducible results were obtained with K_3PO_4 available from Fluka (catalog number 04347, Riedel-de Haën product; free-flowing, fine granule of uniform size) and dried under high vacuum at 150 °C for 3 days. The dried K_3PO_4 was then stored in a nitrogen-filled glovebox. It is important to note that the particle size of K_3PO_4 is critical for reproducible kinetics, i.e., using K_3PO_4 purchased from Alfa Aesar or Aldrich (both of variable size ranging from fine powder to large chunks) led to irreproducible

kinetics and in some instances complete inhibition of the reaction. 2-Pyrrolidinone (**2**) was purchased from Aldrich and distilled over 4 Å molecular sieves prior to its use. 3,5-dimethyliodobenzene (**1**) was also purchased from Aldrich and distilled from CaH_2 prior to its use. Toluene was purchased from J.T. Baker in CYCLE-TAINER solvent delivery kegs, was vigorously purged with argon for 2 h, and then purified by passing through two packed columns of neutral alumina under argon pressure. All reagents with the exception of copper(I) iodide were stored and weighed out inside a nitrogen-filled glovebox.

Analytical methods: ^1H NMR and ^{13}C NMR were recorded on either a Varian 500 MHz Fourier transform NMR spectrometer with chemical shifts reported with respect to residual deuterated solvent peaks. Kinetics experiments were performed in an Omnical SuperCRC reaction calorimeter.

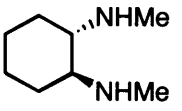

Preparation of racemic *trans-N,N'*-dimethyl-1,2-cyclohexanediamine (3). A procedure reported by Betschart et al. was adapted with small modifications.[55] A solution of racemic *trans*-1,2-cyclohexanediamine (10.0 mL, 0.041 mmol) in ethyl formate (50 mL, 0.25 mmol) was heated at 50 °C for 8 h. The resulting thick, white suspension was allowed to reach room temperature and then was filtered. The filter cake was washed with ethyl acetate (80 mL) and the solid was dried under vacuum to give 5.38 g (77% yield) of *trans-N,N'*-diformyl-1,2-cyclohexanediamine.

A 500 mL three-necked-round bottom flask equipped with a large Teflon-coated stirbar, reflux condenser, and gas inlet was charged with $LiAlH_4$ (8.8 g, 0.23 moles) and purged with argon. THF (250 mL) was added and the resulting suspension cooled to 0 °C. *trans-N,N'*-diformyl-1,2-cyclohexanediamine (11.6 g, 68 moles) was added as a solid over 0.5 h (CAUTION: hydrogen gas evolution!). The cooling bath was replaced with an oil bath and the slightly cloudy, colorless solution was heated at 65 °C for 24 h under a slow stream of argon. The resulting white suspension was cooled to 0 °C and then carefully quenched by dropwise addition of water (10 mL; CAUTION: violently exothermic reaction, evolution of hydrogen gas!) followed by a 20% aq NaOH solution (75 mL). The resulting gelatinous suspension was stirred at room temperature for 1 h, mixed with Celite (35 g), and filtered eluting with THF (500 mL). The colorless filtrate was concentrated using a rotary evaporator. The residue was dissolved in a solution of 10% aq HCl (100 mL) in water (100 mL) and the resulting solution was extracted with dichloromethane (3x~200 mL). The aqueous phase was made basic with 20% aq NaOH (100 mL) and extracted with dichloromethane (3x~200 mL). The organic layers were combined, dried (K_2CO_3), and concentrated using a rotary evaporator. The residue was transferred into a 25 mL flask and distilled under vacuum to give 8.0 g (93% yield) of *trans-N,N'*-dimethyl-1,2-cyclohexanediamine as a colorless liquid.

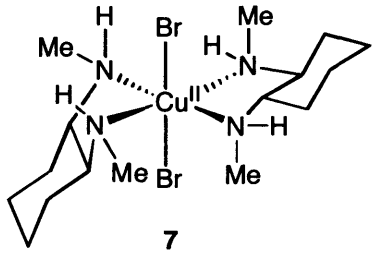

7

Preparation of bis(*N,N'*-dimethyl-1,2-cyclohexanediamine)$CuBr_2$ (7). $CuBr_2$ (2.55 g, 11.4 mmol) was added at ambient temperature to a 250 mL round bottom flask containing MeOH (50 mL). To this solution was added **3** (3.3 g, 23.2 mmol) and the resulting mixture was allowed to stir at room temperature overnight. The mixture was filtered, affording a blue solid, and dried under vacuum. Crystallization from a mixture of $CHCl_3$ and heptanes afforded the product in 87 %. Anal. Calcd (found) for $C_{16}H_{36}Br_2CuN_4$: C, 37.84 (37.78); H, 7.15 (7.09); N, 11.03 (10.91); Br, 31.47 (31.36).

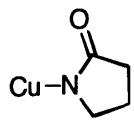

8

Preparation of Copper(I)-pyrrolidinoate (8). 2-pyrrolidinone (**2**) (260 mg, 3.05 mmol) was added at ambient temperature to toluene (10 mL) containing mesitylcopper (500 mg, 2.75 mmol) inside a nitrogen-filled glovebox. The colorless mixture was allowed to stir for 15 minutes at ambient temperature prior to the removal of volatiles under high vacuum. The resulting white solid was washed with hexanes (25 mL) and dried under vacuum affording 350 mg (86 %) of an air-sensitive white solid. Iodometric analysis was performed by dissolving 250 mg in 5 mL of 6N HNO_3 and following the procedure for titration by de la Camp and Seely.[56] ^1H NMR (C_6D_6,

500 MHz) δ 1.58 (br m, 2H), 2.04 (br m, 2H), 3.20 (br m, 2H). ^{13}C NMR (C_6D_6, 125 MHz) δ 25.09, 31.37, 52.83, 185.12.

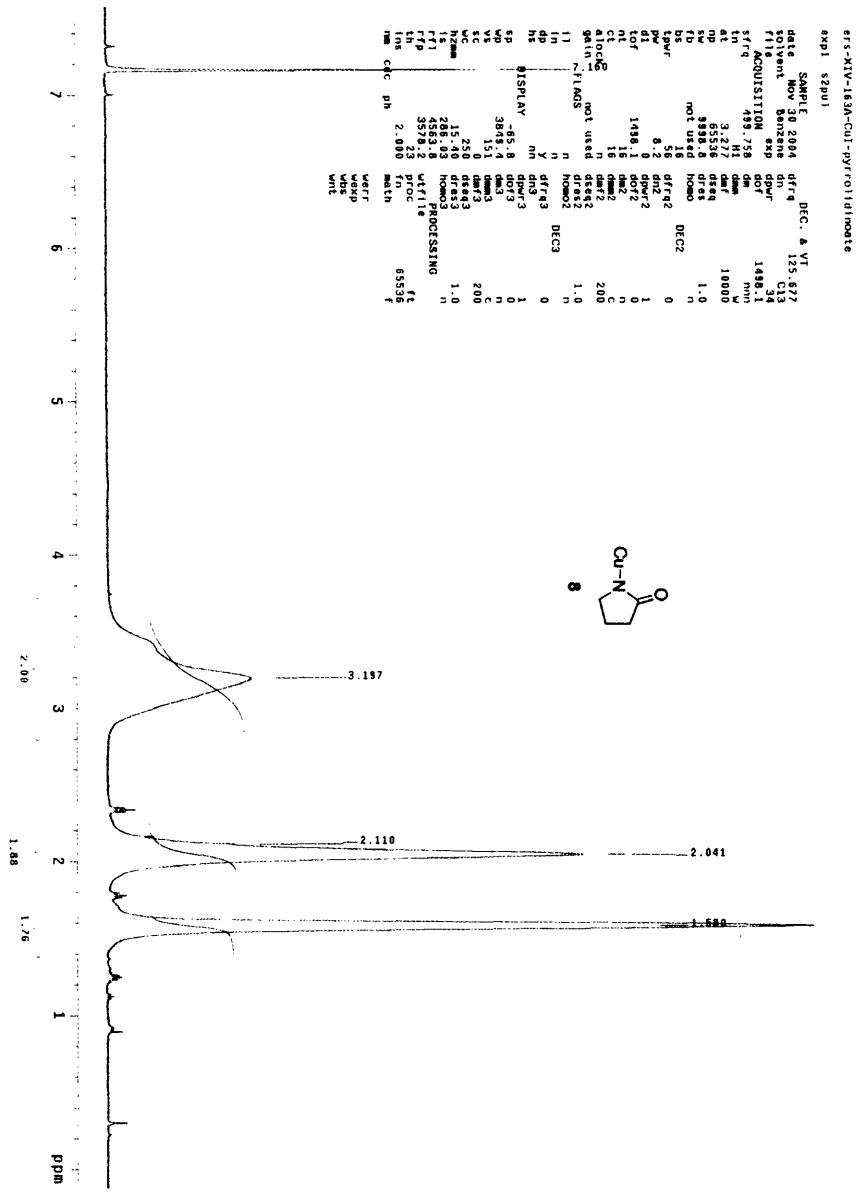

Experimental Procedure for Kinetic Studies Using Reaction Calorimetry. Reactions were performed in an Omnical SuperCRC reaction calorimeter. The instrument contains an internal magnetic stirrer and a differential scanning calorimeter (DSC), which compares the heat released or consumed in a sample vessel to an empty reference vessel. The reaction vessels were 16 mL borosilicate screw-thread vials fit with opentop black phenolic screw caps and white PTFE septa (KimbleBrand) charged with Teflon stir bars. Sample volumes did not exceed 2.5 mL. In a typical calorimetry experiment, a solution of copper iodide and diamine in toluene was added to a reaction vessel containing K_3PO_4, which was placed in the calorimeter and stirred for one hour, allowing the contents of the vessel to reach thermal equilibrium. Simultaneously, a syringe containing 3,5-dimethyliodobenzene and 2-pyrrolidinone was placed in the sample injection port of the calorimeter and was allowed to thermally equilibrate. The reaction was initiated by injecting the mixture of aryl iodide and amide into the stirred catalyst-K_3PO_4 solution. The temperature of the DSC was held constant at 363 K using the internal temperature controller in the calorimeter, ensuring that the reaction would proceed under isothermal conditions. A raw data curve was produced by measuring the heat flow from the sample vessel every fifteen seconds during the reaction. Due to the delay between the instantaneous moment heat is evolved from the reaction vessel and the time the thermophile sensor detects the heat flow, the raw data curve must be calibrated. To accomplish this calibration, a constant amount of current was passed through a resistor in the sample chamber of the calorimeter thereby producing a known quantity of heat. This process results in a response curve, which is then transformed into a square wave allowing for the response time of the instrument to be calculated using the WinCRC software. Application of the response time to the raw data results in a "tau corrected data curve." The tau corrected data curve is a plot of heat flow (mJ s^{-1}) versus time. The reaction rate, which

is directly proportional to the heat flow (eq 1), fraction conversion (eq 2), and instantaneous concentrations of reactants/products can all be calculated from this tau corrected data curve. Conversion measured by GC analysis was compared to conversion measured by heat flow (Figure S1). Agreement between the two methods validates the use of reaction calorimetry to follow the copper-catalyzed amidation of aryl iodides.

$$q = \Delta H_{rxn} \cdot V \cdot r \tag{28}$$

q is the reaction heat flow, ΔH_{rxn} is the heat of reaction, V is the reaction volume, and r is the reaction rate

$$fractional\ conversion = \frac{\int_0^t q \cdot dt}{\int_0^{t_f} q \cdot dt} \tag{29}$$

The numerator represents the area under the heat flow to any time point t and the denominator represents the total area under the heat flow curve.

Monitoring the Decay of Cu(II) Species by EPR. $CuBr_2$ (12.0 mg, 0.054 mmol), **3** (22.3 mg, 0.157 mmol), and K_3PO_4 (320 mg, 1.51 mmol) were added to a 16 mL reaction vessel containing toluene (1 mL) inside a nitrogen-filled glovebox. The vessel was capped with a PTFE septum and opentop screw cap and the vessel was brought outside of the glovebox and placed in an 80 °C oil bath with stirring under a positive flow of argon. Upon equilibrating the reaction mixture at 80 °C for 0.5 h, **2** (110 mg, 1.29 mmol) was added via syringe. Placing the vessel in liquid nitrogen immediately quenched the reaction at each time point. The contents of the vessel were diluted with toluene (1 mL), 0.4 mL was removed and placed in an EPR tube for analysis.

^{1}H NMR experiments with 8. An NMR tube was charged with 1 mL of a solution containing **8** (76 mg, 0.51 mmol) and **3** (76 mg, 0.52 mmol) in toluene-d_8 (5 mL total volume) inside a nitrogen-filled glovebox. The tube was capped with a PTFE septum and opentop screw cap and brought outside of the glovebox and placed in a 500 MHz NMR spectrometer cooled to 273 K. Upon addition of **1** (120 mg, 0.52 mmol) to the NMR tube, data was collected every minute. The concentration of **9** and **5** were determined by integrating relative to ferrocene, which was used as an internal standard in a capillary tube. Likewise, the kinetic studies where [**9**] = [**1**], i.e., *rate* = k_{app}[**9**]^2, was analyzed in an analogous manner.

Figure 23. Representative Kinetics for the Arylation of **9**.

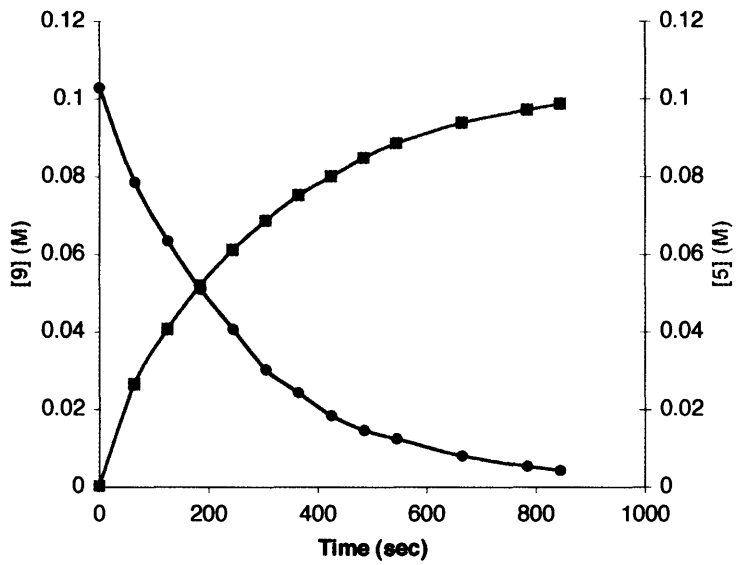

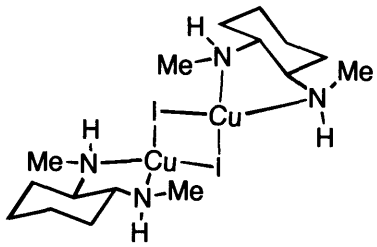

(*R,R,R,R*)-**6**

X-ray Structure Data for (*R,R,R,R*)-*6*

Table 4. Crystal data and structure refinement for **6**.

Identification code	05063t	
Empirical formula	$C_{16}H_{36}Cu_2I_2N_4$	
Formula weight	665.32	
Temperature	100(2) K	
Wavelength	0.71073 Å	
Crystal system	Monoclinic	
Space group	P2(1)	
Unit cell dimensions	a = 8.4715(10) Å	a= 90°.
	b = 7.5995(9) Å	b= 90.054(2)°.
	c = 36.754(4) Å	g = 90°.
Volume	2366.2(5) $Å^3$	
Z	4	
Density (calculated)	1.851 Mg/m^3	
Absorption coefficient	4.412 mm^{-1}	
F(000)	1272	
Crystal size	0.36 x 0.25 x 0.17 mm^3	
Theta range for data collection	0.55 to 28.32°.	
Index ranges	-11<=h<=11, -10<=k<=10, -48<=l<=48	
Reflections collected	46740	
Independent reflections	11686 [R(int) = 0.0337]	
Completeness to theta = 28.32°	99.4 %	
Absorption correction	SADABS	
Refinement method	Full-matrix least-squares on F^2	
Data / restraints / parameters	11686 / 2 / 468	
Goodness-of-fit on F^2	1.301	
Final R indices [I>2sigma(I)]	R1 = 0.0414, wR2 = 0.0962	
R indices (all data)	R1 = 0.0418, wR2 = 0.0963	

Absolute structure parameter	0.09(3)
Largest diff. peak and hole	1.732 and -1.542 e.Å^{-3}

Table 5. Atomic coordinates (x 10^4) and equivalent isotropic displacement parameters (Å^{2}x 10^3) for **6**. U(eq) is defined as one third of the trace of the orthogonalized U^{ij} tensor.

	x	y	z	U(eq)
I(1)	6198(1)	7387(1)	1510(1)	20(1)
I(2)	3795(1)	3015(1)	835(1)	25(1)
Cu(1)	4168(1)	6428(1)	1040(1)	20(1)
Cu(2)	5481(1)	3932(1)	1369(1)	21(1)
C(1)	3487(8)	2556(12)	2007(2)	25(2)
N(1)	7572(7)	2464(9)	1449(2)	21(1)
N(2)	5071(7)	3276(8)	1925(2)	16(1)
I(4)	-1198(1)	6556(1)	6510(1)	20(1)
I(3)	1205(1)	10927(1)	5835(1)	24(1)
Cu(5)	-481(1)	10011(1)	6369(1)	21(1)
Cu(7)	831(1)	7515(1)	6039(1)	19(1)
N(6)	-70(7)	10668(8)	6924(2)	16(1)
N(5)	-2572(7)	11492(9)	6449(2)	20(1)
N(7)	972(7)	6031(8)	5557(2)	17(1)
C(23)	-1381(8)	11810(10)	7053(2)	16(1)
C(6)	6384(8)	2130(10)	2054(2)	16(1)
N(8)	1731(8)	7092(9)	1088(2)	20(1)
N(3)	4029(7)	7914(8)	556(2)	16(1)
C(2)	1163(10)	7639(14)	1448(3)	30(2)
N(9)	3264(8)	6857(8)	6088(2)	19(1)
C(16)	3839(10)	6312(14)	6452(2)	31(2)
C(24)	-2905(7)	11391(9)	6840(2)	16(1)
C(14)	2664(8)	6045(9)	5452(2)	15(1)
C(20)	3091(10)	4828(10)	5138(2)	24(2)
C(7)	7906(7)	2554(9)	1841(2)	16(1)
C(4)	1352(8)	8350(10)	791(2)	18(1)

C(12)	8879(11)	3076(14)	1217(2)	33(2)
C(15)	3650(9)	5580(9)	5792(2)	18(1)
C(21)	-3876(11)	10838(14)	6216(2)	36(2)
C(13)	-91(9)	6712(11)	5267(2)	24(2)
C(19)	4850(10)	4754(11)	5058(2)	24(2)
C(22)	1506(8)	11386(12)	7009(2)	24(2)
C(5)	2339(8)	7897(9)	452(2)	15(1)
C(3)	5094(9)	7236(11)	267(2)	24(2)
C(17)	5412(9)	5501(10)	5708(2)	25(2)
C(10)	9529(9)	1532(13)	2377(2)	30(2)
C(8)	6665(8)	2270(11)	2465(2)	21(1)
C(11)	9233(8)	1320(10)	1966(2)	23(2)
C(18)	5770(10)	4210(10)	5397(3)	29(2)
C(9)	8031(10)	1119(12)	2592(2)	31(2)
C(32)	-1668(8)	11673(11)	7466(2)	20(1)
C(25)	1922(10)	9123(10)	140(2)	24(2)
C(26)	147(10)	9179(11)	59(2)	26(2)
C(28)	-408(9)	8444(10)	710(2)	26(2)
C(29)	-4529(9)	12424(13)	7378(2)	30(2)
C(30)	-4236(8)	12628(10)	6965(2)	23(2)
C(27)	-778(10)	9727(11)	396(3)	29(2)
C(31)	-3035(10)	12830(12)	7590(2)	30(2)

—

Table 6. Bond lengths [Å] and angles [°] for **6**.

I(1)-Cu(1)	2.5450(10)
I(1)-Cu(2)	2.7439(11)
I(2)-Cu(2)	2.5253(11)
I(2)-Cu(1)	2.7192(11)
Cu(1)-N(3)	2.110(6)
Cu(1)-N(8)	2.133(7)
Cu(1)-Cu(2)	2.5094(13)
Cu(2)-N(1)	2.114(7)
Cu(2)-N(2)	2.133(6)
C(1)-N(2)	1.480(9)
N(1)-C(7)	1.469(9)
N(1)-C(12)	1.473(10)
N(2)-C(6)	1.489(9)
I(4)-Cu(7)	2.5468(10)
I(4)-Cu(5)	2.7445(11)
I(3)-Cu(5)	2.5274(11)
I(3)-Cu(7)	2.7185(11)
Cu(5)-N(5)	2.119(7)
Cu(5)-N(6)	2.127(6)
Cu(5)-Cu(7)	2.5106(13)
Cu(7)-N(7)	2.106(6)
Cu(7)-N(9)	2.129(7)
N(6)-C(22)	1.476(9)
N(6)-C(23)	1.488(9)
N(5)-C(24)	1.468(9)
N(5)-C(21)	1.483(10)
N(7)-C(14)	1.484(9)
N(7)-C(13)	1.488(9)
C(23)-C(32)	1.539(10)
C(23)-C(24)	1.542(9)
C(6)-C(8)	1.535(10)
C(6)-C(7)	1.544(9)
N(8)-C(2)	1.468(11)
N(8)-C(4)	1.486(10)

N(3)-C(5)	1.481(9)
N(3)-C(3)	1.486(9)
N(9)-C(16)	1.482(10)
N(9)-C(15)	1.494(10)
C(24)-C(30)	1.538(10)
C(14)-C(20)	1.523(10)
C(14)-C(15)	1.543(10)
C(20)-C(19)	1.519(11)
C(7)-C(11)	1.535(10)
C(4)-C(28)	1.522(10)
C(4)-C(5)	1.540(10)
C(15)-C(17)	1.526(10)
C(19)-C(18)	1.525(13)
C(5)-C(25)	1.519(10)
C(17)-C(18)	1.539(12)
C(10)-C(9)	1.528(12)
C(10)-C(11)	1.539(12)
C(8)-C(9)	1.523(11)
C(32)-C(31)	1.524(10)
C(25)-C(26)	1.533(11)
C(26)-C(27)	1.524(13)
C(28)-C(27)	1.542(12)
C(29)-C(31)	1.518(12)
C(29)-C(30)	1.544(12)

Cu(1)-I(1)-Cu(2)	56.50(3)
Cu(2)-I(2)-Cu(1)	57.03(3)
N(3)-Cu(1)-N(8)	83.7(2)
N(3)-Cu(1)-Cu(2)	146.65(17)
N(8)-Cu(1)-Cu(2)	124.55(17)
N(3)-Cu(1)-I(1)	117.20(17)
N(8)-Cu(1)-I(1)	121.90(18)
Cu(2)-Cu(1)-I(1)	65.76(3)
N(3)-Cu(1)-I(2)	105.70(18)
N(8)-Cu(1)-I(2)	97.87(18)
Cu(2)-Cu(1)-I(2)	57.59(3)

I(1)-Cu(1)-I(2)	122.66(4)
N(1)-Cu(2)-N(2)	83.1(2)
N(1)-Cu(2)-Cu(1)	146.85(18)
N(2)-Cu(2)-Cu(1)	124.51(16)
N(1)-Cu(2)-I(2)	115.81(17)
N(2)-Cu(2)-I(2)	126.01(17)
Cu(1)-Cu(2)-I(2)	65.38(3)
N(1)-Cu(2)-I(1)	107.09(18)
N(2)-Cu(2)-I(1)	94.49(17)
Cu(1)-Cu(2)-I(1)	57.75(3)
I(2)-Cu(2)-I(1)	122.44(4)
C(7)-N(1)-C(12)	114.0(6)
C(7)-N(1)-Cu(2)	105.8(4)
C(12)-N(1)-Cu(2)	112.5(6)
C(1)-N(2)-C(6)	113.4(6)
C(1)-N(2)-Cu(2)	115.4(5)
C(6)-N(2)-Cu(2)	108.6(4)
Cu(7)-I(4)-Cu(5)	56.50(3)
Cu(5)-I(3)-Cu(7)	57.04(3)
N(5)-Cu(5)-N(6)	83.0(2)
N(5)-Cu(5)-Cu(7)	147.00(18)
N(6)-Cu(5)-Cu(7)	124.57(16)
N(5)-Cu(5)-I(3)	115.76(17)
N(6)-Cu(5)-I(3)	126.00(17)
Cu(7)-Cu(5)-I(3)	65.31(3)
N(5)-Cu(5)-I(4)	107.27(18)
N(6)-Cu(5)-I(4)	94.53(17)
Cu(7)-Cu(5)-I(4)	57.77(3)
I(3)-Cu(5)-I(4)	122.41(4)
N(7)-Cu(7)-N(9)	83.6(2)
N(7)-Cu(7)-Cu(5)	146.79(18)
N(9)-Cu(7)-Cu(5)	124.49(17)
N(7)-Cu(7)-I(4)	117.28(18)
N(9)-Cu(7)-I(4)	121.98(18)
Cu(5)-Cu(7)-I(4)	65.73(3)
N(7)-Cu(7)-I(3)	105.71(18)

N(9)-Cu(7)-I(3)	97.72(18)
Cu(5)-Cu(7)-I(3)	57.64(3)
I(4)-Cu(7)-I(3)	122.68(4)
C(22)-N(6)-C(23)	113.0(6)
C(22)-N(6)-Cu(5)	116.0(5)
C(23)-N(6)-Cu(5)	108.8(4)
C(24)-N(5)-C(21)	113.9(6)
C(24)-N(5)-Cu(5)	105.6(4)
C(21)-N(5)-Cu(5)	111.3(6)
C(14)-N(7)-C(13)	113.3(6)
C(14)-N(7)-Cu(7)	105.6(4)
C(13)-N(7)-Cu(7)	112.5(5)
N(6)-C(23)-C(32)	113.2(6)
N(6)-C(23)-C(24)	110.0(6)
C(32)-C(23)-C(24)	110.6(5)
N(2)-C(6)-C(8)	112.8(6)
N(2)-C(6)-C(7)	109.9(6)
C(8)-C(6)-C(7)	110.9(6)
C(2)-N(8)-C(4)	114.2(6)
C(2)-N(8)-Cu(1)	117.4(5)
C(4)-N(8)-Cu(1)	107.4(4)
C(5)-N(3)-C(3)	113.6(6)
C(5)-N(3)-Cu(1)	105.3(4)
C(3)-N(3)-Cu(1)	112.6(5)
C(16)-N(9)-C(15)	113.8(6)
C(16)-N(9)-Cu(7)	117.3(5)
C(15)-N(9)-Cu(7)	107.7(4)
N(5)-C(24)-C(30)	113.7(6)
N(5)-C(24)-C(23)	108.9(5)
C(30)-C(24)-C(23)	109.6(6)
N(7)-C(14)-C(20)	115.0(6)
N(7)-C(14)-C(15)	108.1(6)
C(20)-C(14)-C(15)	110.2(6)
C(19)-C(20)-C(14)	113.7(7)
N(1)-C(7)-C(11)	114.0(6)
N(1)-C(7)-C(6)	109.1(5)

C(11)-C(7)-C(6)	109.4(6)
N(8)-C(4)-C(28)	112.7(6)
N(8)-C(4)-C(5)	109.5(6)
C(28)-C(4)-C(5)	112.5(6)
N(9)-C(15)-C(17)	112.7(6)
N(9)-C(15)-C(14)	108.8(6)
C(17)-C(15)-C(14)	112.0(6)
C(20)-C(19)-C(18)	110.7(7)
N(3)-C(5)-C(25)	114.4(6)
N(3)-C(5)-C(4)	108.4(6)
C(25)-C(5)-C(4)	110.4(6)
C(15)-C(17)-C(18)	111.6(6)
C(9)-C(10)-C(11)	110.5(7)
C(9)-C(8)-C(6)	112.2(6)
C(7)-C(11)-C(10)	110.5(6)
C(19)-C(18)-C(17)	109.5(6)
C(8)-C(9)-C(10)	110.8(7)
C(31)-C(32)-C(23)	112.2(6)
C(5)-C(25)-C(26)	113.0(7)
C(27)-C(26)-C(25)	110.8(7)
C(4)-C(28)-C(27)	112.1(6)
C(31)-C(29)-C(30)	110.4(7)
C(24)-C(30)-C(29)	110.5(6)
C(26)-C(27)-C(28)	109.3(6)
C(29)-C(31)-C(32)	111.2(7)

Symmetry transformations used to generate equivalent atoms:

Table 7. Anisotropic displacement parameters ($Å^2 x\ 10^3$) for **6**. The anisotropic displacement factor exponent takes the form: $-2p^2[\ h^2\ a^{*2}U^{11} + ... + 2\ h\ k\ a^*\ b^*\ U^{12}\ ]$

	U^{11}	U^{22}	U^{33}	U^{23}	U^{13}	U^{12}
I(1)	23(1)	14(1)	22(1)	-3(1)	0(1)	-6(1)
I(2)	37(1)	13(1)	24(1)	-3(1)	-6(1)	-5(1)
Cu(1)	21(1)	17(1)	21(1)	1(1)	-1(1)	0(1)
Cu(2)	25(1)	19(1)	19(1)	1(1)	-2(1)	0(1)
C(1)	9(3)	32(4)	35(4)	1(3)	3(3)	-6(3)
N(1)	22(3)	19(3)	21(3)	-7(3)	6(2)	-6(3)
N(2)	11(3)	18(3)	21(3)	-3(2)	2(2)	5(2)
I(4)	23(1)	14(1)	22(1)	3(1)	0(1)	-6(1)
I(3)	37(1)	13(1)	24(1)	3(1)	6(1)	-5(1)
Cu(5)	25(1)	20(1)	19(1)	-1(1)	2(1)	0(1)
Cu(7)	21(1)	17(1)	20(1)	-1(1)	1(1)	0(1)
N(6)	10(3)	17(3)	20(3)	4(2)	-2(2)	4(2)
N(5)	17(3)	24(3)	20(3)	8(3)	-5(2)	-6(3)
N(7)	16(3)	11(3)	23(3)	-1(2)	0(2)	-3(2)
C(23)	13(3)	15(3)	19(3)	0(3)	1(2)	-1(2)
C(6)	13(3)	17(3)	19(3)	-1(3)	-1(2)	-2(2)
N(8)	25(3)	16(3)	17(3)	-1(2)	5(2)	-10(3)
N(3)	14(3)	9(3)	25(3)	1(2)	0(2)	-2(2)
C(2)	24(4)	30(5)	37(5)	-4(4)	0(3)	5(3)
N(9)	24(3)	16(3)	19(3)	1(2)	-7(2)	-10(2)
C(16)	28(4)	36(6)	29(4)	5(4)	0(3)	3(4)
C(24)	7(3)	13(3)	28(4)	1(3)	-4(2)	-2(2)
C(14)	21(3)	8(3)	17(3)	3(2)	0(2)	0(2)
C(20)	33(4)	11(3)	27(4)	1(3)	0(3)	6(3)
C(7)	8(3)	12(3)	29(4)	1(3)	4(2)	0(2)
C(4)	18(3)	14(4)	22(4)	-1(3)	3(3)	-3(3)
C(12)	35(5)	38(5)	25(4)	-4(4)	14(3)	-6(4)
C(15)	23(4)	10(3)	20(4)	1(3)	-2(3)	-5(3)
C(21)	38(5)	44(5)	26(4)	7(4)	-16(4)	-13(4)
C(13)	25(4)	19(4)	29(4)	1(3)	-9(3)	-2(3)
C(19)	25(4)	13(4)	35(5)	-3(3)	9(3)	2(3)

C(22)	10(3)	30(4)	32(4)	-4(3)	-2(3)	-4(3)
C(5)	20(3)	7(3)	19(3)	-3(2)	-1(2)	0(2)
C(3)	22(3)	18(3)	31(4)	1(3)	8(3)	-1(3)
C(17)	18(4)	16(4)	41(5)	-5(3)	-5(3)	3(3)
C(10)	23(4)	28(4)	39(5)	0(4)	-10(3)	8(3)
C(8)	17(3)	26(4)	20(3)	-2(3)	5(3)	6(3)
C(11)	11(3)	17(4)	42(5)	-4(3)	0(3)	4(3)
C(18)	21(4)	13(3)	52(5)	0(3)	6(3)	6(3)
C(9)	28(4)	29(5)	36(5)	3(4)	-3(3)	2(3)
C(32)	12(3)	26(4)	22(3)	3(3)	-5(2)	5(3)
C(25)	37(4)	12(3)	24(4)	1(3)	1(3)	2(3)
C(26)	24(4)	16(4)	37(5)	5(3)	-10(3)	1(3)
C(28)	17(4)	18(4)	43(5)	5(3)	6(3)	2(3)
C(29)	19(3)	28(4)	44(5)	-1(4)	13(3)	5(3)
C(30)	12(3)	18(4)	40(4)	5(3)	-1(3)	4(3)
C(27)	20(4)	16(4)	52(5)	1(4)	-7(3)	6(3)
C(31)	27(4)	28(4)	35(4)	-7(3)	4(3)	2(3)

Table 8. Hydrogen coordinates (x 10^4) and isotropic displacement parameters ($Å^2$x 10^3) for **6**.

	x	y	z	U(eq)
H(1A)	3318	1478	1866	37
H(1B)	2681	3426	1941	37
H(1C)	3413	2288	2267	37
H(99)	7420(110)	1290(40)	1420(30)	31
H(23)	-1087	13057	6998	19
H(6)	6089	884	1999	20
H(2A)	1698	8727	1521	45
H(2B)	1391	6712	1626	45
H(2C)	22	7842	1438	45
H(16A)	3332	5203	6522	46
H(16B)	3578	7224	6630	46
H(16C)	4986	6149	6444	46
H(24)	-3224	10156	6899	19
H(14)	2943	7273	5379	18
H(20A)	2716	3626	5196	29
H(20B)	2530	5227	4917	29
H(7)	8225	3788	1900	20
H(4)	1689	9545	875	21
H(12A)	9143	4294	1280	49
H(12B)	8561	3015	961	49
H(12C)	9805	2325	1256	49
H(15)	3315	4384	5876	21
H(21A)	-4164	9643	6291	54
H(21B)	-3533	10824	5961	54
H(21C)	-4793	11614	6241	54
H(13A)	231	7907	5200	36
H(13B)	-1180	6731	5357	36
H(13C)	-26	5945	5053	36

H(19A)	5216	5924	4976	29
H(19B)	5049	3899	4861	29
H(22A)	1687	12453	6866	36
H(22B)	2314	10509	6950	36
H(22C)	1562	11673	7269	36
H(5)	2062	6672	376	18
H(3A)	4766	6046	197	35
H(3B)	6180	7206	358	35
H(3C)	5037	8011	54	35
H(17A)	5992	5129	5929	30
H(17B)	5788	6690	5641	30
H(10A)	10386	728	2454	36
H(10B)	9869	2753	2429	36
H(8A)	6891	3511	2529	26
H(8B)	5692	1915	2595	26
H(11A)	10213	1593	1831	28
H(11B)	8938	86	1913	28
H(18A)	6916	4215	5344	35
H(18B)	5466	3003	5470	35
H(9A)	7750	-135	2558	37
H(9B)	8225	1322	2854	37
H(32A)	-1898	10434	7529	24
H(32B)	-697	12027	7597	24
H(25A)	2489	8735	-81	29
H(25B)	2289	10325	200	29
H(26A)	-58	10024	-140	31
H(26B)	-211	8002	-22	31
H(59A)	-976	8830	931	31
H(62B)	-795	7256	644	31
H(29A)	-5381	13234	7454	36
H(29B)	-4874	11205	7431	36
H(30A)	-5216	12350	6830	28
H(30B)	-3943	13861	6911	28
H(27A)	-1924	9709	342	35
H(27B)	-483	10939	467	35
H(31A)	-3228	12634	7853	36

H(31B)	-2752	14083	7556	36
H(61)	1210(80)	6280(110)	1030(19)	0(17)
H(65)	5120(80)	4350(100)	2045(19)	0(16)
H(66)	-160(80)	9740(100)	7062(19)	0(16)
H(67)	3760(90)	7740(110)	6030(20)	4(18)
H(64)	4260(100)	8890(120)	610(20)	10(20)
H(68)	640(90)	5100(120)	5610(20)	6(18)

—

References

(1) (a) Ullmann, F. *Chem. Ber.* **1901**, *34*, 2174. (b) Ullmann, F. *Chem. Ber.* **1903**, *36*, 2382. (c) Ullmann, F.; Sponagel, P. *Chem. Ber.* **1905**, *38*, 2211. (d) Goldberg, I. *Chem. Ber.* **1906**, *39*, 1691.

(2) For an older review highlighting the application of the Ullmann/Goldberg reaction in synthesis, see: Lindley, J. *Tetrahedron* **1984**, *40*, 1433.

(3) For reviews on palladium-catalyzed C-N bond formation, see: (a) Jiang, L.; Buchwald, S. L. *Palladium-Catalyzed Aromatic Carbon-Nitrogen Bond Formation. In Metal-Catalyzed Cross-Coupling Reactions*; 2nd Ed; de Meijere, A., Diederich, F., Eds.; Wiley-VCH; Weinheim, 2004; pp 699. (b) Muci, A. R.; Buchwald, S. L. *Top. Curr. Chem.* **2002**, *219*, 131. (c) Hartwig, J. F. In *Handbook of Organopalladium Chemistry for Organic Synthesis*; Negishi, E., Ed.; Wiley-Interscience: New York, 2002; pp 1051.

(4) (a) Shen, Q.; Shekhar, S.; Stambuli, J. P.; Hartwig, J. F. *Angew. Chem. Int. Ed.* **2005**, *44*, 1371. (b) Huang, X.; Anderson, K. W.; Zim, D.; Jiang, L.; Klapars, A.; Buchwald, S. L. *J. Am. Chem. Soc.* **2003**, *125*, 6653. (c) Harris, M. C.; Huang, X.; Buchwald, S. L. *Org. Lett.* **2002**, *4*, 2885. (d) Link, J. T.; Sorensen, B.; Liu, G.; Pei, Z.; Reilly, E. B.; Leitza, S.; Okasinski, G. *Bioorg. Med. Chem. Lett.* **2001**, *11*, 973. (e) Prashad, M.; Hu, B.; Lu, Y.; Draper, R.; Har, D.; Repic, O.; Blacklock, T. J. *J. Org. Chem.* **2000**, *65*, 2612. (f) Batch, A.; Dodd, R. H. *J. Org. Chem.* **1998**, *63*, 872. (g) Willoughby, C. A.; Chapman, K. T. *Tetrahedron Lett.* **1996**, *37*, 7181. (h) Ward, Y. D.; Farina, V. *Tetrahedron Lett.* **1996**, *37*, 6993.

(5) (a) Yin, J.; Buchwald, S. L. *J. Am. Chem. Soc.* **2002**, *124*, 6043. (b) Cacchi, S.; Fabrizi, G.; Goggiamani, A.; Zappia, G. *Org. Lett.* **2001**, *3*, 2539. (c) Artamkina, G. A.; Sergeev, A. G.;

Beletskaya, I. P. *Tetrahedron. Lett.* **2001**, *42*, 4381. (d) Yin, J.; Buchwald, S. L. *Org. Lett.* **2000**, *2*, 1101. (e) Shakespeare, W. C. *Tetrahedron Lett.* **1999**, *40*, 2035.

(6) Kiyomori, A.; Marcoux, J.-F.; Buchwald, S. L. *Tetrahedron Lett.* **1999**, *40*, 2657.

(7) Goodbrand, H. B.; Hu, N.-X. *J. Org. Chem.* **1999**, *64*, 670.

(8) Gujadhur, R. K.; Bates, C. G.; Venkataraman, D. *Org. Lett.* **2001**, *3*, 4315.

(9) Kwong, F. Y.; Klapars, A.; Buchwald, S. L. *Org. Lett.* **2002**, *4,* 581.

(10) Ma, D.; Cai, Q.; Zhang, H. *Org. Lett.* **2003**, *5*, 2453.

(11) Kwong, F. Y.; Buchwald, S. L. *Org. Lett.* **2003**, *5*, 793.

(12) (a) Antilla, J. C.; Baskin, J. M.; Barder, T. E.; Buchwald, S. L. *J. Org. Chem.* **2004**, *69*, 5578. (b) Zanon, J.; Klapars, A.; Buchwald, S. L. *J. Am. Chem. Soc.* **2003**, *125*, 2890. (c) Jiang, L.; Job, G. E.; Klapars, A.; Buchwald, S. L. *Org. Lett.* **2003**, *5*, 3667. (d) Klapars, A.; Buchwald, S. L. *J. Am. Chem. Soc.* **2002**, *124*, 14844. (e) Antilla, J. C.; Klapars, A.; Buchwald, S. L. *J. Am. Chem. Soc.* **2002**, *124*, 11684. (f) Klapars, A.; Huang, X.; Buchwald, S. L. *J. Am. Chem. Soc.* **2002**, *124*, 7421. (g) Klapars, A.; Antilla, J. C.; Huang, X.; Buchwald, S. L. *J. Am. Chem. Soc.* **2001**, *123*, 7727.

(13) For a critical review concerning copper-catalyzed cross coupling reactions, see: Beletskaya, I. P.; Cheprakov, A. V. *Coord. Chem. Rev.* **2004**, *248*, 2337. For other more recent reviews, see: (a) Ley, S. V.; Thomas, A. W. *Angew. Chem. Int. Ed.* **2003**, *42*, 5400. (b) Kunz, K.; Scholz, U.; Ganzer, D. *Synlett* **2003**, *15*, 2428.

(14) Weston, P. W.; Adkins, H. *J. Am. Chem. Soc.* **1928**, *50*, 859.

(15) Weingarten, H. *J. Org. Chem.* **1964**, *29*, 3624.

(16) Kondratov, S. A.; Shein, S. M. *Zh. Org. Khim.* **1979**, *15*, 2160.

(17) Paine, A. J. *J. Am. Chem. Soc.* **1987**, *109*, 1496.

(18) (a) Aalten, H. L.; van Koten, G.; Grove, D. M.; Kuilman, T.; Piekstra, O. G.; Hulshof, L. A.; Sheldon, R. A. *Tetrahedron* **1989**, *45*, 5565. (b) Resnik, R.; Cohen, T.; Fernando, Q. *J. Am. Chem. Soc.* **1961**, *83*, 3344.

(19) Bacon, R. G. R.; Karim, A. *J. Chem. Soc., Perkin Trans. 1* **1973**, 272.

(20) Whitesides, G. M.; Sadowski, J. S.; Lilburn, J. *J. Am. Chem. Soc.* **1974**, *96*, 2829.

(21) Yamamoto, T.; Ehara, Y.; Kubota, M.; Yamamoto, A. *Bull. Chem. Soc. Jpn.* **1980**, *53*, 1299.

(22) The use of a heterogeneous inorganic base such as K_3PO_4 may limit the reaction rate due to mass transfer effects. However, using different stirring rates resulted in identical reaction rate profiles, thus ruling out the possibility of a mass transfer limited process.

(23) Figure 4 data at constant [ArI], $[Cu]_{total}$, and [Amide] fit to an equation of the form: rate = C_1[1,2-Diamine]/(C_2 + [1,2-Diamine], where C_1 and C_2 are adjustable parameters as in the Michaelis-Menten equation. For details on the Michaelis-Menten equation, see: (a) Walsh, C. *Enzymatic Reaction Mechanisms*; W.H. Freeman and Company: New York, 1979. (b) Fersht, A. *Structure and Mechanism in Protein Science*; W.H. Freeman and Company: New York, 1999.

(24) For previous characterization of related structures, see: (a) Raubenheimer, H. G.; Cronje, S.; Kruger, G. J.; Olivier, P. J. *Polyhedron* **1995**, *14*, 2389. (b) Davies, G.; El-Kady, N.; Onan, K. D.; Shomaly, W.; El-Sayed, M. A.; El-Toukhy, A. *Inorg. Chim. Acta* **1988**, *149*, 21. (c) Davies, G.; El-Kady, N.; El-Sayed, M. A.; El-Toukhy, A.; Schure, M. R. *Inorg. Chim. Acta* **1988**, *149*, 31. (d) Healy, P. C.; Pakawatchai, C.; White, A. H. *J. Chem. Soc., Dalton Trans.* **1985**, 2531. (e) Haitko, D. A. *J. Coord. Chem.* **1984**, *13*, 119.

(25) Enantiomerically pure (R,R)-**3** was used to obtain X-ray quality crystals.

(26) Cotton, F. A.; Wilkinson, G.; Murillo, C. A.; Bochmann, M. *Advanced Inorganic Chemistry*, 6th ed.; Wiley: New York, 1999; pp 856.

(27) Reducing the $CuBr_2$/**3** precatalyst with an equivalent amount of $FeCl_2$ at 80 °C in toluene prior to the addition of the amide and aryl iodide results in an identical reaction rate as premixing the $CuBr_2$/**3** precatalyst with the amide and base for 60 min at 80 °C. A similar observation has previously been made: Tuong, T. D.; Hida, M. *J. Chem. Soc., Perkin Trans. II* **1974**, 676.

(28) $CuBr_2$ is completely insoluble in a toluene solution in the absence of **2**.

(29) Soloman, E. I. In *Copper Coordination Chemistry: Biochemical & Inorganic Perspectives*; Karlin, K. D.; Zubieta, J.; Adenine; New York, 1983; pp 1.

(30) (a) Chiang, T.-C. *J. Chem. Phys.* **1968**, *48*, 1814. (b) Knuehl, B.; Pintauer, T.; Kajiwara, A.; Fischer, H.; Matyjaszewski, K. *Macromolecules* **2003**, *36*, 8291.

(31) For the preparation of similar Cu(II) complexes, see: Kennedy, B. P.; Lever, A. B. P. *J. Am. Chem. Soc.* **1973**, *95*, 6907.

(32) For the characterization of *N*-centered imide radicals, see: (a) Koenig, T.; Hoobler, J. A.; Klopfenstein, C. E.; Hedden, G.; Sunderman, F.; Russell, B. R. *J. Am. Chem. Soc.* **1974**, *96*, 4573. (b) Kaba, R. A.; Ingold, K. U. *J. Am. Chem. Soc.* **1976**, *98*, 7375. (c) Forrester, A. R.; Irikawa, H.; Soutar, G. *Tetrahedron Lett.* **1984**, *25*, 5445.

(33) Decay of the free-radical occurs while in the presence of a proton source, e.g., H_2O, or K_2HPO_4.

(34) (a) Tsuda, T.; Yazawa, T.; Watanabe, K.; Fujii, T.; Saegusa, T. *J. Org. Chem.* **1981**, *46*, 292. (b) Gambarotta, S.; Floriani, C.; Chiesi-Villa, A.; Guastini, C. *J. Chem. Soc., Chem. Commun.* **1983**, 1156. (c) Meyer, E. M.; Gambarotta, S.; Floriani, C.; Chiesi-Villa, A.; Guastini, C. *Organometallics* **1989**, *8*, 1067. (d) Tsuda, T. *Encyclopedia of Reagents for Organic*

Synthesis; Paquette, L., Ed.; Wiley: New York, 1995; p 3271. (e) Eriksson, H.; Håkansson, M. *Organometallics* **1997**, *16*, 4243.

(35) For the synthesis of copper(I)-amides, see: (a) Tsuda, T.; Watanabe, K.; Miyata, K.; Yamamoto, H.; Saegusa, T. *Inorg. Chem.* **1981**, *20*, 2728. (b) Hope, H.; Power, P. P. *Inorg. Chem.* **1984**, *23*, 936. (c) Gamboratta, S.; Bracci, M.; Floriani, C.; Chiesi-Villa, A.; Guastini, C. *J. Chem. Soc., Dalton Trans.* **1987**, 1883.

(36) A similar procedure was used to characterize Cu(I) alkoxides, see ref. 20.

(37) (a) Lopes, C.; Håkansson, M.; Jagner, S. *Inorg. Chim. Acta* **1997**, *254*, 361. (b) Håkansson, M.; Lopes, C.; Jagner, S. *Inorg. Chim. Acta* **2000**, *304*, 178. (c) Gustafsson, B.; Håkansson, M.; Westman, G.; Jagner, S. *J. Organomet. Chem.* **2002**, *649*, 204.

(38) Hibble, S. J.; Eversfield, S. G.; Cowley, A. R.; Chippindale, A. M. *Angew. Chem. Int. Ed.* **2004**, *43*, 628.

(39) Arylation of Cu(I) amidate in the absence of **3** did not precede at temperatures between 0 °C and 90 °C.

(40) As described in ref. 21, PPh_3–ligated Cu(I) amidates also undergo *N*-arylations, however, these reactions were not kinetically characterized either stoichiometrically or in the context of a catalytic reaction.

(41) Bunnett, J. F. *Acc. Chem. Res.* **1978**, *11*, 413.

(42) (a) Kochi, J. K. *J. Am. Chem. Soc.* **1957**, *79*, 2942. (b) Jenkins, C. L.; Kochi, J. K. *J. Am. Chem. Soc.* **1972**, *94*, 843. (c) Jenkins, C. L.; Kochi, J. K. *J. Am. Chem. Soc.* **1972**, *94*, 856.

(43) (a) Whitesides, G. M.; Fischer, W. F.; San Filippo, J.; Bashe, R. W.; House, H. O. *J. Am. Chem. Soc.* **1969**, *91*, 4871. (b) Whitesides, G. M.; Kendall, P. E. *J. Org. Chem.* **1972**, *37*, 3718.

(44) Johnson, C. R.; Dutra, G. A. *J. Am. Chem. Soc.* **1973**, *95*, 7783.

(45) (a) Cohen, T.; Wood, J.; Dietz, A. G. *Tetrahedron Lett.* **1974**, *40*, 3555. (b) Cohen, T.; Lewarchik, R. J.; Tarino, J. Z. *J. Am. Chem. Soc.* **1974**, *96*, 7753. (c) Cohen, T.; Christea, I. *J. Am. Chem. Soc.* **1976**, *98*, 748.

(46) Arai, S.; Hida, M.; Yamagishi, T. *Bull. Chem. Soc. Jpn.* **1978**, *51*, 277.

(47) Bethell, D.; Jenkins, I. L.; Quan, P. M. *J. Chem. Soc., Perkin Trans. II* **1985**, 1789.

(48) For studies demonstrating the relative affinities of aromatic acids to Cu(I), see: Saphier, M.; Burg, A.; Sheps, S.; Cohen, H.; Meyerstein, D. *J. Chem. Soc., Dalton Trans.* **1999**, 1845.

(49) For a review on electron transfer in copper chemistry, see: Rorabacher, D. B. *Chem. Rev.* **2004**, *104*, 651.

(50) Rusonik, I; Cohen, H.; Meyerstein, D. *J. Chem. Soc., Dalton Trans.* **2003**, 2024.

(51) (a) Parr, R. G.; Pearson, R. G. *J. Am. Chem. Soc.* **1983**, *105*, 7512. (b) Pearson, R. G. *J. Am. Chem. Soc.* **1988**, *110*, 7684. (c) Pearson, R. G. *Inorg. Chem.* **1988**, *27*, 734. (c) Pearson, R. G. *J. Org. Chem.* **1989**, *54*, 1423.

(52) Deng, H.; Kebarle, P. *J. Am. Chem. Soc.* **1998**, *120*, 2925.

(53) Arai, S.; Hida, M.; Yamagishi, T.; Ototake, S. *Bull. Chem. Soc. Jpn.* **1977**, *50*, 2982.

(54) Barton, J.; Tino, J.; Horanská, V. *Makromol. Chem.* **1973**, *164*, 215.

(55) Betschart, C.; Schmidt, B.; Seebach, D. *Helv. Chim. Acta* **1988**, *71*, 1999.

(56) de la Camp, U.; Seely, O. *Iodometric Determination of Cu in Brass.* http://www.csudh.edu/oliver/che230/labmanual/copbrass.htm

Chapter Two:

Mechanistic Studies on the Pd-Catalyzed C-N Bond Forming Reaction Using Monophosphinobiaryl Ligands

Introduction

Over the last three decades palladium-catalyzed transformations have emerged as extremely versatile tools in organic synthesis (eqs 1 and 2).[1] The ability to construct a wide array of carbon-carbon and carbon-heteroatom bonds has remained unmatched in other organometallic reactions. The primary reason for this status stems from their generality and tolerance of a variety of functional groups, which makes several of these applications amenable to the synthesis of complex targets.

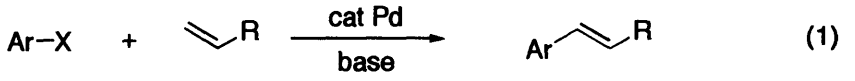

(1)

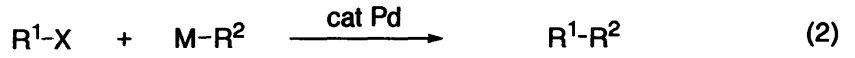

(2)

X = Cl, Br, I, OTf, OTs

R^1 and R^2 = aryl, vinyl, and alkyl

M = MgX, BX_2, ZnX, SnR_3, SiX_3, etc.

The general mechanism for palladium-catalyzed cross-coupling reactions is thought to proceed through sequential stages (Scheme 1).[2] The first stage involves activation of the catalyst. Since it is common for $Pd(OAc)_2$ or $[Pd_2(dba)_3]$ (dba = dibenzylideneacetone) to be employed as catalyst precursors, they typically require either reduction of Pd(II) to Pd(0) in the former case or removal of the dba in the latter instance. In some circumstances the dissociation of an equivalent of ligand is also a prerequisite for the formation of an active $L_nPd(0)$ species. Once the active catalyst has been produced, the second stage involves the reaction between an aryl, vinyl, or alkyl halide or sulfonate with the Pd(0) center through an oxidative addition process. In the penultimate step, a transmetalation reaction affords a Pd(II) species containing the two moieties

to be coupled. Finally, reductive elimination of the coupled product occurs in the fourth stage along with the concomitant regeneration of the active Pd(0) catalyst.

Scheme 1. General Mechanism for Pd(0)-catalyzed Cross-Coupling Reactions.

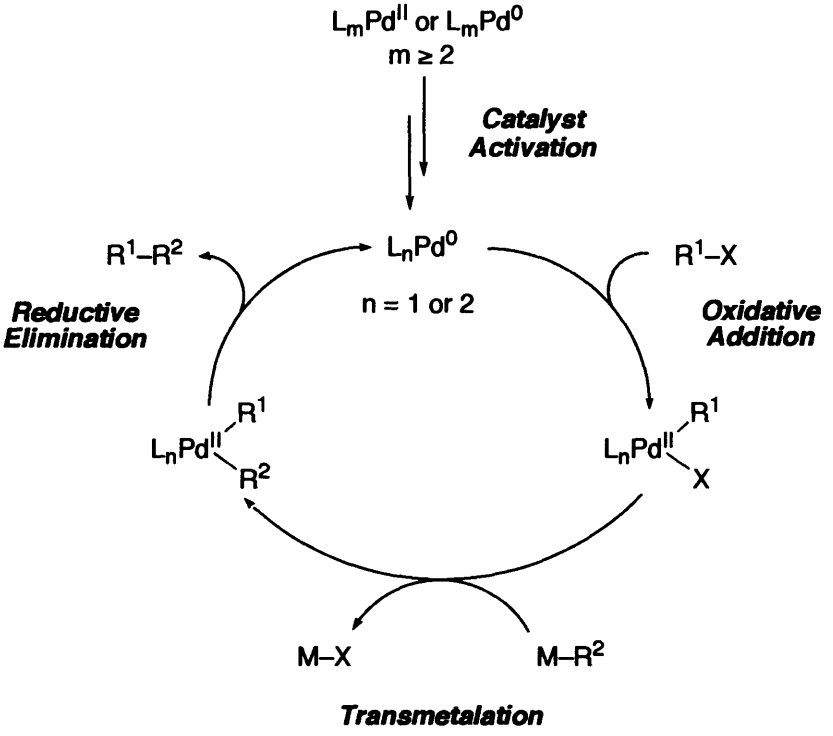

One of the highlights in Pd-catalyzed cross-coupling reactions over the last decade is the development of ligands that promote catalyst turnover and improve catalyst stability. At the forefront of this development is the presence of bulky, electron-rich ligands, e.g., phosphines and carbenes.[3] The logic underlying these advancements in cross-coupling chemistry is based on the premise that highly unsaturated 12-electron LPd(0) complexes are formed, which facilitate the oxidative addition reaction with less reactive substrates.[4] Indeed, catalysts derived from recently developed ligands allow for lower catalyst loadings in addition to facilitating the activation of less reactive substrates such as aryl chlorides/tosylates and alkyl halides/tosylates.[5]

Achievements along these lines have garnered a significant amount of interest in potential industrial applications, specifically, as a result of the growing practicality and economic feasibility of these reactions.

The introduction of PCy_3 and P*t*-Bu_3 as supporting ligands served as the harbinger for catalysts with higher activity and stability. Although the pioneering work of Osborn,[6] Alper,[7] and Milstein[8] on the reactivity of electron-rich Pd(0) complexes underscores the initial applications of bulky, electron-rich ligands in the activation of aryl chlorides, it was not until the late 1990's that a general catalyst system was discovered in which bulky, electron-rich phosphines served as the supporting ligands. More specifically, in 1997, a catalyst system based on PCy_3 was employed for the Pd-catalyzed C–N bond forming reaction with unactivated aryl chlorides, however this system offered limited scope with respect to both the amine and aryl chloride.[9] In 1998, Nishiyama reported on the use of highly active catalysts derived from P*t*-Bu_3 in the C–N bond forming reaction with aryl chlorides.[10] In that same year, Fu demonstrated that the same catalyst was also highly effective in Suzuki-Miyaura couplings.[11] Subsequently, the Pd/ P*t*-Bu_3 system rendered itself as a general catalyst for Stille cross-couplings,[12] Heck reactions,[13] α-arylations of ketones, malonates, and silyl enol ethers,[14] and used further in C–N bond forming reactions.[15] Importantly, the optimal Pd/phosphine ratio was found to be between 1 and 1.5.[11b] This observation was also substantiated through mechanistic studies on the Pd/ P*t*-Bu_3–catalyzed C-N bond forming reaction with aryl chlorides, which found an inhibitory role for higher [P*t*-Bu_3].[16]

Based on the success achieved with the Pd/ P*t*-Bu_3 catalyst system, attempts were made to evaluate the efficacy of other catalysts derived from bulky, electron-rich phosphines and carbenes. As shown in Figure 1, a number of ligands have been employed in Pd-catalyzed cross-

coupling reactions with unactivated substrates, each of which have their own merits. For example, catalysts derived from ligand **3** have been employed in Suzuki-Miyaura couplings as well as C–N and C–O bond forming reactions.[17] Carbenes **5a** and 5**b** have also been employed as supporting ligands in numerous cross-coupling reactions, however, they are typically plagued by the requirement to use strong bases such as KO*t*-Bu and NaO*t*-Bu.[18] Furthermore, catalysts based on **7**[19] and **8**[20] have also demonstrated their utility in a variety of cross-coupling reactions with unactivated aryl chlorides. High turnover numbers (TONs) can be achieved in Suzuki-Miyaura couplings with catalysts based on **9** and in the case of C-N bond forming reactions these catalysts are particularly effective for the coupling of aryl chlorides with 2,6-disubstituted anilines.[21] The first example of the use of an aryl tosylate in cross-coupling chemistry was demonstrated with the catalyst derived from **2**.[22] More recently, using **4**, which is structurally similar to **2**, highly reactive and stable catalysts are generated, thus, promoting the coupling of heteroaryl and aryl chlorides with primary alkylamines.[23]

The most general catalysts in terms of their efficacy in C–C, C–N, and C–O bond forming reactions are those based on the Buchwald group's bulky, electron-rich monophosphinobiaryl ligands (Figure 2). Introduced in 1998, the Pd(0) catalyst based on **10e** demonstrated exceptionally high activity, allowing for room temperature Suzuki-Miyaura couplings with aryl bromides and chlorides as well as room temperature aminations with aryl bromides; including the first room temperature amination with an aryl chloride.[24] While searching for catalysts displaying higher TONs than those observed with **10e**, ligand **11a** was discovered, which further expanded the scope of these cross-coupling reactions.[25,26] More recently, with the introduction of **12**[27] and **13**[28] into this class of ligands, the most general and

active catalyst systems to date for the Suzuki-Miyaura, C-N bond forming reactions, and Sonogashira reactions with aryl chlorides and tosylates have been revealed.

Figure 1. Bulky, Electron-Rich Ligands Used in Pd-Catalyzed Cross-Coupling Reactions.

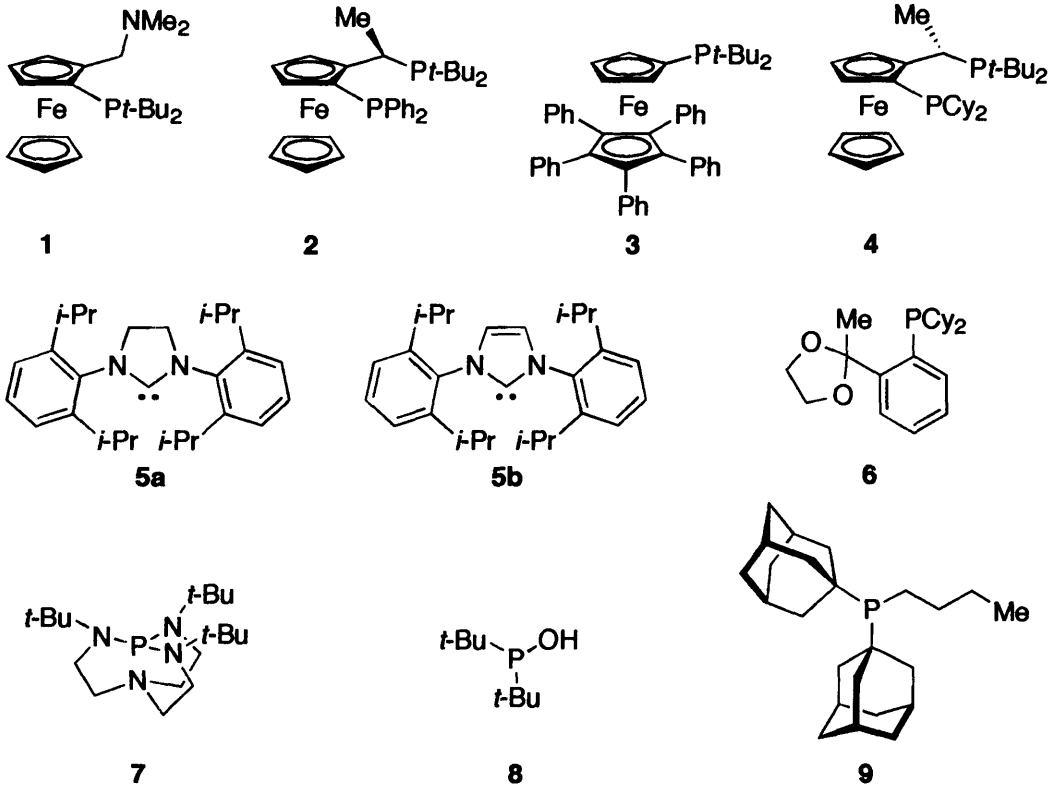

The activity and stability of catalysts derived from the monophosphinobiaryl ligands has been attributed to a combination of electronic and steric properties that favor both the oxidative addition and reductive elimination steps.[25c] The hypothesis for the initial use of bulky, electron-rich ligands was based on the premise that steric properties influence the formation of a monoligated Pd(0) species, which are in turn, responsible for the rapid oxidative addition of the aryl halide/sulfonate. This proposal has been substantiated in the context of oxidative additions

Figure 2. Bulky, Electron-Rich Monophinobiaryl Ligands Used in Pd-Catalyzed C–C, C–N, and C–O Bond Forming Reactions.

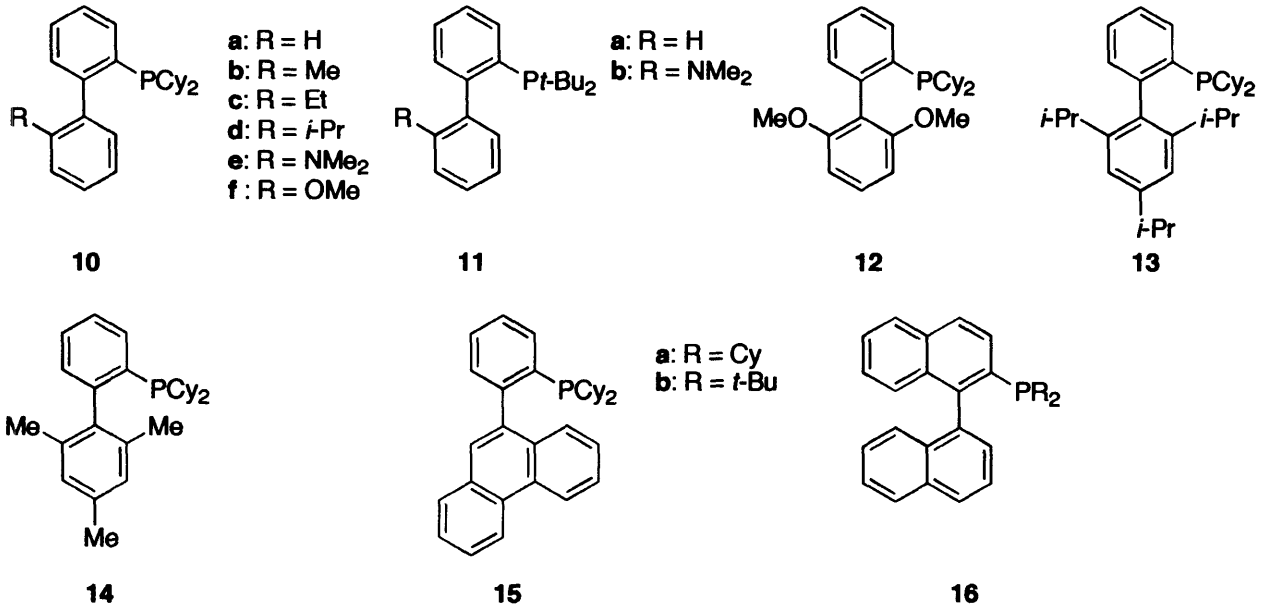

to trialkylphosphine-based Pd(0) complexes. In their systematic study, Brown demonstrated that a more rapid oxidative addition reaction ensues with Pd(0) complexes containing bulkier ligands, i.e., P*t*-Bu_3, in comparison to complexes containing CyP*t*-Bu_2, Cy_2P*t*-Bu, and PCy_3.[29] The reason for this was attributed to the lower energy required for oxidative addition to occur with a monoligated L_1Pd(0) complex. Placing these results in the context of the monophosphinobiaryl ligands, the stability of monoligated Pd(0) species is thought to arise from π interactions between the lower ring of the biaryl moiety and the Pd(0) center. Support for this proposal was initially provided by the X-ray structure of **17**[25o] and later by **18**,[27] both of which display a π interaction. Moreover, stabilization of this type may also account for faster rates of reductive elimination, since destabilization due to the steric properties of the ligand in the Pd(II) species is not the only factor that determines the rate of this process.[30]

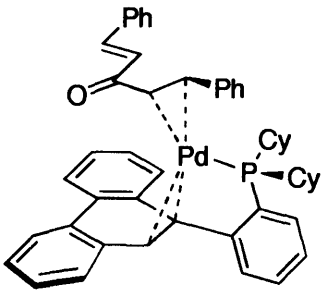

17

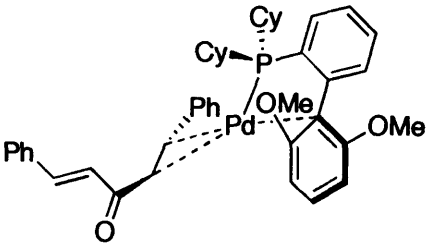

18

On the basis of the aforementioned mechanistic studies, unsaturated Pd(0) and Pd(II) species based on bulky, electron-rich ligands have been postulated to exist within the catalytic process; however, structural evidence supporting these claims has been relatively scarce until recently. A series of tricoordinated Pd(II) compounds with the general formula [(R_3P)Pd(Ph)X] (PR_3 = Ad*P*t-Bu_2, P*t*-Bu_3, **3**; X = Br, I, OTf) were synthesized and characterized by X-ray crystallography.[31] Not only do these complexes display the T-shaped geometry expected for the unsaturated Pd(II) upon oxidative addition, they also suggest that stabilization of these complexes occurs through agostic interactions. Furthermore, the rate of oxidative addition to generate these T-shaped complexes was consistent with the rates obtained from the catalytic processes. In the context of C–N bond forming reactions, the T-shaped Pd(II) complexes with the formula [(R_3P)Pd(*p*-anisyl)NAr_2] (PR_3 = **3**, FcP*t*-Bu_2; Ar = 3,5-$(CF_3)_2$-C_6H_3) were also isolated and characterized by X-ray crystallography.[32] As one would expect, the overall rates of C–N reductive elimination of the triarylamine from these complexes follow the order: [(**3**)Pd(*p*-anisyl)NAr_2] > [(*t*-Bu_3P)Pd(*p*-anisyl)NAr_2] > [(FcP*t*-Bu_2) (*p*-anisyl)NAr_2], which suggests a dependence on the size of the ligand in promoting the reductive elimination, i.e., the bulkier the ligand, the faster the reductive elimination. Moreover, comparing the rates of reductive elimination from three-coordinate complexes to those from four-coordinate complexes indicate

that the former process occurs more rapidly. Taken together, these results provide considerable insight into the effects of bulky, electron-rich ligands on the individual steps in the catalytic process. They also provide further motivation to elucidate other factors that could improve catalyst activity and lifetime.

This report provides a systematic mechanistic analysis of $Pd(OAc)_2$/ monophosphino-biaryl–catalyzed C–N bond forming reaction with aryl chlorides. The results provide insights into the relationship between the steady-state concentration of active Pd and the size and substitution pattern of the monophosphinobiaryl ligands. These insights into the nature of catalyst activation help highlight the importance of establishing a high concentration of active catalyst. The catalyst derived from the bulkiest ligand in the series, the tri-*i*-propyl ligand **13**, exhibits both accelerated rate and the increased stability required for practical application of this reaction.

Results and Discussion

Protocol for Kinetic Examination. We began by examining the reaction shown in eq 3 in order to measure the differences in reaction rates for the catalytic systems generated from biaryl ligands **10a–d**, **11a**, and **12–14**. The reaction rates were determined by monitoring the progress in sequential reactions using reaction calorimetry. We have shown previously how such a protocol allows the examination of features such as catalyst activation while also providing a complete kinetic profile for estimating reaction rate constants in a multi-step mechanism.[33] This approach also helps to address the question of catalyst activation and stability by comparing initial rates for reactions commencing after the catalyst has already undergone numerous

turnovers. In the case of a process in which catalyst activation is slow, the reaction rates for each subsequent reaction should increase, while catalyst deactivation or positive-order substrate dependencies will yield decreasing reaction rates as the turnover numbers increase.

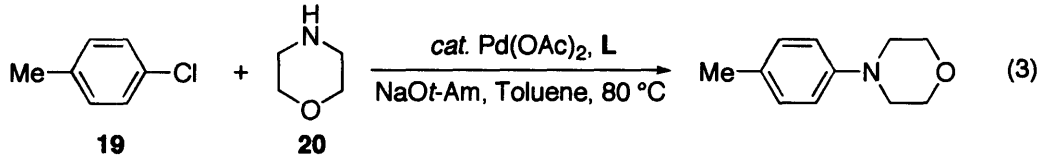

19 **20** (3)

A typical experiment for the coupling of *p*-chlorotoluene (**19**) with morpholine (**20**) in toluene at 80 °C (eq 3) was carried out with four consecutive injections of the reactants to a solution containing the $Pd(OAc)_2$ precatalyst along with the ligand and NaO*t*-Am equilibrated at 80 °C for 1 h. The amine was either added with the catalyst prior to commencement of the first injection of aryl chloride or added in the first injection with the aryl chloride. The remaining three injections only contained aryl chloride. This reaction protocol allowed us to examine the influence of the presence of the amine on activation of the Pd(II) precatalyst.[34] Between 20 – 35 turnovers were accomplished in each reaction.

Comparison of Reaction Rates with Different Catalysts. Figure 3 compares the initial activity as well as the long-term stability of catalysts derived from ligands **11a** and **13**. Exceptional reactivity in Pd-catalyzed C-N bond forming processes has been observed previously for catalyst systems based on these two ligands.[25c,28] Both catalyst systems are very active, with that derived from **11a** giving an initial rate about 40% lower than that based on **13** (Figure 3). Their relative activity following three reactions (ca. 110 turnovers), however, is markedly different (Figure 3 inset). The catalyst with ligand **13** retains its original activity while the reaction rate for catalyst/ligand **11a** combination has decreased by more than an order of

magnitude. These results further exemplify the utility of monitoring the catalyst from one set of turnovers to the next.

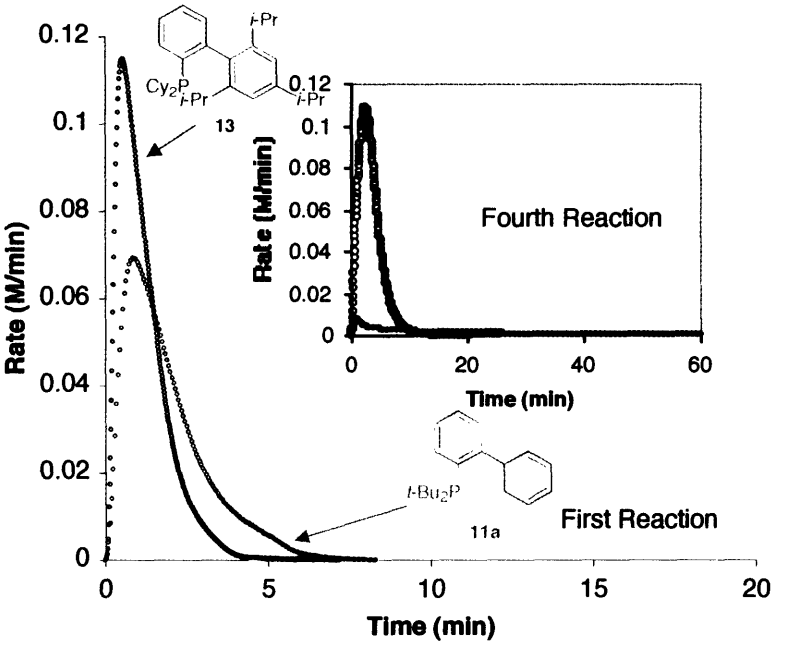

Figure 3. Reaction rate vs. time for the coupling of morpholine ($[\mathbf{20}]_o$ = 0.74 M – 0.78 M) with *p*-chlorotoluene (4 x $[\mathbf{19}]_o$ = 0.15 M) using $[Pd(OAc)_2]$ = 4.2 mM and $[NaO\textit{t}\text{-Am}]_o$ = 0.8 M: (o) [**13**] = 16.5 mM, (o) [**11a**] = 16.5 mM. (a) Reaction 1 is initiated by adding all of **20** and the first aliquot of **19**. The subsequent reactions were performed by adding additional aliquots of **19**. (b) Reaction 4 is taken after the reaction had undergone 110 turnovers (75 min into the reaction). Setting the time equal to 0 for reaction 4 is only for reference.

Figure 4 depicts the comparison of the activity and stability between catalysts based on ligands **12** – **14**, by plotting the reaction rate as a function of reaction progress for four consecutive reactions. The rates for catalyst systems based on **12** and **14** are significantly lower than that observed using ligand **13**. It is important to note that the concentrations of $Pd(OAc)_2$ and **13** used in the sequential reaction experiment is half of that used in the case of ligands **12** and **14**. The dramatic effect of the size of the substituents in the 2′and 6′ positions of the monophosphinobiaryl ligand is revealed by the factor of five difference in reaction rate across

the ligand series **12 – 14**. More specifically, the order in reaction rate follows: Pd/**13** > Pd/**14** > Pd/**12**, suggesting that the more sterically encumbered the biaryl, the faster the rate of the catalytic process.[35] Another intriguing feature of these reactions is the remarkable stability of each of these catalysts over multiple turnovers, as indicated by the nearly identical reaction rates from one reaction to the next.

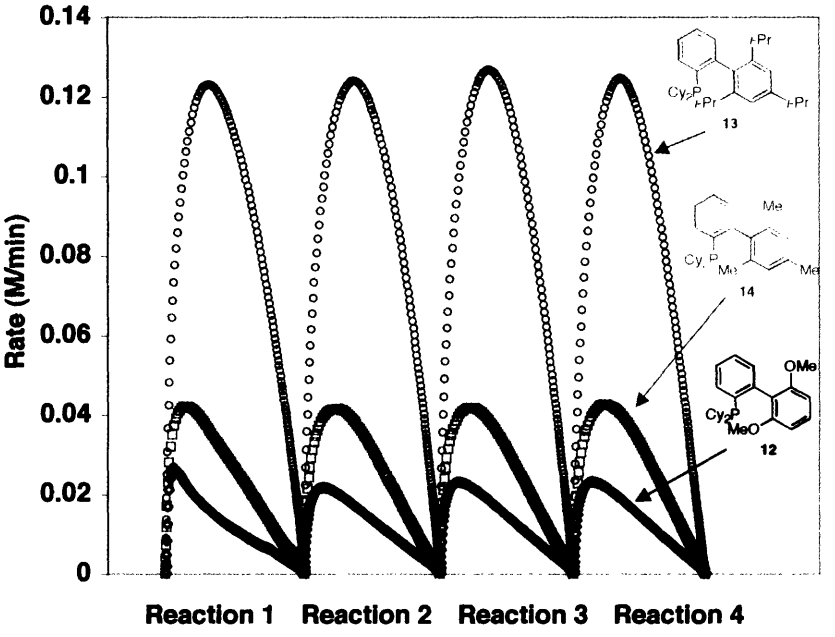

Figure 4. Sequential reaction experiment for the amination of *p*-chlorotoluene (4 x $[\mathbf{19}]_0 = 0.15$ M) with morpholine ($[\mathbf{20}]_0 = 0.74$ M – 0.78 M) using $[NaO\textit{t}\text{-Am}]_0 = 0.8$ M: (blue o) $[Pd(OAc)_2]$ = 4.2 mM, [**13**] = 12.7 mM (**13** : Pd = 3), (red □) $[Pd(OAc)_2]$ = 8.3 mM, [**14**] = 25 mM (**14** : Pd = 3), (black ◊) $[Pd(OAc)_2]$ = 8.3 mM, [**12**] = 25 mM (**12** : Pd = 3). The reaction was performed by adding all of **20** and the first aliquot of **19** in the first reaction of the sequence. Note: the L:Pd ratio is 3 for all of these reactions

A similar protocol as that mentioned above was used to examine catalysts based on the 2′-substituted biaryl ligands **10b – 10d** (Figure 5). The reaction rates for all of these catalysts are lower than those described in Figure 4 (the catalyst derived from **10d** exhibits a higher rate than

that based on **12**, however, when the **12** : Pd ratio is 2, the reaction rate for this catalyst is significantly higher, *vide infra*). Furthermore, the amination with catalysts derived from **10b** – **10d** no longer maintains a constant reaction rate for each consecutive reaction like those in Figure 4; the reaction rate actually *increases* for each consecutive reaction. This observation suggests that catalyst activation (Stage 1 Scheme 1) is *slower* than the reactions taking place within the catalytic cycle. Thus, as more turnovers occur, more catalyst enters into the cycle. This emphasizes the importance of the 2′,6′-substitution pattern in generating highly active catalysts. Ligands with the 2′,6′-substitution pattern not only generate catalysts that provide higher reaction rates, they also prevent a slow catalyst activation process from occurring.

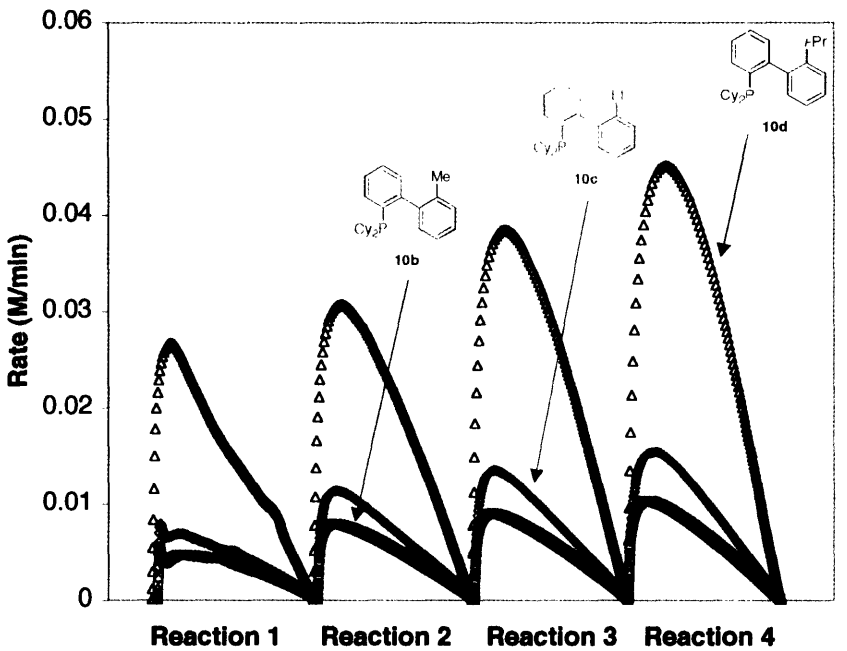

Figure 5. Sequential reaction experiment for the amination of *p*-chlorotoluene (4 x $[\mathbf{19}]_o = 0.15$ M) with morpholine ($[\mathbf{20}]_o = 0.74$ M – 0.78 M) using $[NaO\textit{t}\text{-Am}]_o = 0.8$ M and $[Pd(OAc)_2] = 8.3$ mM: (green Δ) [**10d**] = 16.5 mM (**10d** : Pd = 2), (red ◊) [**10c**] = 16.5 mM (**10c** : Pd = 2), (blue □) [**10b**] = 16.5 mM (**10b** : Pd = 2). The reaction was performed by adding all of **20** and the first aliquot of **19** in the first reaction of the sequence. Note: the L:Pd ratio is 2 for all of these reactions.

The general mechanism outlined in Scheme 2 describes a proposed catalyst activation process that may result from the use of the monophosphinobiaryl ligands.[36] Ligand dissociation from $L_2Pd(X)_2$ (**I**) generates the monophosphine complex **II**. This step should be sensitive to the size of the phosphine, with larger phosphines resulting in a more favorable equilibrium. Once the monophosphine complex **II** forms, amine association occurs which is followed by deprotonation resulting in the Pd(II) amide (**IV**). β-Hydride elimination then ensues to afford **V** which readily undergoes reductive elimination to generate the active Pd(0) species.[37]

Scheme 2. Proposed Mechanism for Catalyst Activation Involving the Amine.

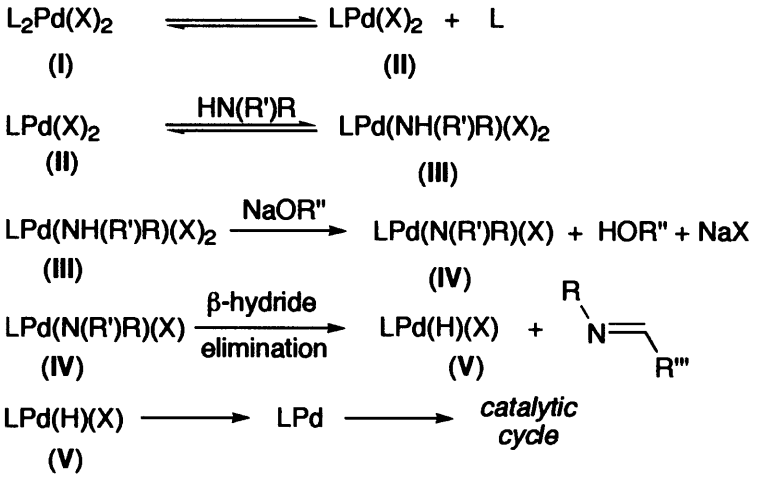

To investigate this proposed mechanism, the catalyst was incubated with the amine prior to the commencement of the reaction through the addition of the aryl chloride (Figures 6 and 7). If catalyst activation is slow as in the case with ligands **10b – 10d**, allowing the catalyst to incubate with the amine prior to the commencement of the reaction should then facilitate this activation process. In contrast, with catalysts based on ligands **12 – 14**, where slow catalyst activation is presumed not to be present, amine incubation should have little effect. In the event, incubating the catalyst/base mixture with the amine has a significant influence on the reaction

rate with *all* of the catalysts. Comparing the rates obtained from this protocol (Figure 6) to those in Figure 4, the rate nearly doubles upon incubating. Surprisingly, a constant reaction rate for each consecutive reaction is maintained with the exception of the *N*-arylation with the Pd/**13** catalyst, where the reaction rate slightly decreases with each subsequent reaction. This effect arises from catalyst deactivation, a process that was validated by the adding extra **20** in

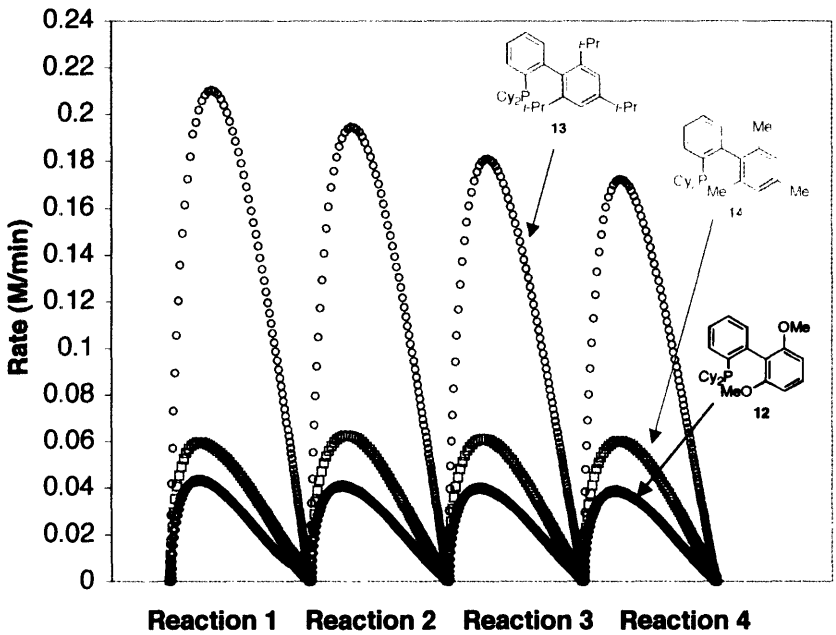

Figure 6. Sequential reaction experiment for the amination of *p*-chlorotoluene (4 x $[\mathbf{19}]_0 = 0.15$ M) with morpholine ($[\mathbf{20}]_0 = 0.74$ M – 0.78 M) using $[NaO\textit{t}\text{-Am}]_0 = 0.8$ M: (blue o) $[Pd(OAc)_2]$ = 2.5 mM, [**13**] = 7.6 mM (**13** : Pd = 3), (red □) $[Pd(OAc)_2]$ = 8.3 mM, [**14**] = 25 mM (**14** : Pd = 3), (black ◊) $[Pd(OAc)_2]$ = 8.3 mM, [**12**] = 25 mM (**12** : Pd = 3). The reaction was performed by mixing the catalyst with **20** and NaO*t*-Am for 60 min at 80 °C prior to the addition of the first aliquot of **19**.

the fourth reaction, making the total [**20**] equal to the second reaction. More specifically, if the *decreasing* reaction rates were a result of a reaction rate dependence on [amine] then the additional amount of **20** in the last reaction should lead to a reaction rate which was identical to that observed in the second reaction; however, this was not the case. It is also important to

mention that the rate enhancement observed upon incubating the catalyst with the amine becomes less significant at higher concentrations of catalyst. That is, when increasing the concentrations of $Pd(OAc)_2$ to 8.3 mM and the [**13**] to 16.5 mM (these concentrations are identical to those used with catalysts based on **10b – 10d**), the difference in reaction rate upon incubating the catalyst with the amine was insignificant. This implies that rate of catalyst activation is directly related to the concentration of the catalyst.

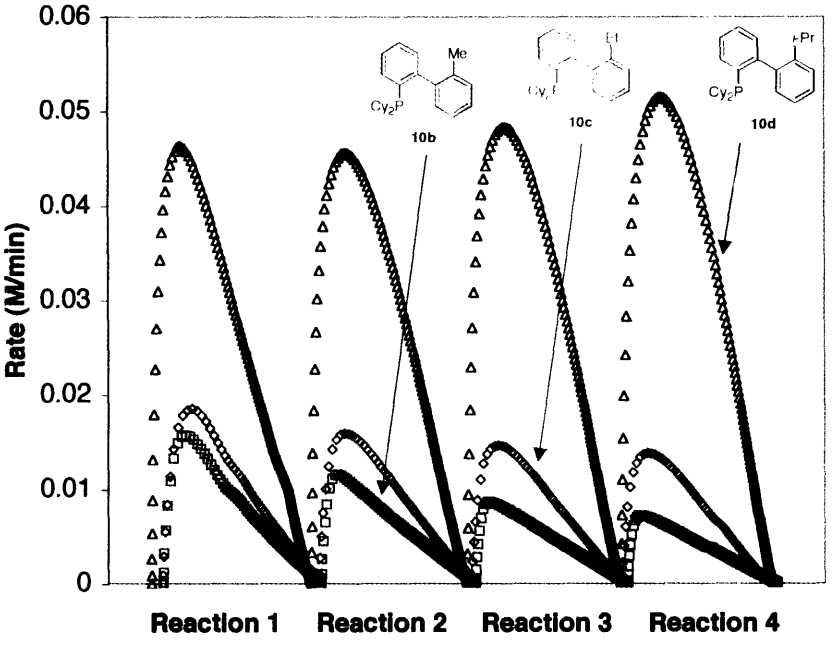

Figure 7. Sequential reaction experiment for the amination of *p*-chlorotoluene (4 x $[\mathbf{19}]_o = 0.15$ M) with morpholine ($[\mathbf{20}]_o = 0.74$ M – 0.78 M) using $[NaO\textit{t}\text{-Am}]_o = 0.8$ M and $[Pd(OAc)_2] = 8.3$ mM: (green Δ) [**10d**] = 16.5 mM (**10d** : Pd = 2), (red ◊) [**10c**] = 16.5 mM (**10c** : Pd = 2), (blue □) [**10b**] = 16.5 mM (**10b** : Pd = 2). The reaction was performed by mixing the catalyst with **20** and NaO*t*-Am for 60 min at 80 °C prior to the addition of the first aliquot of **19**.

The rate profiles become drastically different upon incubating catalysts based on ligands **10b – 10d** with the amine (Figure 7). Not only is there an overall increase in reaction rate relative to that described in Figure 5, the consecutive reactions display *decreasing* reaction rates with ligands **10b** and **10c**. Using the catalyst based on **10d**, higher reactions rates are also

observed in the amine incubation, however, the reaction rates still increase with each consecutive reaction, albeit, the slope of the rate increase is less pronounced in this case. This suggests either that catalyst activation is much slower for this catalyst relative to those based on **10b** and **10c** or that less catalyst deactivation occurs with the system derived from **10d** relative to those derived from **10b** and **10c**. Further comparison between the studies carried out with amine incubation and those without, indicates that the reaction rate of the *first* reaction in the sequence where incubation was employed was higher than the *last* in the sequence with no amine incubation (Figure 5). Importantly, these results support the original hypothesis for the effect of the amine during catalyst activation, in that incubating the catalyst with the amine facilitates catalyst activation through a pathway involving the amine.

The proposed role for the amine in activating the catalyst was investigated by studying the kinetic isotope effects (KIE's) using morpholine-d_8 (**20**-d_8) as a substrate. For the catalyst system derived from ligand **10b**, a primary KIE may be anticipated for the initial reactions when carried out *without* amine incubation, because the overall reaction rate is influenced by the rate of catalyst activation (formation of LPd(0) in Scheme 2). By contrast, no KIE would be expected using catalysts derived from **10b** in reactions carried out *with* amine incubation, since catalyst activation is suggested to be complete prior to the beginning of the coupling reaction. Similarly, no KIE should be observed with the bulkiest ligand **13**, since catalyst activation in this case is not a turnover-limiting process as evidenced by the identical reaction rates obtained for consecutive reactions. Results shown in Table 1 confirm these predictions, showing no KIE for catalysts based on ligand **13** and positive but steadily decreasing KIE's in reactions using ligand **10b** under the same conditions as in Figure 5, where catalyst activation is occurring concomitant with the catalytic reaction.[38] Although the magnitude of the KIE values reported here for the

amine activation process with catalysts based on **10b** are similar to those reported for the catalytic alcohol oxidation (values range between 1.3 and 2.5),[39] larger KIE's, which range from 5.9 to 7, have been observed for β-hydride elimination from other metal alkoxide, amide, and amine complexes.[40] At present, it is unclear what isotope-dependent factors contribute to the magnitudes of the isotope effects since the structure of the various species along the amine activation pathway have not been elucidated. However, to obtain high KIE values the vibration in the transition state for β-hydride elimination must be minimal and/or the difference in vibrational energy levels must be small; these conditions may not be met under the present circumstances.

Table 1. Kinetic Isotope Effects.

Ligand	k_H/k_D 1st Injection	k_H/k_D 2nd Injection	k_H/k_D 3rd Injection	k_H/k_D 4th Injection
10b	1.58 ± 0.01	1.53 ± 0.02	1.34 ± 0.03	1.17 ± 0.02
10b w/ amine incubation	1.04 ± 0.02	1.03 ± 0.01	1.08 ± 0.04	1.08 ± 0.04
13	1.01 ± 0.07	0.90 ± 0.09	0.88 ± 0.08	0.96 ± 0.05

Scheme 3. Proposed Mechanism for the Effect of Ligand Size on the Reaction Rate.

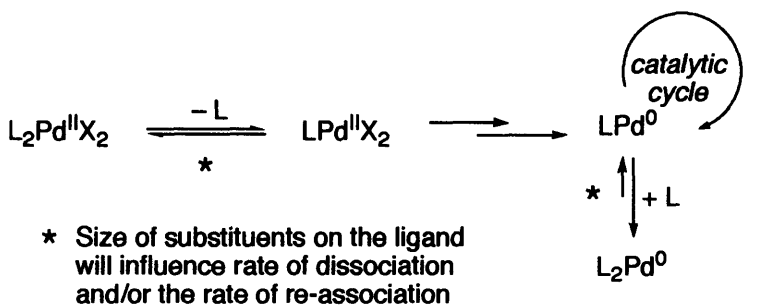

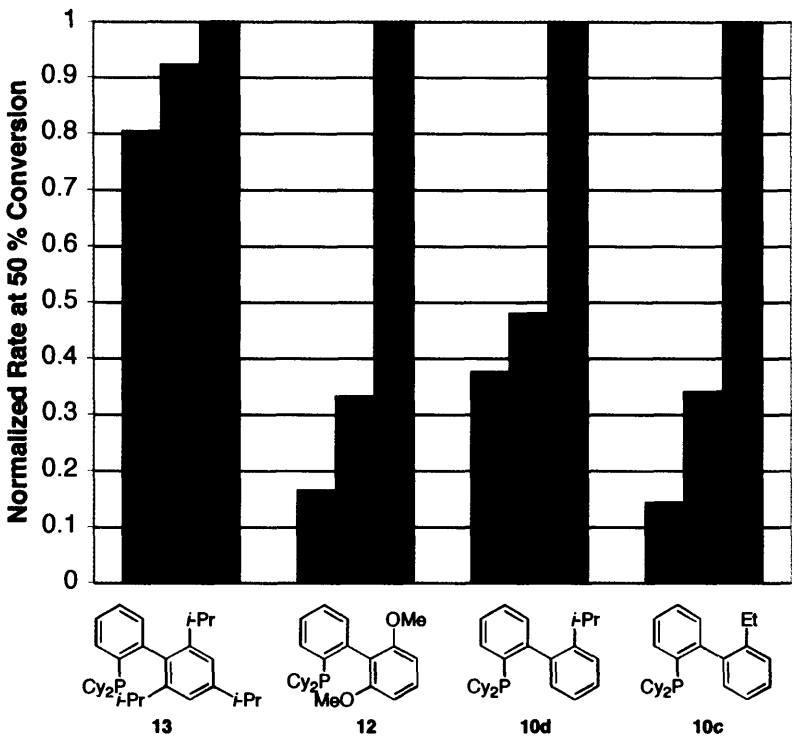

Figure 8. Normalized rate (rate at 50 % conversion/ maximum rate) of ligands **13**, **12**, **10d**, and **10c** with varying ligand: Pd ratios. Ligand: Pd ratios: **4 : 1 (green)**, **3 : 1** (red), **2 : 1** (blue). The conditions used for these experiments were identical to those in Figures 4 and 5.

Effect of Ligand Size on the Reaction Rate. Although the difference in rate profiles for the catalysts based on the 2′,6′-disubstituted biaryl ligands and those based on the 2′-substituted ligands indicate that two different catalyst activation pathways exist, they are similar in the sense that the size of the substituents dramatically influences the reaction rate. More specifically, the sensitivity of reaction rate to the size of the substituent on the phosphine ligand suggests that dissociation of the phosphine from a bisphosphine Pd(0) or Pd(II) complex is required prior to the introduction of the active catalyst into catalytic cycle (Scheme 3). Thus, slower reaction rates may be the result of a slower rate of phosphine dissociation from bisphosphine complexes. Alternatively, the size of the substituents on the phosphine ligand may influence the rate at which

ligand re-association occurs, with smaller substituents facilitating a faster re-association process. Each of these possibilities are supported by the observation that the rate displays a small dependence on the L:Pd ratio for the largest ligand **13**, while the rate dependence becomes more significant for the smaller ligands **12**, **10d**, and **10c** (Figure 8).

Scheme 4. Proposed Mechanism for the Formation of **21** (X-ray structure also shown) from a Mixture of **13** and $Pd(OAc)_2$ in Toluene at Room Temperature.

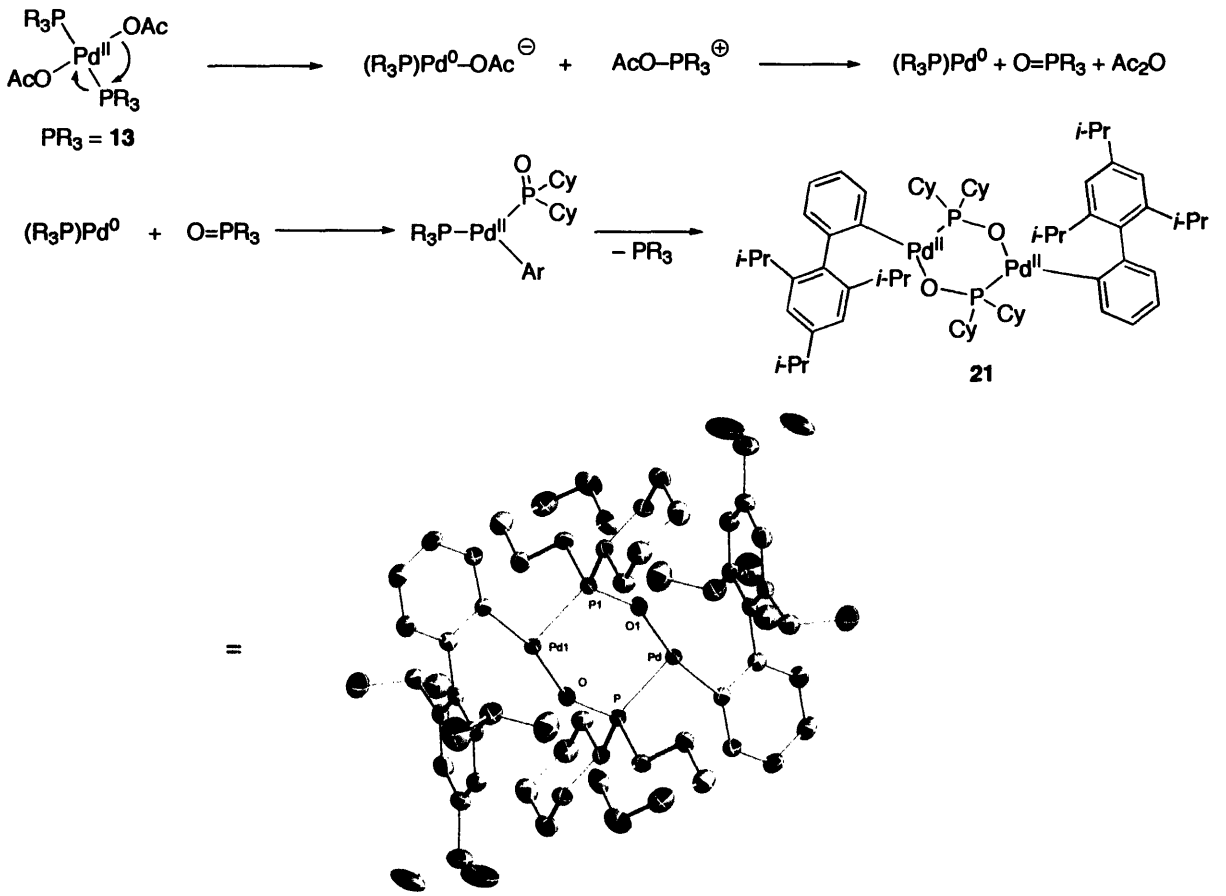

Palladium Speciation With Different Catalysts. ^{31}P NMR spectroscopic studies were conducted to gain insights into the differences in Pd speciation while using catalysts based on 2′,6′-disubstituted biaryl ligands versus those based on 2′-substituted biaryl ligands. Addition of 3 equiv of **13** to $Pd(OAc)_2$ in toluene-d_8 at 22 °C results in a single resonance at 41.1 ppm in

addition to free ligand. The integration data reveal that only 2 equiv of **13** coordinates to Pd(II). Although this spectrum does not change over a 60 °C temperature range (20 – 80 °C), attempts to isolate the complex were unsuccessful. This may be a result of the decomposition of Pd(II) into Pd(0), a process that is quite common with Pd(II) carboxylates in the presence of phosphine ligands. Allowing this same solution to stand overnight, however, resulted in the precipitation of yellow crystals. X-ray crystallographic analysis of this material revealed the structure of **21**. The formation of which presumably occurs through a pathway similar to the standard autoreduction process for Pd(II) carboxylates; however, upon generation of the phosphine oxide of **13** an oxidative addition reaction ensues with the concomitantly formed Pd(0). Subsequently, dimerization with the loss of **13** results in **21** (Scheme 4).[41]

To glean more structural information regarding the possible formation of *trans*-(**13**)$_2$Pd(OAc)$_2$ from the mixture of Pd(OAc)$_2$ and **13**, complex **22** was synthesized from (MeCN)$_2$PdCl$_2$ and **13**. The X-ray structure of **22** is shown below, which indeed displays a square planar Pd(II) center containing two phosphine ligands oriented in such a way that an inversion center exists at Pd(II). More importantly, the ^{31}P NMR of this complex in toluene-d_8 displays a single resonance at 45.5 ppm, suggesting that the complex that results from the mixture of Pd(OAc)$_2$ and **13** is geometrically and electronically similar.

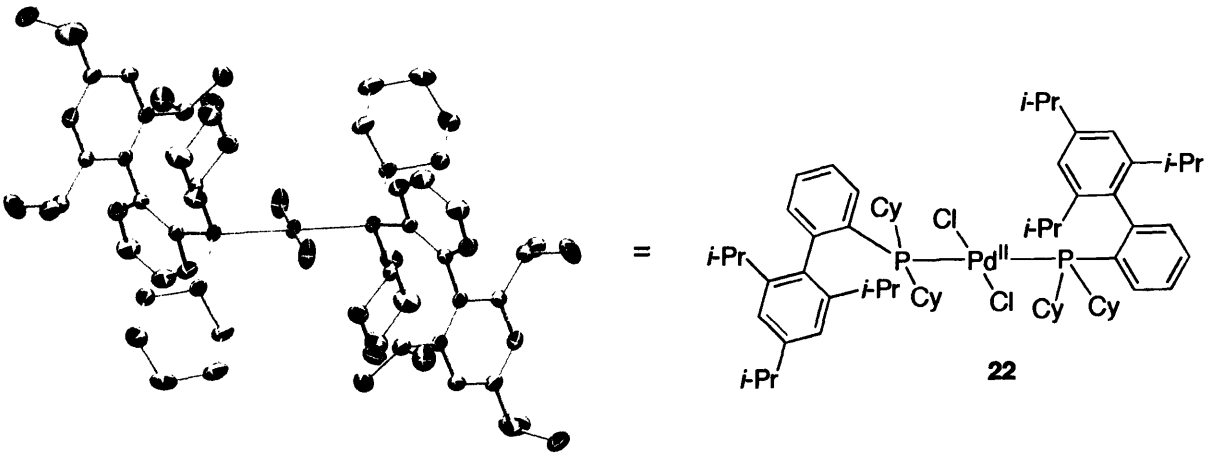

Addition of either NaO*t*-Am or a NaO*t*-Am/morpholine mixture to a solution of the catalyst (1:3 $Pd(OAc)_2$: **13**) in toluene-d_8 alters the structure of the initial catalyst complex. Following the addition of 150 equiv of NaO*t*-Am to the catalyst mixture at 60 °C, the ^{31}P NMR spectrum indicates that the original Pd(II) complex is no longer present. Instead, a new resonance appears at 32 ppm along with an increase in the intensity for free **13** (Figure 9 II). Furthermore, upon addition of 120 equiv of morpholine (**20**) to this mixture, the signal intensity for the species at 32 ppm decays within seconds, affording a very broad resonance at 23 ppm (Figure 10 II, broad resonance can not be seen). These results are consistent with the rapid displacement of acetate within the original Pd(II) complex by alkoxide. However, it is uncertain whether the resulting complex contains either one or two phosphine ligands. The increase in free **13** suggests that ligand dissociation occurs, however, this may just be the result of the formation of other species existing in low concentrations that are equilibrating with the free phosphine. Nevertheless, the species at 32 ppm reacts rapidly with the amine, consistent with a rapid catalyst activation process. The kinetic studies involving the multiple reaction protocol in Figure 4 also support this conclusion as evidenced by the initial reaction rate that is maintained over sequential

reactions. Thus, on the basis of these observations, the reduction of Pd(II) to Pd(0) is not the turnover-limiting process when ligands such as **12–14** are employed.

The differences in reactions rates obtained with (Figure 6) and without amine incubation (Figure 4) must therefore arise from differences in Pd speciation. For example, incubating the catalyst/base mixture with the amine may prevent the formation of a less active Pd complex or complexes. Indeed, monitoring the catalytic reaction by ^{31}P NMR at 60 °C indicates that there exists a difference in Pd speciation upon amine incubation. In the catalytic reaction where the Pd/**13** catalyst is not incubated with the amine (the amine and aryl chloride are added simultaneously to initiate the reaction), the resonance at 32 ppm immediately gives way to a new resonance at 63 ppm (Figure 9 III and IV). This new species maintains a relatively constant concentration throughout the reaction, as indicated by its presence even after 12 min when the reaction is > 90 % complete. In contrast, incubating the catalyst/base mixture with the

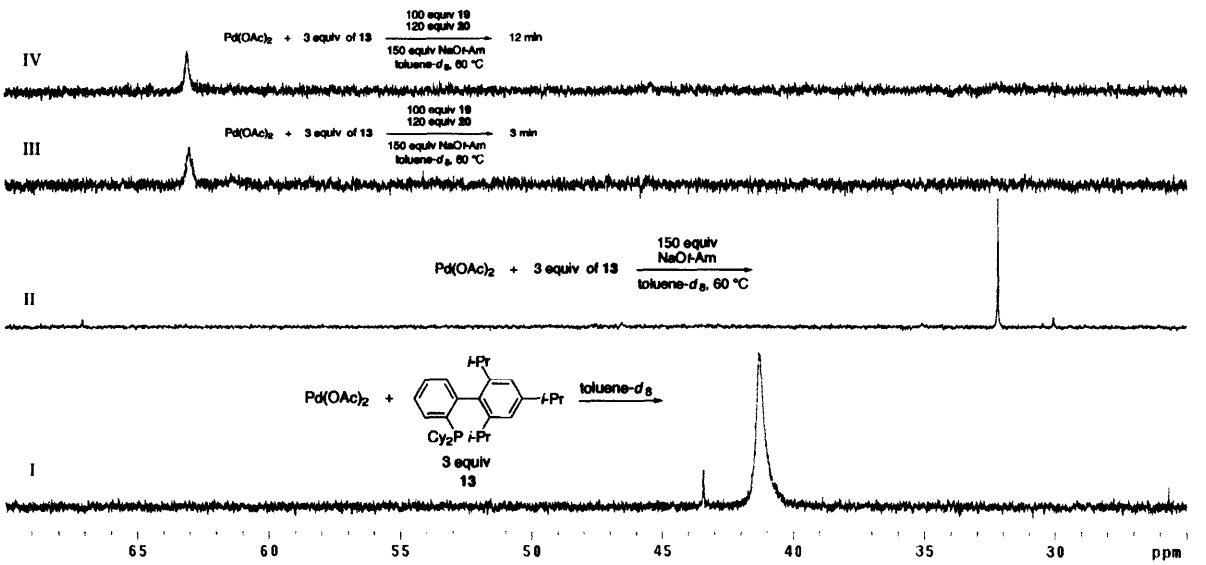

Figure 9. ^{31}P NMR spectra of a (I) solution containing $Pd(OAc)_2$ (18 mM), **13** (55 mM) in 1 mL of toluene-d_8 at 60 °C, (II) solution containing $Pd(OAc)_2$ (18 mM), **13** (55 mM), and NaO*t*-Am (2.0 M) in 1 mL of toluene-d_8 at 60 °C, (III) solution of the catalytic reaction 3 min after the simultaneous addition of **19** (0.51 M) and **20** (1.5 M) to the mixture in II, and (IV) solution of the catalytic reaction 12 min after the addition of **19** and **20** to the mixture in II.

amine for 60 min at 60 °C results in the absence of a single observable species by ^{31}P NMR (Figure 10 III and IV). This result supports the original hypothesis in that amine incubation inhibits the formation of a Pd species that either slowly enters into the catalytic reaction or is completely inactive. Although the structure of the species corresponding to 63 ppm in the ^{31}P NMR (Figure 9) has not been elucidated, the formation of this species may account for the difference in reaction rates observed in Figures 4 and 6. It is important to mention that this species does not correspond to a L_2Pd^0 species since the *in situ* generation of the latter complex through the addition of **13** to (TMEDA)Pd(Me)$_2$ produces a broad resonance at 23 ppm.[42] A similar scenario is observed with the other 2′,6′-disubstituted ligands **12** and **14** where an inactive Pd species is formed in the absence of incubating the catalyst with the amine.

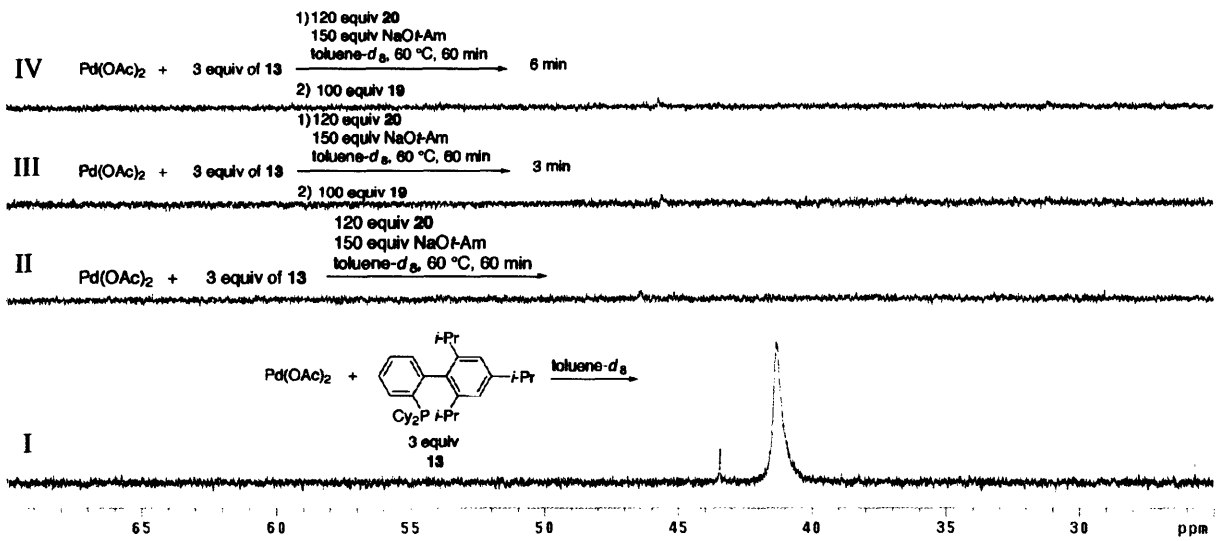

Figure 10. ^{31}P NMR spectra of a (I) solution containing Pd(OAc)$_2$ (18 mM), **13** (55 mM) in 1 mL of toluene-d_8 at 60 °C, (II) solution containing Pd(OAc)$_2$ (18 mM), **13** (55 mM), **20** (1.5 M), and NaO*t*-Am (2.0 M) in 1 mL of toluene-d_8 after 60 min at 60 °C, (III) solution of the catalytic reaction 3 min after the addition of **19** (0.51 M) to the mixture in II, and (IV) solution of the catalytic reaction 6 min after the addition of **19** to the mixture in II.

Catalysts derived from 2′-substituted ligands, such as **10d**, do not display the same pattern in Pd speciation as those derived from the 2′,6′-disubstituted ligands. As shown in Figure 11, mixing $Pd(OAc)_2$ with 2 equiv of **10d** in toluene-d_8 results in the formation of multiple species (Figure 11 I). Changing the temperature over a 60 °C range (20 – 80 °C) does not affect this spectrum, however, addition of NaO*t*-Am at 80 °C causes the resonances to shift (Figure 11 II). Subsequently, upon commencement of the catalytic reaction by adding 100 equiv of **19** and 120 equiv **20** simultaneously to the solution in II, the ^{31}P NMR indicates the absence any new resonances. Even after 18 min when the reaction is complete, based on gas chromatographic measurements, the ^{31}P NMR of the reaction mixture remains the same. These results are in contrast with those obtained with the catalyst based on **13**, where that catalyst was dramatically influenced by the addition of the reaction components. It is possible that the active catalyst is formed in undetectable concentrations and the species that give rise to the resonances in Figure 11 are just spectators. However, the absence of an affect on Pd speciation with ligand **10b** once the amine is added indicates that they may not be innocuous. Instead, the active species may slowly filter into the catalytic cycle, a process that is consistent with the kinetic studies described in Figure 5.

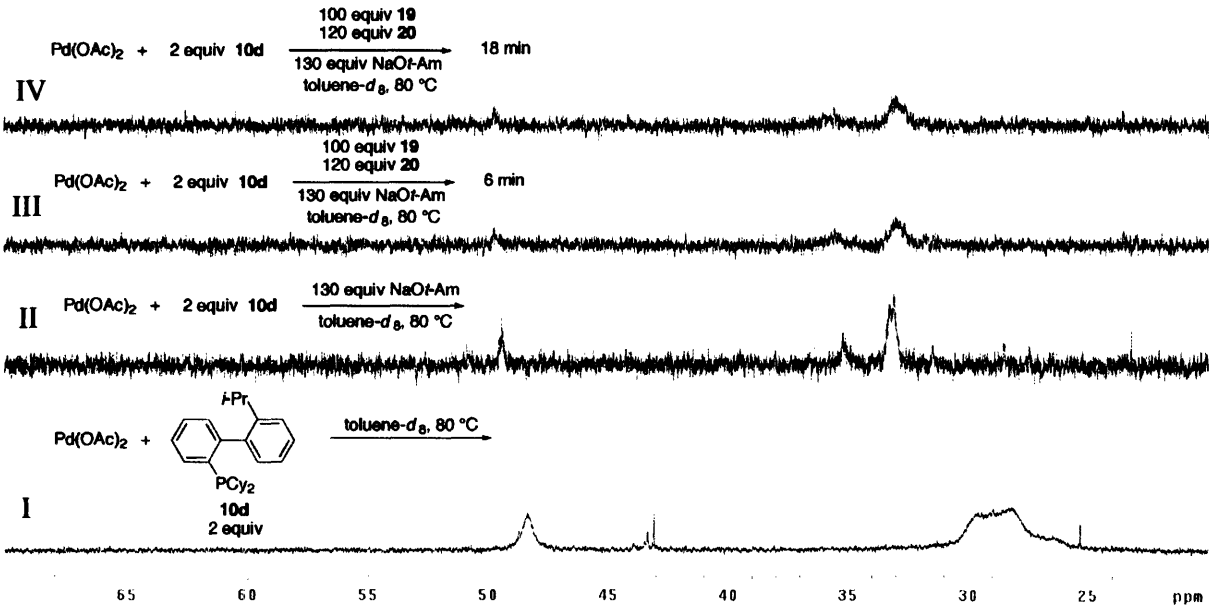

Figure 11. ^{31}P NMR spectra of a (I) solution containing $Pd(OAc)_2$ (18 mM), **10d** (36 mM) in 1 mL of toluene-d_8 at 80 °C, (II) solution containing $Pd(OAc)_2$ (18 mM), **10d** (36 mM), and NaO*t*-Am (2.0 M) in 1 mL of toluene-d_8 at 80 °C, (III) solution of the catalytic reaction 6 min after the simultaneous addition of **19** (0.51 M) and **20** (1.5 M) to the mixture in II, and (IV) solution of the catalytic reaction 18 min after the addition of **19** and **20** to the mixture in II.

Since the two classes of ligands afford two distinct patterns both in the kinetic studies as well as the spectroscopic studies, it was hypothesized that the origins of this divergence arise from the formation of palladacycle intermediates.[5a] The possible palladacycles that may form with these ligands are shown in Figure 12. In the first case, a six-membered palladacycle is formed through a process described in Scheme 5, which involves an attack on the coordinated Pd(II) center by the bottom ring of the biaryl ligand.[43] Significantly, a similar palladacycle has been successfully employed as a single-component catalyst.[44] In the second case, the top ring of the biaryl ligand attacks the Pd(II) center in a Friedel-Crafts like fashion generating a four-membered ring palladacycle.[45] Furthermore, on the basis of several studies demonstrating the potential of Pd(II)-mediated cleavage of sp^3 C-H bonds, the third structure in Figure 12 is also a

potential intermediate.[46] Taking into consideration the substitution pattern of the two ligand classes, it would appear that the 2′,6′-disubstituted ligands are incapable of forming the first type of palladacycle, whereas all three types of complexes are possible with the 2′-substituted ligands.

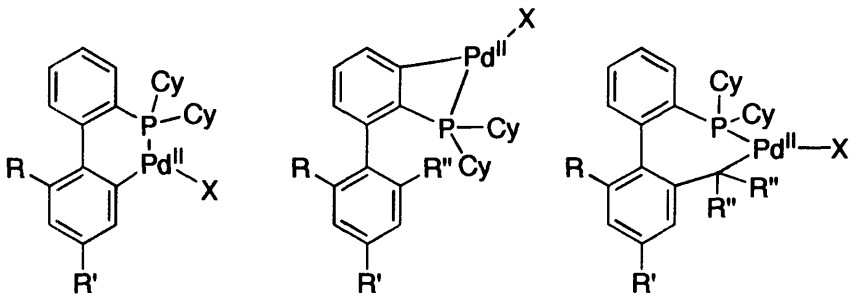

Figure 12. Structures of Potential Palladacycles.

Scheme 5. Formation of Palladacycle Intermediates.

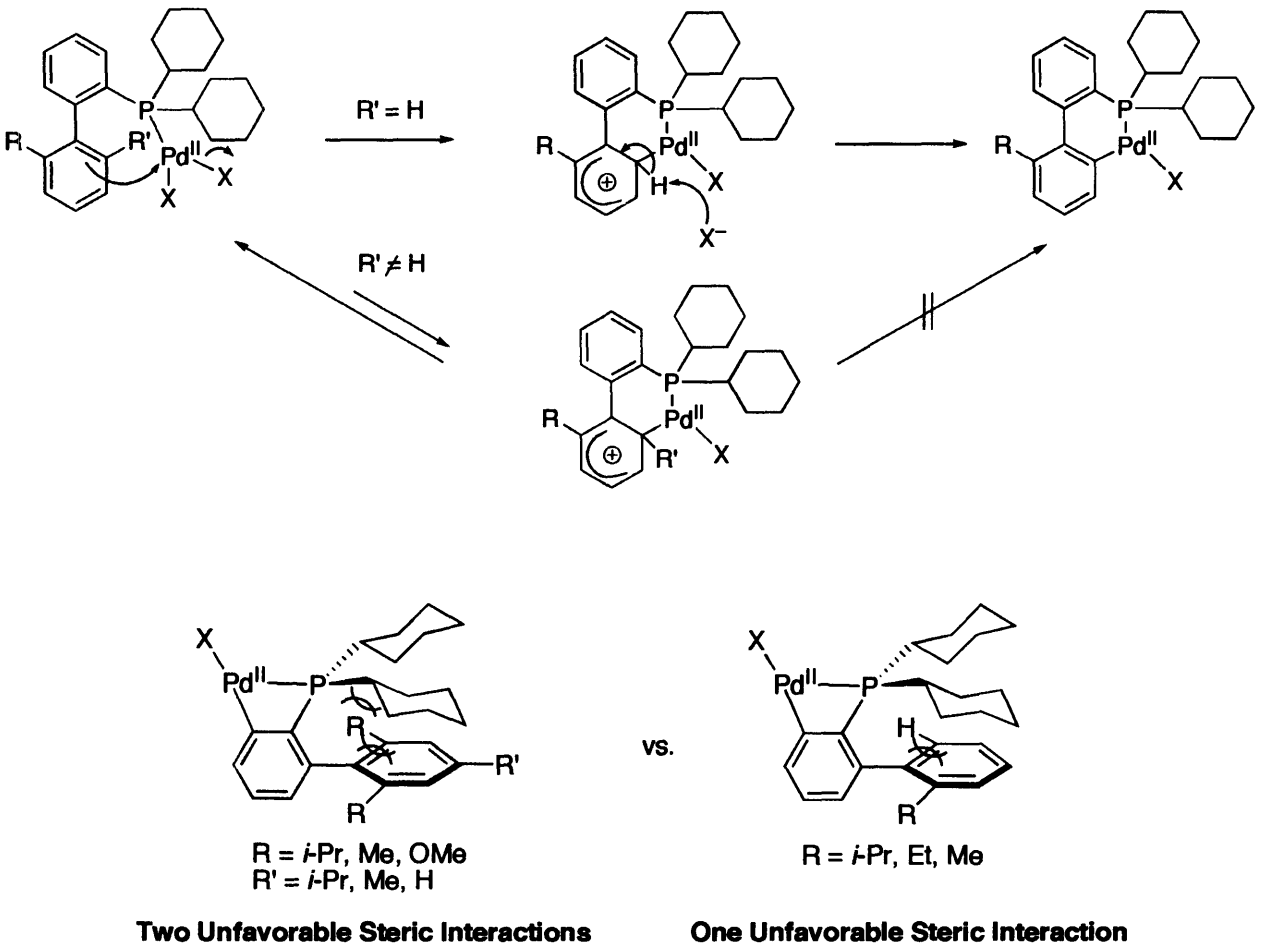

Figure 13. Unfavorable Steric Interactions within Palladacycles.

On the basis of the kinetic and spectroscopic studies, the formation of a stable palladacycle precludes the rapid activation of Pd(II) to Pd(0) through a process similar to that described in Scheme 2. In contrast, this same process can occur rapidly with complexes that do not form palladacycles. Since the main difference between the 2′,6′-disubstituted and 2′-substituted ligands is the rate of catalyst activation, the structure of the palladacycle that would be most consistent with these results is the first complex in Figure 12. However, the second palladacycle cannot be ruled out on the basis of this data alone. For example, if the four-membered ring palladacycle were to form with the 2′,6′-disubstituted ligands, two unfavorable steric interactions between the cyclohexyl groups attached to phosphorus and the two substituents on the bottom ring of the biaryl would result (Figure 13). In contrast, with 2′-substituted ligands only one unfavorable interaction would result, thus, making this complex more energetically favorable than that with the 2′,6′-disubstituted ligands.

To test this hypothesis, morpholine-d_8 (**20**-d_8) was employed as the substrate and the extent of deuterium incorporation into the bottom ring of the monophosphinobiaryl was monitored. If palladacycle formation occurs and the mechanism in Scheme 2 is consistent, then deuterium incorporation into the ligand should be observed with the 2′-substituted ligands (Scheme 6, a similar mechanism can be proposed for the four-membered ring palladacycles). Using 2′,6′-disubstituted ligands, however, deuterium incorporation should not occur since palladacycles are absent in this case. Importantly, Hartwig and Louie have postulated a similar mechanism for the formation of Pd(0) from palladacycles derived from P(*o*-tolyl)$_3$, however, relevance of these palladacycles to the catalytic process was not established.[47]

Scheme 6. Proposed Mechanism for Deuterium Incorporation into Monophosphinobiaryl Ligands.

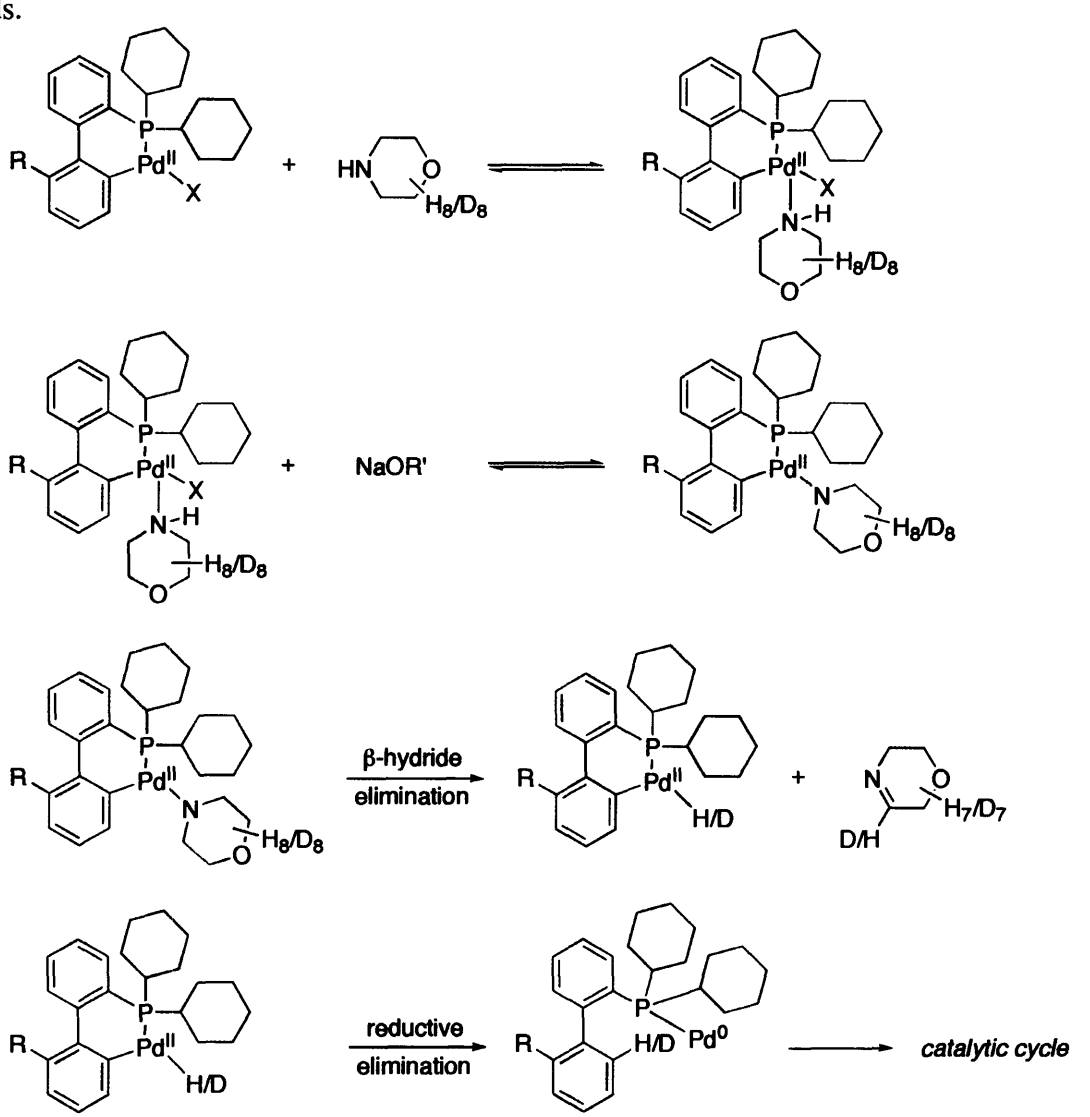

The *N*-arylation of morpholine-d_8 was performed under the standard conditions. However, 1,2-bis(diphenylphosphino)ethane (dppe) was added at the end of the reaction to sequester the Pd and facilitate the separation of the monophosphinobiaryl ligand in order to investigate the extent and placement of isotope incorporation (eq 4). Upon isolation, ^{2}H NMR, mass spectrometry, and ^{1}H NMR were used to analyze the free ligand. As indicated by ^{2}H NMR,

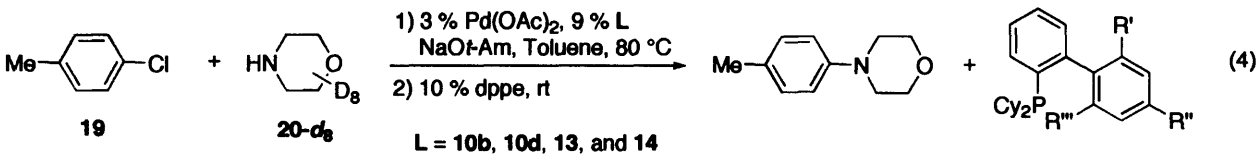

19 20-d_8 (4)

ligands **13** and **14**, both 2′,6′-disubstituted ligands, did not contain deuterium. In contrast, the ^{2}H NMR for both **10b** and **10d** displayed the presence of deuterium in the aromatic region. Furthermore, mass spectrometric analysis of the molecular ion peaks revealed that re-isolated **10d** is 26.5 % enriched with ^{2}H while **10b** is only 7.6% enriched.[46] The difference between the levels of enrichment may arise from the greater propensity of the catalyst based on **10b** to form a bis-ligated Pd(II) complex relative to that based on **10d** due to the smaller size of **10b**. Such a complex may preclude the formation of a palladacycle intermediate. The ^{1}H NMR spectrum of the re-isolated **10d** also supports the results obtained from the mass spectrometric analysis. As revealed by integration, the doublet (J = 7.5 Hz) at 6.9 ppm is the only resonance to decrease in value, which suggests that a single carbon atom has been isotopically labeled (Figure 14). Furthermore, the difference in integration between the authentic sample of **10d** and that from the re-isolated **10d** is ca. 26 %, which is identical to the value obtained from mass spectrometric analysis. Although these results do not definitively support isotope incorporation into the 6′ position (*b* in Figure 14) of the biaryl ligand, previous studies on P-aryl derivatives have shown that the deshielding effect of phosphorus on neighboring protons is most significant at the ortho position (*a* in Figure 14).[49] Thus, the formation of the first palladacycle in Figure 12, which would result in deuterium incorporation into position *b* in Figure 14 is most consistent with the previous studies on P-aryl derivatives. Taken together, these results do indeed support the hypothesis that the formation of palladacycles occurs with 2′-substituted ligands, whereas, with

2′,6′-disubstituted ligands it does not. Moreover, the isolation of isotopically-labeled ligands supports the presence of palladacycles in the catalytic reaction.

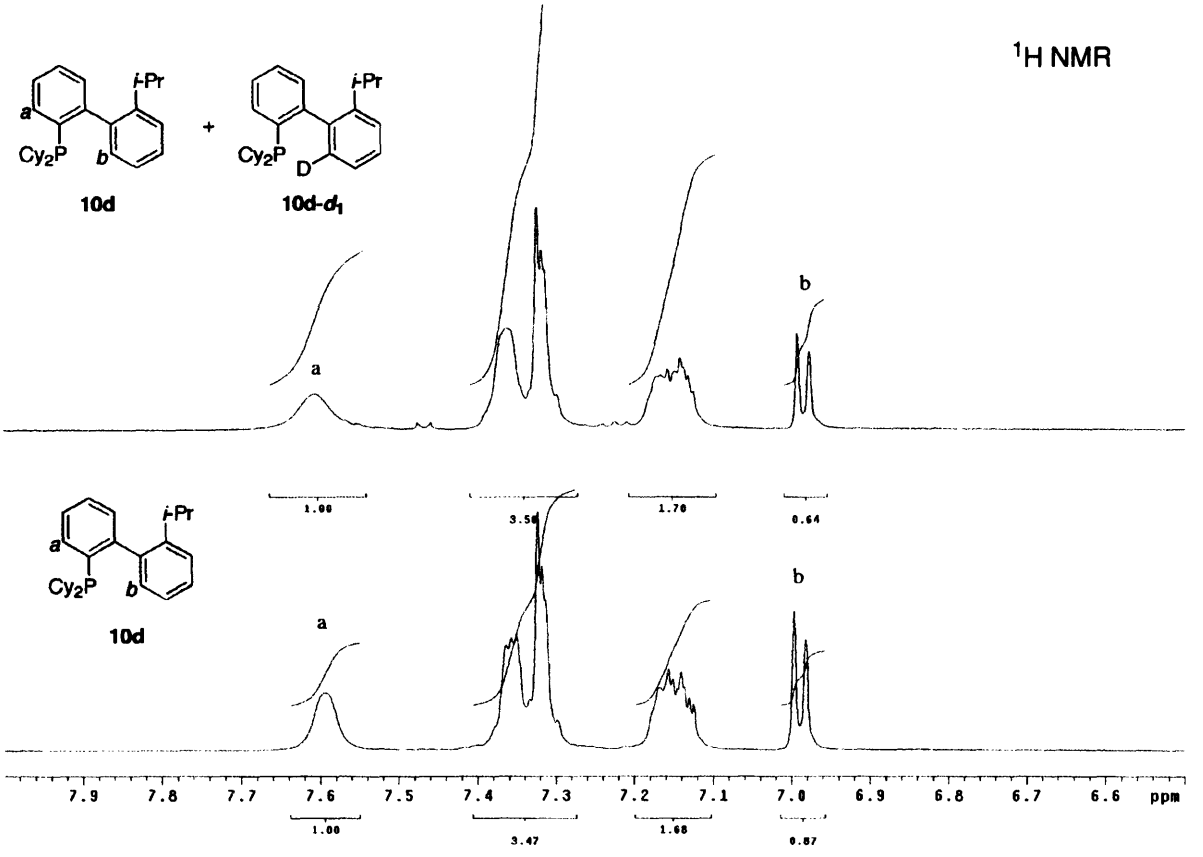

Figure 14. ^{1}H NMR of authentic **10d** (bottom) and re-isolated **10d** containing partially deuterated material (top).

Effects of Various Reducing Agents on the Rate of Pd-Catalyzed C-N Bond Forming Reactions. While the preceding sections have demonstrated that catalyst activation with systems based on the 2′,6′-disubstituted ligands occurs rapidly in the presence of a secondary amine, we wanted to ascertain which factors would facilitate the formation of a more active catalyst. Previous studies concerning the reduction of Pd(II) to Pd(0) have shown that myriad reducing

agents can be employed to promote this process.[1c] Additionally, other activation pathways have been explored in hopes of generating significant concentrations of the highly active $L_1Pd(0)$ species without the necessity to start from a Pd(II) precursor. Beller has demonstrated the utility of 1,6-diene Pd(0) monophosphine complexes (**23**) as catalysts for Suzuki-Miyaura couplings.[50] The higher activity observed with these precatalysts compared to those based on Pd(II) precursors lends credence to the rapid dissociation of the 1,6-diene which immediately produces a monoligated Pd(0) species. More recently, Hartwig has reported that Mingos-type Pd(I) dimer complexes (**24**) were very active for both the amination with various aryl chlorides and simple Suzuki-Miyaura couplings at room temperature.[51] These catalysts, however, suffered from a limited scope and short lifetime.

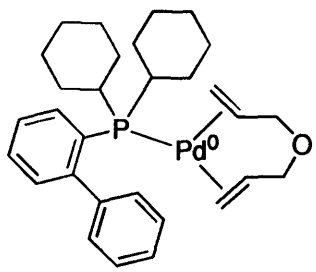

23

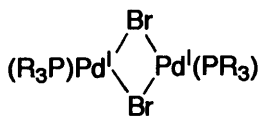

PR_3 = P(1-Ad)*t*-Bu_2, P*t*-Bu_3

24

Since catalysts derived from **13** offer both high activity as well as stability, we sought to develop a catalyst system based on a Pd(II)/**13** precursor that could be rapidly activated at room temperature. To accomplish this goal, several reducing agents were examined for their efficacy in promoting catalyst activation. The *N*-arylation of aniline was studied (eq 5) to avoid complications arising from the substrate induced reduction of Pd(II) to Pd(0). The protocol used to study the reactivity differences between various reducing agents involved incubating the Pd(II)/**13** catalyst system with the reducing agent and base for 60 min at 60 °C prior to the introduction of the aniline and aryl chloride. Plotting turnover frequency (TOF) versus the

equivalents of reducing agent relative to Pd (Figure 12) shows that both the type of reducing agent and its number of equivalents relative to Pd are critical in determining the rate of the overall *N*-arylation reaction. As evidenced by the highest TOF: equiv of reducing agent ratio, the most effective reducing agents are $PhB(OH)_2$, H_2O, *i*-Pr_2NH, and Cy_2NMe, respectively.

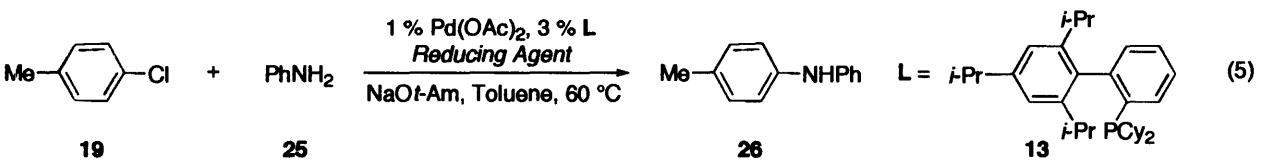

(5)

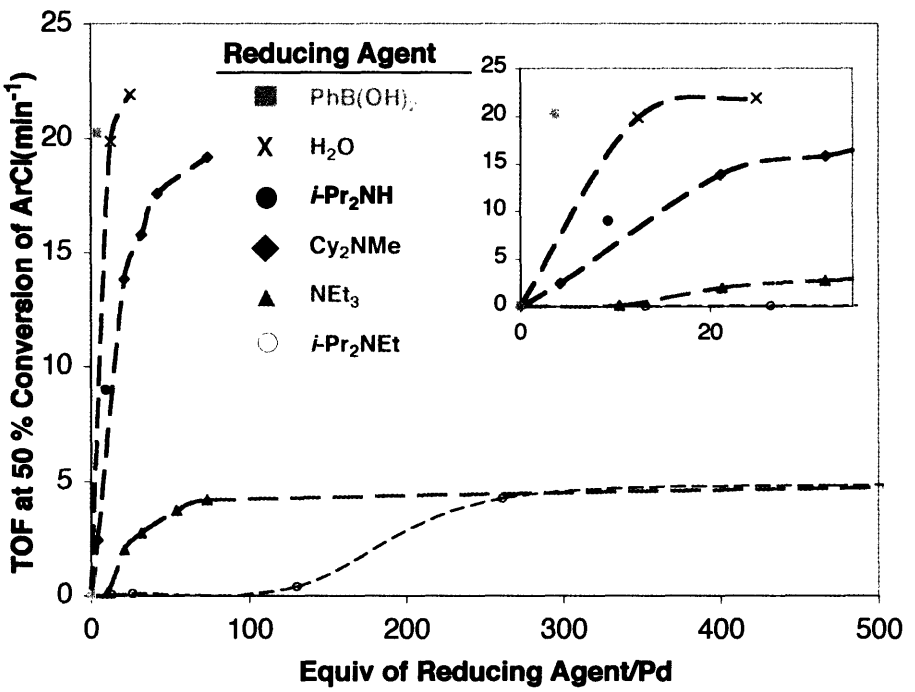

Figure 12. Turnover frequency (TOF) versus concentration of reducing agent. Conditions: $[Pd(OAc)_2]$ = 6.3 mM, [**13**] = 17.2 mM, [**19**] = 0.56 M, [**23**] = 0.85 M, [NaO*t*-Am] = 1.15 M in 1.5 mL of toluene at 60 °C. (■) $[PhB(OH)_2]$ = 14 mM, (X) = $[H_2O]$ = 0.08 – 0.16 M, (●) [*i*-Pr_2NH] = 0.06 M, (◆) $[Cy_2NMe]$ = 0.03 – 0.46 M, (▲) $[Et_3N]$ = 0.07 – 4.08 M, (o) [*i*-Pr_2NEt] = 0.08 – 3.28 M.

Further examination of these four reducing agents in the room temperature activation of the catalyst provided more detailed insight into which system was the most efficacious. In these experiments either the $Pd(OAc)_2$/**13** system or the $Pd(OAc)_2$/**13**/NaO*t*-Am combination was allowed to mix with the reducing agent at room temperature prior to the introduction of the catalyst mixture to a solution of **19**, **25**, and NaO*t*-Am in toluene at 60 °C. At room temperature, both Cy_2NMe and *i*-Pr_2NH were ineffective. More specifically, these reducing agents require extended mixing times with the catalyst at 60 °C before a significant rate enhancement is observed. In contrast, both $PhB(OH)_2$ and H_2O are highly effective reducing agents at room temperature. It is important to note that the $PhB(OH)_2$ used in these studies was recrystallized from H_2O. Since gas chromatographic measurements of the crude reaction mixture indicated an absence of biphenyl, i.e., the byproduct from the reduction of Pd(II) with $PhB(OH)_2$, the reduction of Pd(II) with this source of $PhB(OH)_2$ is most likely due to the H_2O mediated pathway. This suggests that the optimal reducing agent may indeed be H_2O.

Scheme 7. Role of H_2O as a Reducing Agent.

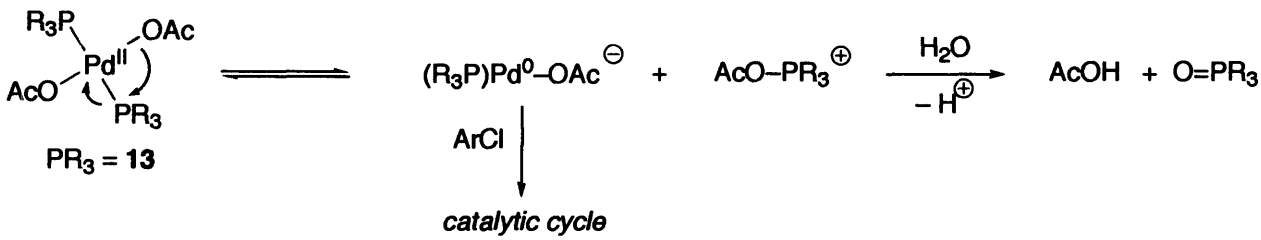

The role of H_2O in the reduction of Pd(II) to Pd(0) was investigated further on the basis of its ability to generate an active catalyst at room temperature. The observation that H_2O promotes the reduction of the $Pd(OAc)_2$/(*R*)-BINAP precatalyst was first described by Hayashi in 1992.[52] Using $^{18}OH_2$, they demonstrated that the ratio of (*R*)-BINAP(^{18}O):(*R*)-BINAP(^{16}O) increased as the reaction progressed, suggesting that an exchange occurs between $^{18}OH_2$ and the

acetate and that the source of oxygen is the acetate group. Subsequently, Amatore and Jutand explored this process more thoroughly in the case of both chelating and non-chelating ligands.[41] Although the reduction of Pd(II) to Pd(0) was not enhanced when PPh_3 was used as a supporting ligand, it was when chelating ligands such as 1,3-bis(diphenylphosphino)propane (dppp) were employed. Furthermore, their results suggested that the role of H_2O in the reduction process was to facilitate the decomposition of the phosphonium ion (Scheme 7), thereby driving the equilibrium between the $(R_3P)_2Pd(OAc)_2$ complex and the anionic palladium species forward

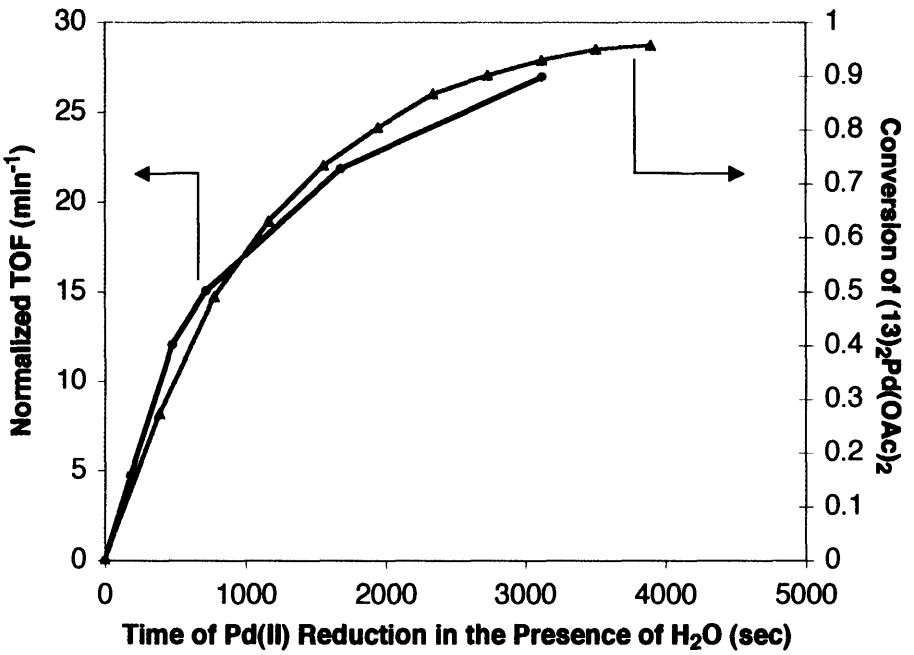

Figure 13. Time course for the reduction of $(\mathbf{13})_2Pd(OAc)_2$ in the presence of H_2O. (●) Normalized TOF (the reaction rate from the *N*-arylation of aniline using the unreduced $Pd(OAc)_2$/**13** was subtracted from the reaction rate obtained from the *N*-arylation of aniline using the same catalyst but pre-reduced with H_2O) vs. time of $Pd(OAc)_2$/**13** reduction in the presence of H_2O. (▲) Conversion of $(\mathbf{13})_2Pd(OAc)_2$ in the presence of H_2O versus time.

through the formation of the phosphine oxide. These findings support Hayashi's in the sense that H_2O facilitates the formation of acetic acid, which then exchanges with the acetate ligand on Pd(II) and undergoes the reduction process.

In regards to the Pd(II)/**13** catalyst system, monitoring the intensity of the ^{31}P NMR resonance at 41.2 ppm (Figure 9), which corresponds to *trans*-(**13**)$_2$Pd(OAc)$_2$, once H_2O had been added to the solution indicates an immediate decay in the concentration of this species with the concomitant formation of the phosphine oxide of **13**. The reduction process is complete in ca. 60 min (Figure 13, ▲). In a separate experiment, aliquots were removed from a mixture containing Pd(OAc)$_2$, 3 equiv of **13**, and 10 equiv of H_2O in toluene at various time points and added to a mixture containing **19**, **25**, and NaO*t*-Am in toluene at 60 °C. The progress of the reaction was then monitored by reaction calorimetry. Plotting the normalized TOF versus time of incubation between the Pd(II)/**13** precatalyst and H_2O indicates that reaction rate is directly proportional to the time required for the reduction of the Pd(II) precursor to occur (Figure 13, ●). These studies suggest that pre-reducing the Pd(II) precatalyst with H_2O may be a viable means to generate a highly active catalyst, however, additional work is necessary in order to fully exploit the potential of this catalyst activation process.

Summary

The Pd/monophosphinobiaryl catalyst system has been applied to a variety of C–C, C–N, and C–O cross-coupling reactions, and this mechanistic study of the C–N bond forming reaction between secondary cyclic amines and aryl chlorides provides insights into the factors that control catalyst activity and stability. Of significance, we have complemented the kinetic study of the *N*-

arylation reaction with direct spectroscopic evidence displaying the difference in Pd speciation between the various catalysts. Such data facilitated the elucidation of the detailed mechanism of catalyst activation with Pd(II) precatalysts and also revealed that the source of slow catalyst activation with catalysts based on 2′-substituted ligands may potentially reside in the propensity of these catalysts to form palladacycles. Thus, this study demonstrates that there exists a direct relationship between the steady-state concentration of active Pd and size and substitution pattern of monophosphinobiaryl ligands used in the amination of aryl chlorides. Furthermore, this study highlights the important role of catalyst activation in achieving maximum reaction rates from a given catalyst system.

Experimental Section

General Considerations: Reagents. $Pd(OAc)_2$ and ligand **11a** were purchased from Strem Chemical Co. and used without further purification. Ligands **10b–10d** and **12–14** were prepared as previously described.[26] NaO*t*-Am was purchased from Aldrich and used without further purification. *p*-Chlorotoluene **19** was purchased from Aldrich and distilled from CaH_2 prior to use. Morpholine **20** was also purchased from Aldrich and distilled from CaH_2 prior to use. Morpholine-d_8 (**20-d_8**) was purchased from Cambridge Isotope Laboratories, Inc. All reagents were handled and stored under nitrogen in a Vacuum Atmosphere glovebox. Toluene was purchased from J.T. Baker in CYCLE-TAINER® solvent delivery kegs, which were vigorously purged with argon for 2 h, and further purified by passing the solvent through two packed columns of neutral alumina and copper (II) oxide under argon pressure.

Procedure for the Kinetics of Sequential Reactions. Reactions were performed in a stirred 16 mL screw capped vial with a PTFE septa under a positive pressure of argon. The reaction vial (typically 2.1 mL or 4.2 mL reaction volume) was placed in the sample compartment of a Omnical SuperCRC reaction calorimeter with an empty vial placed in the reference compartment. The stirred vial was maintained under isothermal conditions at 353 K. The calorimeter recorded the difference in heat flows from the sample vs. reference cells at data collection rates up to 60 min^{-1}. A typical reaction was conducted by adding four identical aliquots of **19** (4 x $[\mathbf{19}]_o$ = 0.15 M) in four different intervals to a thermally equilibrated reaction mixture consisting of 4.2 mM of $Pd(OAc)_2$, 9.2 mM of ligand, 0.8 M of NaO*t*-Am, 0.75 M of **20** and dodecane as an internal standard. Another reaction protocol consisted of adding a mixture of **20** ($[\mathbf{20}]_o$ = 0.75 M) and the first aliquot of **19** ($[\mathbf{19}]_o$ = 0.15 M) to the thermally equilibrated catalyst/NaO*t*-Am mixture and allowing for complete conversion of the aryl chloride before the next aliquot of **19** was added (a total of four identical aliquots of **19** were added to the reaction). The reaction mixture was in each case an orange solution.

Kinetic Data Analysis. A similar analysis to that described in Ch. 1 was used to for the multiple reaction sequence described here, albeit, the analysis was performed on each individual reaction in a sequence. An energy balance around the reaction vessel demonstrates that for the case of a single reaction occurring, the reaction heat flow, q, is proportional to the reaction rate, r, where ΔH_{rxn} is the heat of reaction and V is the reaction volume (eq 6).

$$q = \Delta H_{rxn} \cdot V \cdot r \qquad (6)$$

The heat of reaction from integration of the observed heat flow vs. time curves provided an average value of 188 kJ/mole ± 5% for all four consecutive reactions.

Monitoring the Catalytic Reaction by ^{31}P NMR. $Pd(OAc)_2$ (8.1 mg, 0.036 mmol) and **13** (52 mg, 0.11 mmol) were added to a 5 mL vial and capped with a PTFE septum and opentop screwcap. The vial was evacuated and backfilled with argon 3x prior to bringing the sample inside a nitrogen-filled glovebox. Once inside the glovebox, toluene (1 mL) was added, and the solution was allowed to stir until dissolution was complete. To a NMR tube containing NaO*t*-Am (220 mg, 2.0 mmol) and toluene (0.5 mL) was added 0.5 mL of the solution above. The NMR tube was capped with a PTFE septum and opentop screwcap, the tube was shaken, and the contents were analyzed by ^{31}P NMR at 60 °C. The concentrations of the *trans*-(**13**)$_2$Pd(OAc)$_2$ complex and free **13** were determined by integrating with respect to PPh_3, which was used as an internal standard in a capillary tube. To the NMR tube at 60 °C was than added a mixture of **19** (65 mg, 0.51 mmol) and **20** (130 mg, 1.5 mmol) via syringe and data was collected every 3 min. A similar procedure was used for the catalyst based on ligand **10d**. The procedure used to incubate the catalyst with the amine, however, is slightly different. In this case, **20** (130 mg, 1.5 mmol) was added to the NMR tube and the contents were equilibrated at 60 °C for 60 min in the spectrometer prior to analysis by ^{31}P NMR.

The full ^{31}P NMR spectrum of the mixture containing $Pd(OAc)_2$ (8.1 mg, 0.036 mmol) and **13** (52 mg, 0.11 mmol) is shown below.

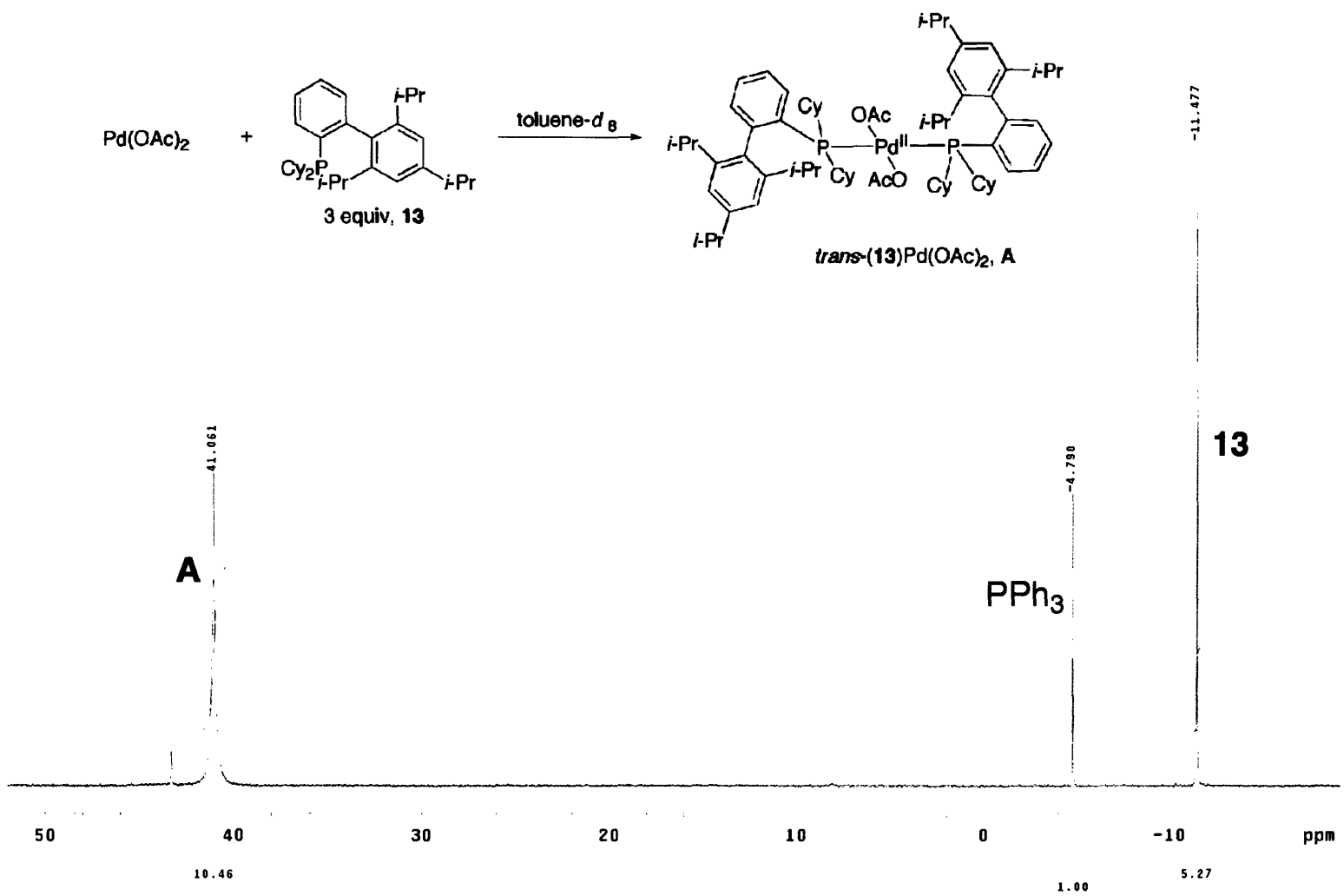
Pd(OAc)2
+
i-Pr
Cy2P
i-Pr
i-Pr
3 equiv, 13
toluene-d 8
Cy
OAc
i-Pr
i-Pr
i-Pr
P
Pd
P
i-Pr
Cy
AcO
Cy
Cy
i-Pr
i-Pr
trans-(13)Pd(OAc)2, A
-11.477
41.061
-4.790
A
13
PPh3
50
40
30
20
10
0
-10
ppm
10.46
1.00
5.27

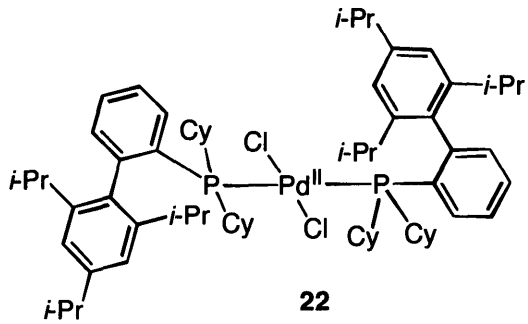

22

Preparation of *trans*-(13)$_2$PdCl$_2$ (22). A 50 mL Schlenk flask was charged with $(MeCN)_2PdCl_2$ (105 mg, 0.40 mmol) and **13** (395 mg, 0.83 mmol). The flask was evacuated and backfilled with argon 3x prior to the addition of toluene (5 mL). The mixture was allowed to stir at room temperature overnight prior to the removal of solvent under vacuum. Trituration of the resulting residue with Et_2O (30 mL) followed by filtration afforded a yellow solid, which was dissolved in $CHCl_3$ and layered with MeOH to obtain the title compound as pure yellow crystals (322 mg, 71 %). ^{1}H NMR (CH_2Cl_2): δ 8.38 (br s, 2 H), 7.39 (m, 4 H), 7.04 (m, 6 H), 2.92 (sept, 4 H, C**H**$(CH_3)_2$), 2.80 – 0.3 (br m, 41 H). ^{31}P {^{1}H} NMR: δ 45.5.

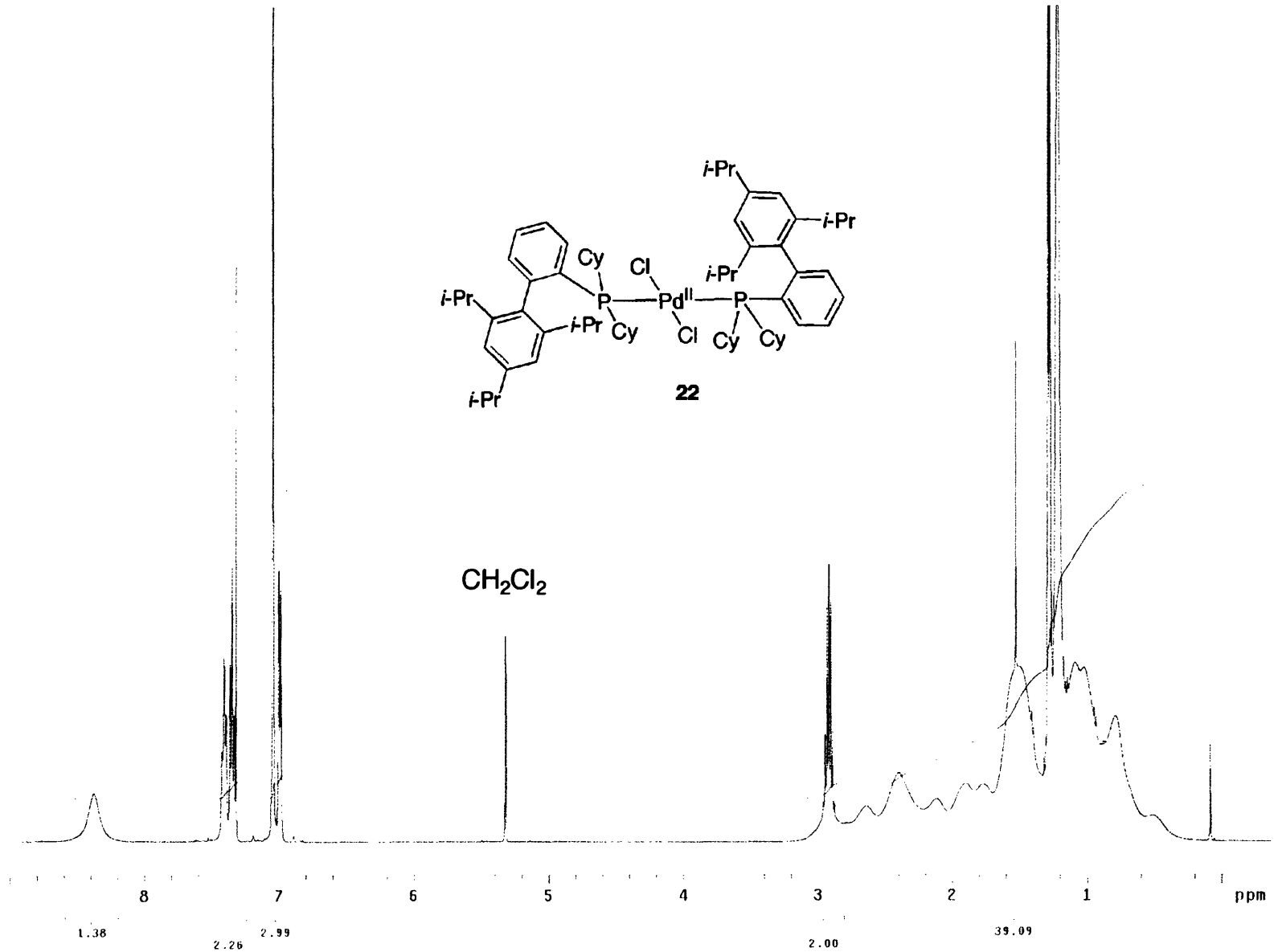
i-Pr
i-Pr
i-Pr
Cy
Cl
P
Pd
II
P
i-Pr
i-Pr
Cy
Cl
Cy
Cy
i-Pr
22
CH2Cl2
8
7
6
5
4
3
2
1
ppm
1.38
2.26
2.99
2.00
39.09

XPhos2PdCl2-31P

expl s2pul

SAMPLE		DEC. & VT	
date	Apr 23 2005	dfrq	300.101
solvent	CD2Cl2	dn	H1
file	/data/export/~	dpwr	39
home/slbuch/4es/mr~		dof	0
hat/XPhos2PdCl2-31~		dm	yyy
	P.fid	dmm	w
ACQUISITION		dmf	11000
sfrq	121.485	PROCESSING	
tn	P31	lb	1.00
at	0.800	wtfile	
np	128000	proc	ft
sw	80000.0	fn	not used
fb	44000		
bs	16	werr	
tpwr	62	wexp	
pw	10.0	wbs	
dl	0.250	wnt	
tof	2337.3		
nt	256		
ct	130		
alock	n		
gain	not used		
FLAGS			
il	n		
in	n		
dp	y		
DISPLAY			
sp	-1822.5		
wp	10932.6		
vs	151		
sc	0		
wc	250		
hzmm	43.73		
is	354.40		
rfl	37148.4		
rfp	0		
th	20		
ins	100.000		
nm no ph			

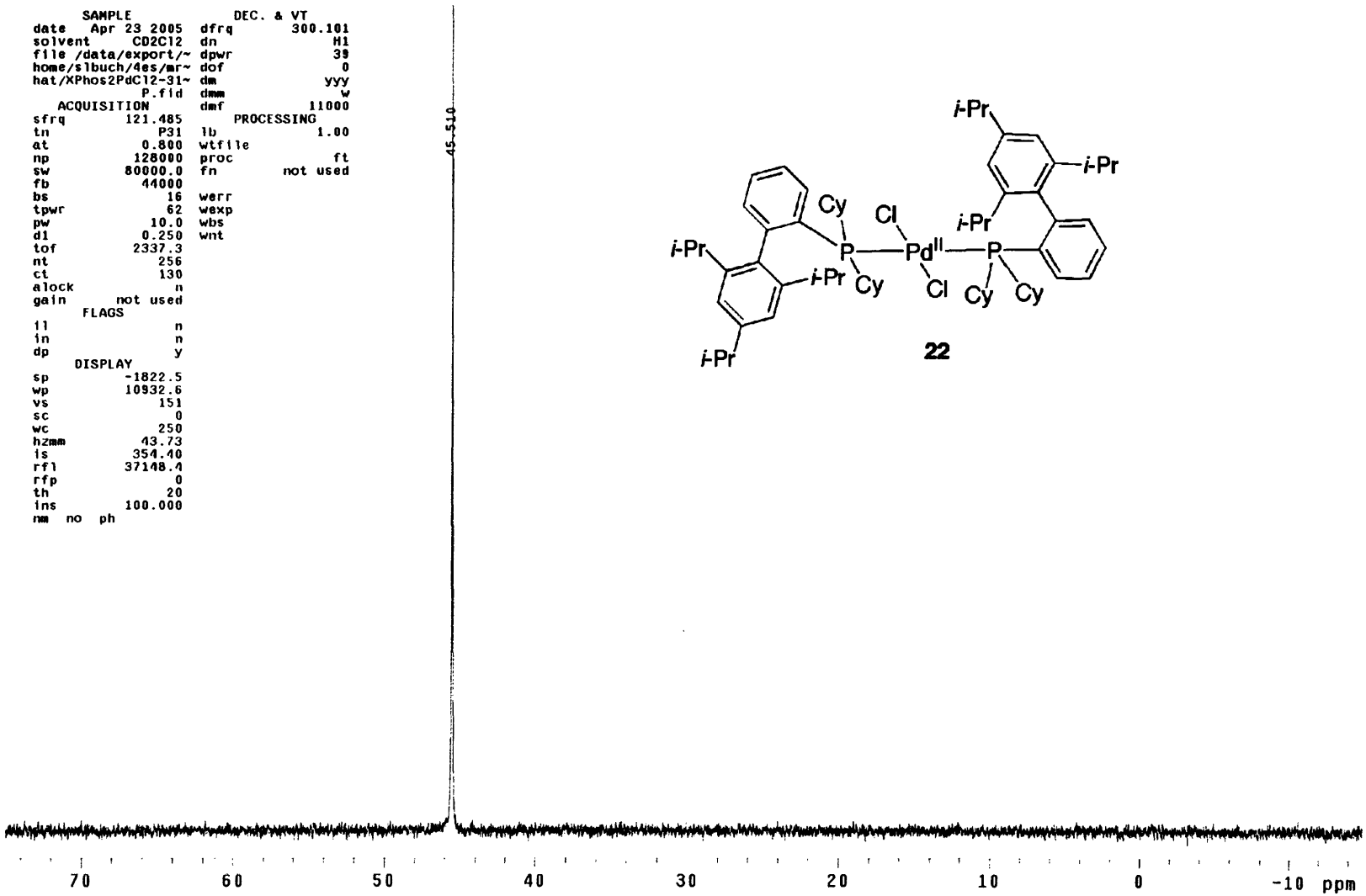

22

Isolation of Ligand After the *N*-Arylation Reaction. $Pd(OAc)_2$ (16.1 mg, 0.07 mmol) and **10b** (69.8 mg, 0.19 mmol) were added to an oven-dried Schlenk tube containing a Teflon-coated stir bar. The tube was capped with a Teflon-screwcap and evacuated and backfilled with argon 3x. Once the tube was brought into a nitrogen-filled glovebox, toluene (1 mL) was added and the solution was allowed to stir until complete dissolution. NaO*t*-Am (310 mg, 2.81 mmol) was then added to this mixture along with toluene (1 mL). The tube was recapped and brought outside the glovebox and placed in an 80 °C oil bath with stirring. After allowing the mixture to equilibrate at 80 °C for 60 min the screwcap was removed and replaced with a rubber septum under a positive flow of argon. To this mixture was then added **19** (180 mg, 1.42 mmol) and **20-d_8** (205 mg, 2.15 mmol) via syringe. The rubber septum was replaced with the screwcap and the reaction mixture was allowed to stir at 80 °C for 8 h. The tube was removed from the oil bath and allowed to cool to room temperature. The screwcap was removed under a positive flow of argon and dppe (150 mg, 0.38 mmol) was added. The resulting mixture was allowed to stir at room temperature overnight. The contents were then diluted with EtOAc (5 mL) and filtered through a pad of Celite. The filtrate was concentrated *in vacuo* and chromatographed on silica gel (30 g) using a 95:5 mixture of hexanes:Et_2O as the eluent, which afforded **10b** (37 mg, 53 % recovery). A similar procedure was used for catalysts based on **10d** (42 mg, 60 % recovery), **13** (53 mg, 62 % recovery), and **14** (28 mg, 40 % recovery). The ^2H NMR (CH_2Cl_2) for **10b** and **10d** in addition to the EI-MS data for **10d** are shown on the following pages.

^2H NMR

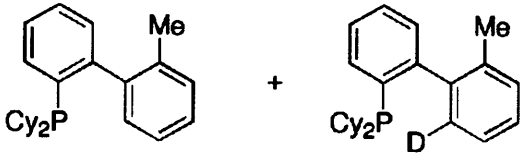

10b **10b-d_1**

$CD_2Cl_2/CHDCl_2$

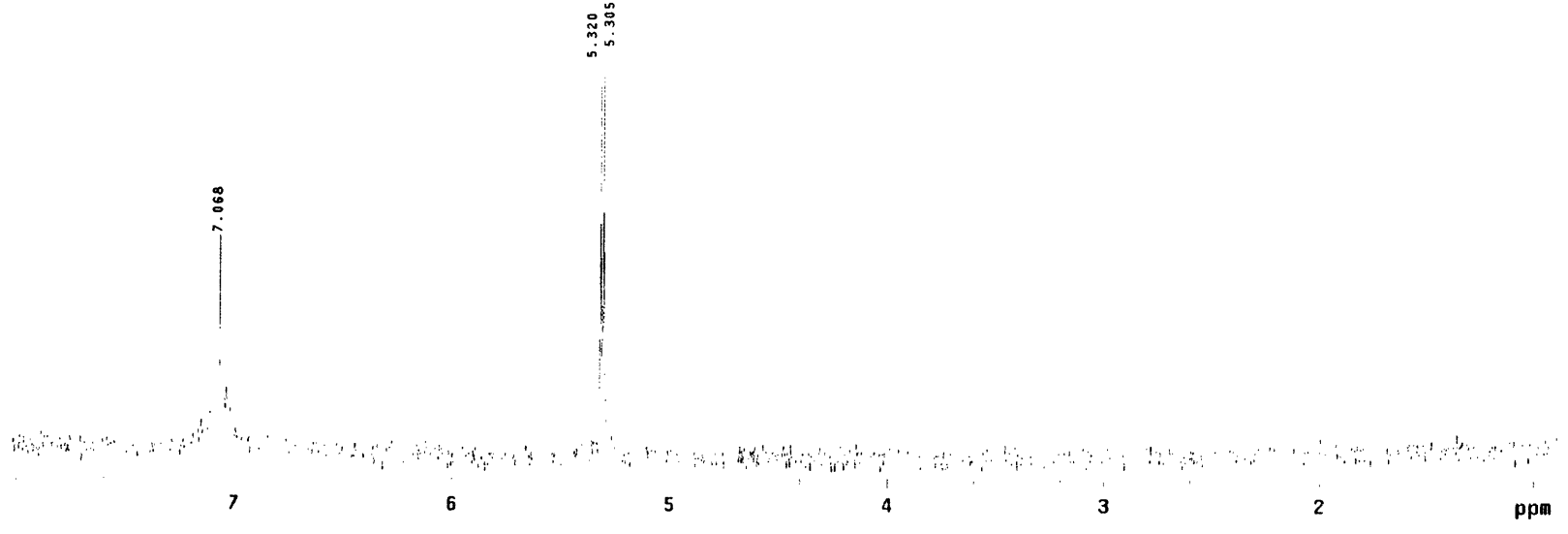

^{2}H NMR

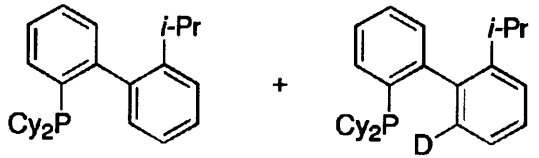

10d

+

10d-d_1

$CD_2Cl_2/CHDCl_2$

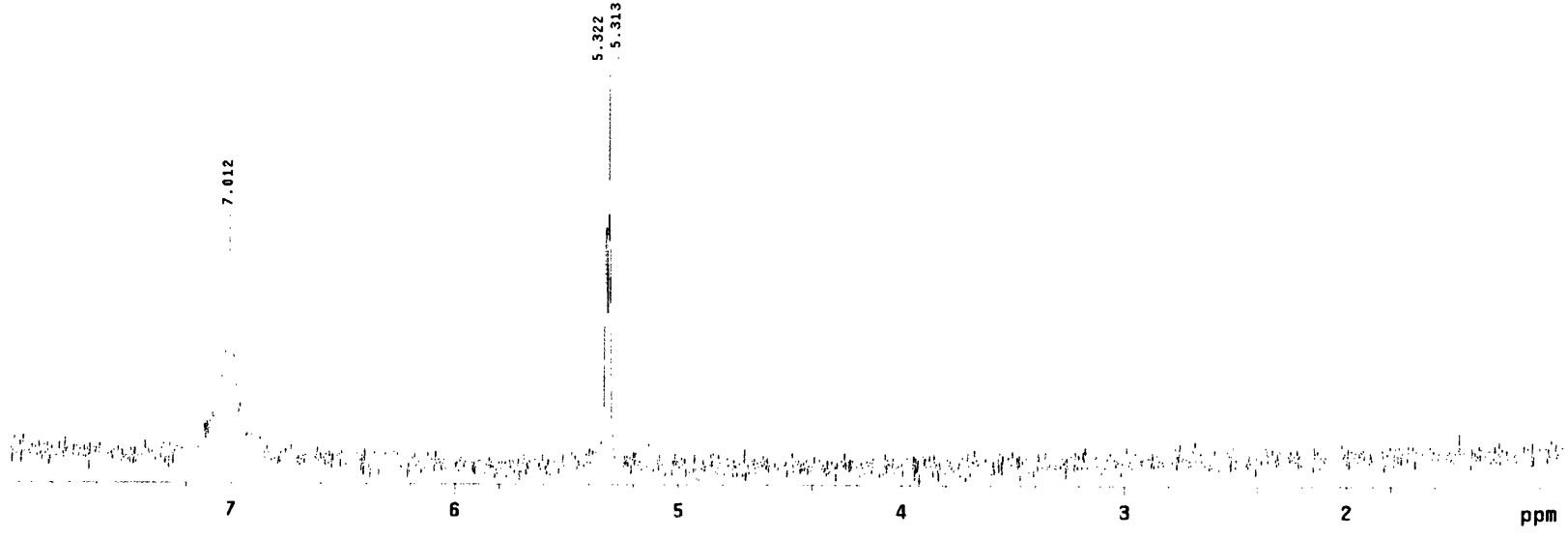

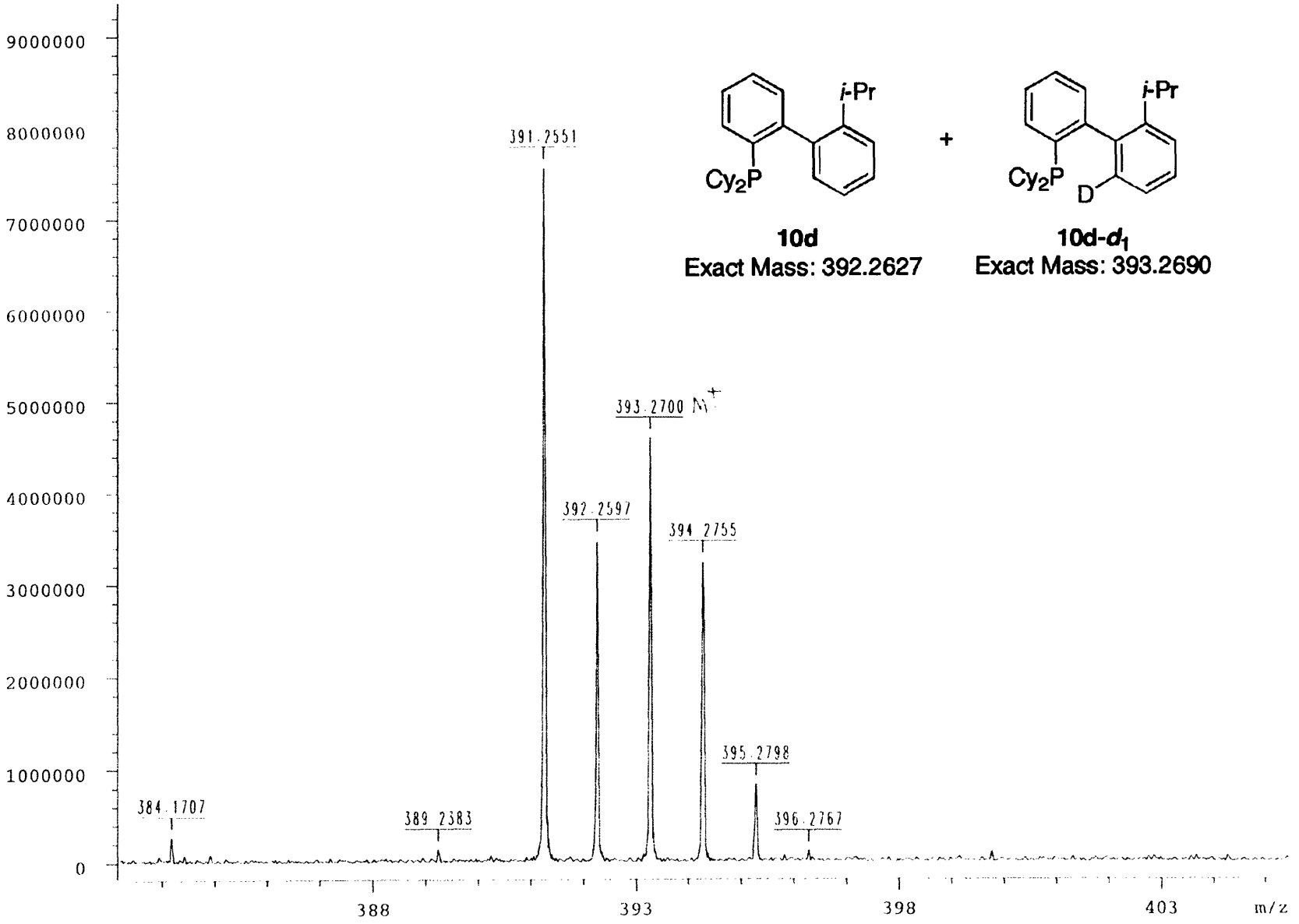
9000000
8000000
7000000
6000000
5000000
4000000
3000000
2000000
1000000
0
384.1707
389.2383
391.2551
392.2597
393.2700
394.2755
395.2798
396.2767
388
393
398
403
m/z
i-Pr
Cy2P
+
i-Pr
Cy2P
D
10d
Exact Mass: 392.2627
10d-d1
Exact Mass: 393.2690

Kinetics of the *N*-Arylation of Aniline (25) Using Pd/13 Precatalyst in the Presence of Cy_2NMe: $Pd(OAc)_2$ (10 mg, 0.04 mmol) and **13** (56 mg, 0.12 mmol) were added to a 5 mL vial which was then capped with a PTFE septum and opentop screwcap. The vial was evacuated and backfilled with argon 3x and brought inside a nitrogen-filled glovebox. Once inside the glovebox, toluene (1 mL) was added to the vial and the mixture was allowed to stir until complete dissolution. From this mixture 250 μL was removed via syringe and added to a 16 mL reaction calorimeter vial containing NaO*t*-Am (225 mg, 2.04 mmol), Cy_2NMe (92.0 mg, 0.47 mmol), and toluene (1.25 mL). The vial was capped with a PTFE septum and opentop screwcap and brought outside the glovebox and placed into a reaction calorimeter, preheated to 80 °C, under a positive flow of argon. The contents of the reaction vessel were allowed to equilibrate inside the calorimeter for 60 min before a mixture of **19** (127 mg, 1.00 mmol) and **25** (140 mg, 1.50 mmol) were added via a syringe that had simultaneously been thermally equilibrated in the calorimeter along with the reaction vessel. The temporal heat flow was monitored every 3 sec.

Monitoring the Reduction of *trans*-$(13)_2Pd(OAc)_2$ in the Presence of H_2O by ^{31}P NMR: $Pd(OAc)_2$ (10 mg, 0.04 mmol) and **13** (56 mg, 0.12 mmol) were added to a 5 mL vial, which was then capped with a PTFE septum and opentop screwcap. The vial was evacuated and backfilled 3x with argon and brought inside the glovebox. Toluene (0.5 mL) was then added and the mixture was allowed to stir until complete dissolution. The contents of the vial were removed and placed in a NMR tube. The vial was rinsed with toluene (0.5 mL), which was then added to the NMR tube. The NMR tube was capped with a PTFE septum and opentop screwcap and placed in the spectrometer, which was maintained at 20 °C. Upon obtaining a ^{31}P NMR spectrum for the initial mixture, H_2O (5 mg, 0.28 mmol) was injected into the tube via syringe and the reaction was monitored every 6.5 min.

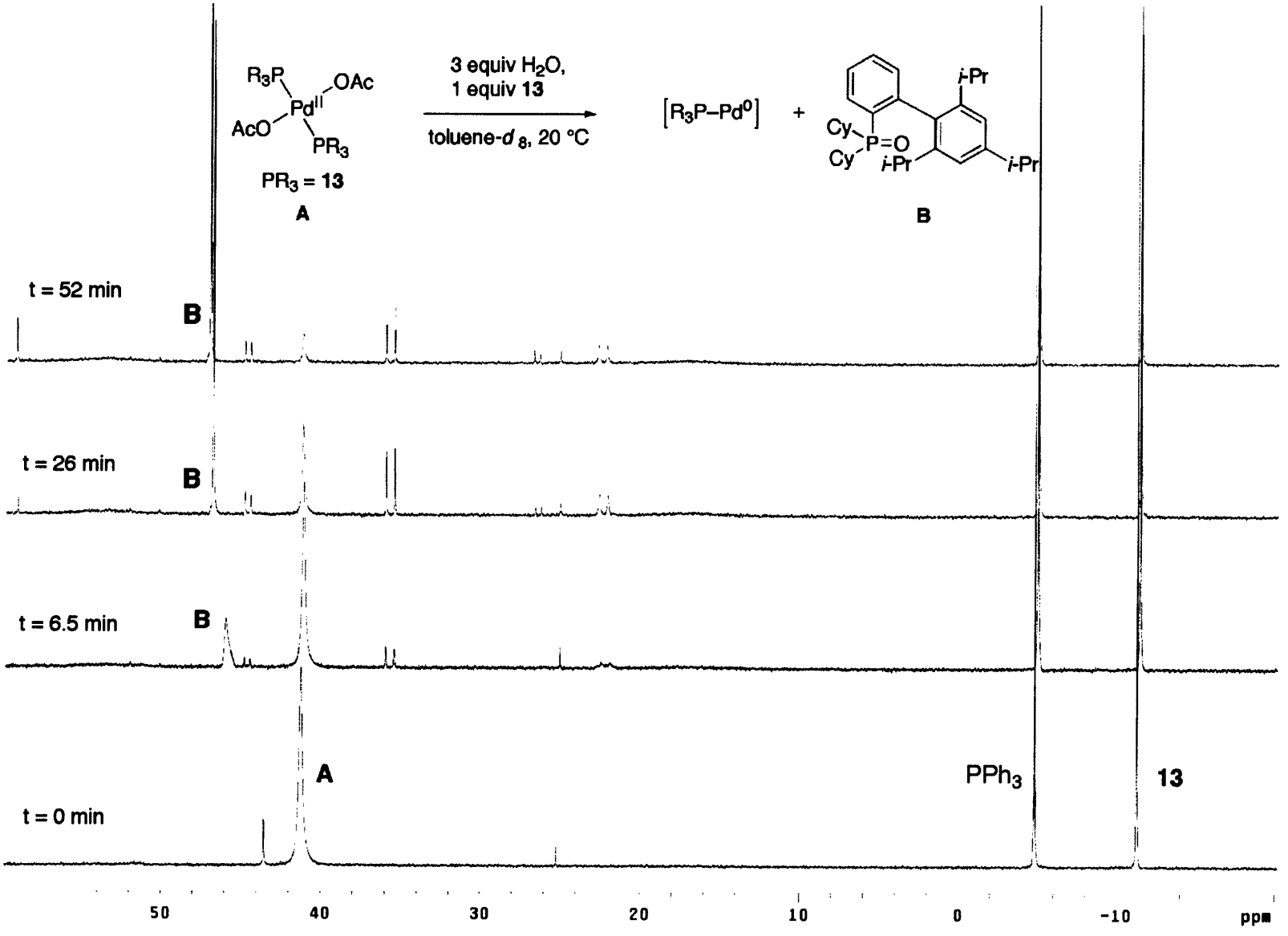
R3P
OAc
Pd(II)
AcO
PR3
PR3 = 13
A
3 equiv H2O,
1 equiv 13
toluene-d8, 20 °C
[R3P–Pd0]
+
i-Pr
Cy
P=O
Cy
i-Pr
i-Pr
B
t = 52 min
B
t = 26 min
B
t = 6.5 min
B
A
t = 0 min
PPh3
13
50
40
30
20
10
0
-10
ppm

Kinetics of *N*-Arylation of Aniline (25) Using Pd/13 Precatalyst in the Presence of H_2O: $Pd(OAc)_2$ (10 mg, 0.04 mmol) and **13** (56 mg, 0.12 mmol) were added to a 5 mL vial which was then capped with a PTFE septum and opentop screwcap. The vial was evacuated and backfilled with argon 3x and toluene (1 mL) was added. The mixture was allowed to stir at room temperature under a postive flow of argon until complete dissolution. To this mixture was added H_2O (5 mg, 0.28 mmol), which had been degassed by bubbling argon through a flask containing H_2O overnight. The resulting mixture was allowed to stir at room temperature for various amounts of time. At a given time point, 250 μL of this solution was removed via syringe and placed in a calorimeter preheated to 60 °C. The contents of the syringe were allowed to thermally equilibrate at 60 °C for 30 s prior to their addition to a reaction vial containing **19** (127 mg, 1.00 mmol), **25** (140 mg, 1.50 mmol), and NaO*t*-Am (225 mg, 2.04 mmol) in toluene (1.25 mL), which had been thermally equilibrated for 60 min at 60 °C under a positive flow of argon. The resulting temporal heat flow was monitored every 3 sec.

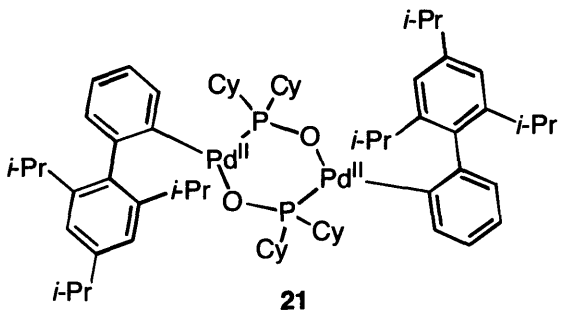

21

X-ray Structure Data for 21.

Table 2..

Identification code	04024	
Empirical formula	$C_{73}H_{110}O_4P_2Pd$	
Formula weight	1175.86	
Temperature	194(2) K	
Wavelength	0.71073 Å	
Crystal system	Monoclinic	
Space group	P2(1)/c	
Unit cell dimensions	a = 14.9487(10) Å	a= 90°.
	b = 14.1546(10) Å	b= 94.6670(10)°.
	c = 16.9735(11) Å	g = 90°.
Volume	3579.6(4) $Å^3$	
Z	2	
Density (calculated)	1.091 Mg/m^3	
Absorption coefficient	0.345 mm^{-1}	
F(000)	1260	
Crystal size	0.90 x 0.22 x 0.17 mm^3	
Theta range for data collection	1.88 to 23.28°.	
Index ranges	-16<=h<=16, -15<=k<=11, -18<=l<=18	
Reflections collected	15849	
Independent reflections	5156 [R(int) = 0.0188]	
Completeness to theta = 23.28°	99.9 %	
Absorption correction	SADABS	
Refinement method	Full-matrix least-squares on F^2	
Data / restraints / parameters	5156 / 0 / 423	
Goodness-of-fit on F^2	1.030	
Final R indices [I>2sigma(I)]	R1 = 0.0251, wR2 = 0.0662	

R indices (all data)	R1 = 0.0268, wR2 = 0.0675
Largest diff. peak and hole	0.647 and -0.318 e.Å^{-3}

Table 3. Atomic coordinates (x 10^4) and equivalent isotropic displacement parameters (Å^{2}x 10^3). U(eq) is defined as one third of the trace of the orthogonalized U^{ij} tensor.

	x	y	z	U(eq)
O	-605(1)	9209(1)	-378(1)	30(1)
P(2)	-217(1)	8739(1)	387(1)	23(1)
Pd(1)	967(1)	9508(1)	916(1)	22(1)
C(1)	1438(1)	8497(2)	1652(1)	23(1)
C(2)	2308(2)	10586(2)	1997(1)	28(1)
C(3)	2285(1)	8802(2)	1957(1)	24(1)
C(4)	2618(1)	9742(2)	1674(1)	25(1)
C(5)	-975(2)	9426(2)	1753(1)	33(1)
C(6)	2686(2)	11445(2)	1776(1)	35(1)
C(7)	1098(2)	7672(2)	1969(1)	28(1)
C(8)	2446(2)	7452(2)	2821(1)	36(1)
C(9)	2789(2)	8284(2)	2536(1)	32(1)
C(10)	1602(2)	7154(2)	2544(1)	33(1)
C(11)	-1722(2)	9354(2)	2320(2)	39(1)
C(12)	-2036(2)	8810(2)	651(2)	36(1)
C(13)	-1102(1)	8690(2)	1089(1)	26(1)
C(14)	3291(2)	9778(2)	1134(1)	29(1)
C(15)	3642(2)	10648(2)	948(1)	34(1)
C(16)	-2650(2)	9442(2)	1884(2)	44(1)
C(17)	3653(2)	8879(2)	780(1)	36(1)
C(18)	3362(2)	11489(2)	1265(1)	36(1)
C(19)	3839(2)	12408(2)	1079(2)	50(1)
C(20)	4635(2)	8715(2)	1063(2)	63(1)
C(21)	-2774(2)	8727(2)	1215(2)	46(1)
C(22)	3532(2)	8884(2)	-124(2)	56(1)
C(23)	3249(2)	13216(2)	880(3)	80(1)

C(24)	4540(3)	12659(3)	1723(3)	110(2)
C(26)	1633(2)	10574(2)	2629(1)	33(1)
C(27)	-863(2)	7041(2)	-267(1)	29(1)
C(28)	-2(1)	7512(2)	99(1)	25(1)
C(29)	745(2)	7474(2)	-470(1)	33(1)
C(30)	876(2)	11292(2)	2467(2)	45(1)
C(31)	2118(2)	10718(2)	3452(2)	49(1)
C(34)	904(2)	6463(2)	-743(2)	38(1)
C(35)	46(2)	6022(2)	-1117(2)	40(1)
C(36)	-686(2)	6040(2)	-548(2)	36(1)
C(61)	3108(5)	6252(4)	216(4)	135(3)
C(62)	3813(3)	6040(4)	836(4)	41(1)
C(63)	3741(3)	5892(3)	1569(3)	79(1)
C(64)	4583(4)	5629(5)	2111(4)	50(2)
C(65)	5326(4)	5614(4)	1850(3)	118(2)
C(66)	5419(4)	5923(6)	1007(3)	62(2)
C(67)	4691(3)	5989(4)	564(3)	102(2)
C(75)	5326(4)	5614(4)	1850(3)	118(2)
C(71)	3108(5)	6252(4)	216(4)	135(3)
C(72)	3033(8)	6288(6)	847(7)	96(3)
C(73)	3741(3)	5892(3)	1569(3)	79(1)
C(74)	4502(7)	5738(6)	1383(7)	101(3)
C(76)	4171(9)	6102(8)	8(7)	123(4)
C(77)	4691(3)	5989(4)	564(3)	102(2)

—

Table 4. Bond lengths [Å] and angles [°].

O-P(2)	1.5302(15)
O-Pd(1)#1	2.0842(15)
P(2)-C(28)	1.839(2)
P(2)-C(13)	1.852(2)
P(2)-Pd(1)	2.2055(6)
Pd(1)-C(1)	1.991(2)
Pd(1)-O#1	2.0842(15)
C(1)-C(3)	1.397(3)
C(1)-C(7)	1.398(3)
C(2)-C(6)	1.404(3)
C(2)-C(4)	1.409(3)
C(2)-C(26)	1.533(3)
C(3)-C(9)	1.397(3)
C(3)-C(4)	1.512(3)
C(4)-C(14)	1.416(3)
C(5)-C(13)	1.535(3)
C(5)-C(11)	1.535(3)
C(6)-C(18)	1.385(3)
C(7)-C(10)	1.392(3)
C(8)-C(10)	1.377(3)
C(8)-C(9)	1.388(3)
C(11)-C(16)	1.524(4)
C(12)-C(21)	1.522(4)
C(12)-C(13)	1.537(3)
C(14)-C(15)	1.386(3)
C(14)-C(17)	1.525(3)
C(15)-C(18)	1.384(4)
C(16)-C(21)	1.522(4)
C(17)-C(20)	1.525(4)
C(17)-C(22)	1.530(4)
C(18)-C(19)	1.530(4)
C(19)-C(23)	1.466(4)
C(19)-C(24)	1.495(5)
C(26)-C(30)	1.528(3)

C(26)-C(31)	1.534(4)
C(27)-C(36)	1.525(3)
C(27)-C(28)	1.536(3)
C(28)-C(29)	1.536(3)
C(29)-C(34)	1.529(3)
C(34)-C(35)	1.518(4)
C(35)-C(36)	1.518(3)
C(61)-C(62)	1.459(7)
C(62)-C(63)	1.274(7)
C(62)-C(67)	1.429(7)
C(63)-C(64)	1.542(8)
C(64)-C(65)	1.230(8)
C(65)-C(66)	1.513(8)
C(66)-C(67)	1.274(7)

P(2)-O-Pd(1)#1	144.85(10)
O-P(2)-C(28)	104.39(9)
O-P(2)-C(13)	108.64(9)
C(28)-P(2)-C(13)	106.57(10)
O-P(2)-Pd(1)	111.53(6)
C(28)-P(2)-Pd(1)	115.00(7)
C(13)-P(2)-Pd(1)	110.32(7)
C(1)-Pd(1)-O#1	165.35(7)
C(1)-Pd(1)-P(2)	97.57(6)
O#1-Pd(1)-P(2)	94.66(4)
C(3)-C(1)-C(7)	117.55(19)
C(3)-C(1)-Pd(1)	105.89(15)
C(7)-C(1)-Pd(1)	136.11(16)
C(6)-C(2)-C(4)	118.6(2)
C(6)-C(2)-C(26)	119.9(2)
C(4)-C(2)-C(26)	121.3(2)
C(1)-C(3)-C(9)	121.3(2)
C(1)-C(3)-C(4)	117.85(18)
C(9)-C(3)-C(4)	120.80(19)
C(2)-C(4)-C(14)	119.6(2)
C(2)-C(4)-C(3)	119.73(19)

C(14)-C(4)-C(3)	120.5(2)
C(13)-C(5)-C(11)	111.3(2)
C(18)-C(6)-C(2)	122.4(2)
C(10)-C(7)-C(1)	121.1(2)
C(10)-C(8)-C(9)	119.7(2)
C(8)-C(9)-C(3)	119.9(2)
C(8)-C(10)-C(7)	120.4(2)
C(16)-C(11)-C(5)	111.7(2)
C(21)-C(12)-C(13)	111.3(2)
C(5)-C(13)-C(12)	109.46(19)
C(5)-C(13)-P(2)	113.31(15)
C(12)-C(13)-P(2)	110.70(15)
C(15)-C(14)-C(4)	118.8(2)
C(15)-C(14)-C(17)	120.0(2)
C(4)-C(14)-C(17)	121.2(2)
C(18)-C(15)-C(14)	122.9(2)
C(21)-C(16)-C(11)	111.0(2)
C(20)-C(17)-C(14)	111.4(2)
C(20)-C(17)-C(22)	110.4(2)
C(14)-C(17)-C(22)	111.9(2)
C(15)-C(18)-C(6)	117.7(2)
C(15)-C(18)-C(19)	119.3(2)
C(6)-C(18)-C(19)	122.9(2)
C(23)-C(19)-C(24)	110.8(3)
C(23)-C(19)-C(18)	115.4(2)
C(24)-C(19)-C(18)	111.2(2)
C(12)-C(21)-C(16)	111.6(2)
C(30)-C(26)-C(2)	112.7(2)
C(30)-C(26)-C(31)	111.4(2)
C(2)-C(26)-C(31)	110.3(2)
C(36)-C(27)-C(28)	111.59(18)
C(27)-C(28)-C(29)	111.03(18)
C(27)-C(28)-P(2)	110.97(15)
C(29)-C(28)-P(2)	110.56(15)
C(34)-C(29)-C(28)	111.20(19)
C(35)-C(34)-C(29)	111.4(2)

C(34)-C(35)-C(36)	110.8(2)
C(35)-C(36)-C(27)	111.5(2)
C(63)-C(62)-C(67)	117.4(5)
C(63)-C(62)-C(61)	128.7(6)
C(67)-C(62)-C(61)	114.0(6)
C(62)-C(63)-C(64)	119.5(4)
C(65)-C(64)-C(63)	120.4(5)
C(64)-C(65)-C(66)	119.4(5)
C(67)-C(66)-C(65)	116.1(5)
C(66)-C(67)-C(62)	125.1(5)

Symmetry transformations used to generate equivalent atoms:
#1 -x,-y+2,-z

Table 5. Anisotropic displacement parameters ($Å^2 x\ 10^3$). The anisotropic displacement factor exponent takes the form: $-2p^2[\ h^2\ a^{*2}U^{11} + ... + 2\ h\ k\ a^*\ b^*\ U^{12}\ ]$

	U^{11}	U^{22}	U^{33}	U^{23}	U^{13}	U^{12}
O	37(1)	22(1)	28(1)	4(1)	-9(1)	-3(1)
P(2)	24(1)	19(1)	24(1)	3(1)	-2(1)	0(1)
Pd(1)	23(1)	20(1)	23(1)	4(1)	-1(1)	-2(1)
C(1)	25(1)	22(1)	22(1)	0(1)	1(1)	3(1)
C(2)	28(1)	28(1)	27(1)	0(1)	-4(1)	-1(1)
C(3)	25(1)	22(1)	26(1)	-1(1)	4(1)	3(1)
C(4)	20(1)	29(1)	24(1)	2(1)	-5(1)	-2(1)
C(5)	32(1)	37(1)	29(1)	-2(1)	3(1)	-2(1)
C(6)	41(1)	25(1)	37(1)	-2(1)	-4(1)	0(1)
C(7)	32(1)	27(1)	27(1)	2(1)	1(1)	-4(1)
C(8)	41(1)	35(1)	32(1)	10(1)	-3(1)	9(1)
C(9)	26(1)	35(1)	33(1)	5(1)	-3(1)	4(1)
C(10)	45(1)	26(1)	29(1)	6(1)	4(1)	0(1)
C(11)	42(2)	43(2)	34(1)	1(1)	10(1)	5(1)
C(12)	26(1)	41(2)	41(1)	-8(1)	-3(1)	5(1)
C(13)	25(1)	24(1)	31(1)	3(1)	2(1)	1(1)
C(14)	23(1)	35(1)	29(1)	2(1)	-2(1)	-1(1)

C(15)	28(1)	43(2)	32(1)	5(1)	2(1)	-6(1)
C(16)	35(1)	49(2)	48(2)	5(1)	13(1)	10(1)
C(17)	32(1)	39(1)	38(1)	0(1)	10(1)	4(1)
C(18)	32(1)	38(1)	37(1)	7(1)	-4(1)	-10(1)
C(19)	51(2)	41(2)	57(2)	12(1)	0(1)	-15(1)
C(20)	46(2)	70(2)	74(2)	-6(2)	1(2)	21(2)
C(21)	25(1)	51(2)	61(2)	-3(1)	2(1)	3(1)
C(22)	73(2)	53(2)	43(2)	-7(1)	8(2)	13(2)
C(23)	61(2)	47(2)	130(3)	21(2)	1(2)	-16(2)
C(24)	97(3)	80(3)	139(4)	50(3)	-63(3)	-63(2)
C(26)	37(1)	27(1)	34(1)	-5(1)	7(1)	0(1)
C(27)	29(1)	25(1)	33(1)	0(1)	3(1)	-2(1)
C(28)	27(1)	22(1)	24(1)	1(1)	0(1)	1(1)
C(29)	31(1)	32(1)	36(1)	1(1)	6(1)	-2(1)
C(30)	45(2)	38(2)	53(2)	-6(1)	14(1)	8(1)
C(31)	61(2)	54(2)	34(2)	-4(1)	10(1)	-4(2)
C(34)	37(1)	36(1)	42(1)	-3(1)	11(1)	6(1)
C(35)	48(2)	33(1)	39(1)	-10(1)	4(1)	4(1)
C(36)	37(1)	27(1)	42(1)	-4(1)	-1(1)	-2(1)
C(61)	141(5)	102(4)	149(5)	-26(4)	-72(5)	41(4)
C(62)	29(3)	34(3)	57(4)	-2(3)	-14(3)	4(2)
C(63)	65(2)	71(3)	102(3)	-23(2)	23(2)	-12(2)
C(64)	45(4)	74(4)	30(3)	-2(3)	-2(3)	-20(3)
C(65)	96(4)	122(4)	127(4)	-57(3)	-53(3)	39(3)
C(66)	37(3)	109(6)	38(3)	6(3)	-3(3)	6(3)
C(67)	84(3)	161(5)	62(3)	-11(3)	7(2)	-23(3)
C(75)	96(4)	122(4)	127(4)	-57(3)	-53(3)	39(3)
C(71)	141(5)	102(4)	149(5)	-26(4)	-72(5)	41(4)
C(72)	106(8)	61(5)	128(9)	-8(6)	51(7)	-10(5)
C(73)	65(2)	71(3)	102(3)	-23(2)	23(2)	-12(2)
C(74)	92(7)	58(5)	145(10)	-15(5)	-39(7)	0(5)
C(76)	148(10)	129(9)	95(8)	-15(7)	24(7)	6(8)
C(77)	84(3)	161(5)	62(3)	-11(3)	7(2)	-23(3)

Table 6. Hydrogen coordinates (x 10^4) and isotropic displacement parameters ($Å^2$x 10^3).

	x	y	z	U(eq)
H(5A)	-978	10067	1520	39
H(5B)	-386	9327	2051	39
H(6)	2470	12017	1984	42
H(7)	513	7462	1790	34
H(8)	2793	7089	3205	43
H(9)	3365	8501	2734	38
H(10)	1361	6591	2747	40
H(11A)	-1674	8739	2598	47
H(11B)	-1641	9860	2722	47
H(12A)	-2074	9437	391	44
H(12B)	-2125	8321	235	44
H(13)	-1079	8050	1339	32
H(15)	4095	10669	587	41
H(16A)	-3114	9337	2260	52
H(16B)	-2729	10088	1667	52
H(17)	3299	8335	969	43
H(19)	4165	12279	599	60
H(20A)	4996	9248	900	95
H(20B)	4845	8131	830	95
H(20C)	4695	8663	1641	95
H(21A)	-2769	8081	1439	55
H(21B)	-3364	8829	919	55
H(22A)	2891	8923	-297	84
H(22B)	3782	8302	-328	84
H(22C)	3845	9431	-325	84
H(23A)	2898	13360	1329	119
H(23B)	2841	13062	416	119
H(23C)	3613	13767	763	119
H(24A)	4808	13269	1604	164

H(24B)	5007	12171	1761	164
H(24C)	4265	12701	2227	164
H(26)	1353	9932	2621	39
H(27A)	-1313	7020	130	34
H(27B)	-1116	7424	-720	34
H(28)	207	7152	587	29
H(29A)	577	7876	-936	40
H(29B)	1308	7728	-203	40
H(30A)	1122	11933	2513	67
H(30B)	428	11206	2851	67
H(30C)	593	11196	1932	67
H(31A)	2568	10219	3554	74
H(31B)	1682	10690	3852	74
H(31C)	2415	11335	3475	74
H(34A)	1364	6465	-1132	45
H(34B)	1135	6077	-285	45
H(35A)	165	5361	-1268	48
H(35B)	-157	6375	-1603	48
H(36A)	-505	5637	-85	43
H(36B)	-1245	5776	-812	43
H(61A)	3052	5727	-162	203
H(61B)	3261	6832	-60	203
H(61C)	2537	6341	452	203
H(63)	3173	5942	1780	94
H(64)	4526	5478	2650	60
H(65)	5837	5410	2174	142
H(66)	5986	6059	819	74
H(67)	4736	6005	9	122
H(75A)	5626	6226	1929	177
H(75B)	5713	5184	1579	177
H(75C)	5208	5346	2363	177
H(71)	2619	6301	-176	162
H(72)	2502	6580	1000	115
H(73)	3571	5790	2089	94
H(76)	4346	6107	-518	148
H(77)	5306	6068	475	12

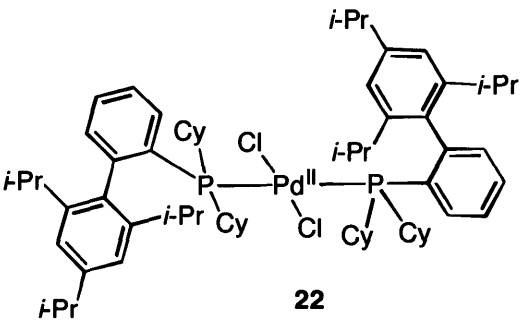

22

X-ray Structure Data for 22.

Table 7. Crystal data and structure refinement.

Identification code	03148t	
Empirical formula	$C_{68}H_{100}Cl_8P_2Pd$	
Formula weight	1369.42	
Temperature	193(2) K	
Wavelength	0.71073 Å	
Crystal system	Triclinic	
Space group	P-1	
Unit cell dimensions	a = 9.6212(15) Å	a= 89.314(2)°.
	b = 13.507(2) Å	b= 72.367(2)°.
	c = 15.100(2) Å	g = 72.398(2)°.
Volume	1775.7(5) $Å^3$	
Z	1	
Density (calculated)	1.281 Mg/m^3	
Absorption coefficient	0.645 mm^{-1}	
F(000)	720	
Crystal size	0.36 x 0.33 x 0.27 mm^3	
Theta range for data collection	2.22 to 23.29°.	
Index ranges	-10<=h<=9, -14<=k<=15, -16<=l<=10	
Reflections collected	7303	
Independent reflections	5039 [R(int) = 0.0131]	
Completeness to theta = 23.29°	98.4 %	
Absorption correction	SADABS	
Refinement method	Full-matrix least-squares on F^2	
Data / restraints / parameters	5039 / 0 / 365	
Goodness-of-fit on F^2	1.007	

Final R indices [I>2sigma(I)]	R1 = 0.0366, wR2 = 0.0909
R indices (all data)	R1 = 0.0385, wR2 = 0.0924
Extinction coefficient	0.0028(5)
Largest diff. peak and hole	0.912 and -0.880 e.Å^{-3}

Table 8. Atomic coordinates (x 10^4) and equivalent isotropic displacement parameters (Å^{2}x 10^3). U(eq) is defined as one third of the trace of the orthogonalized U^{ij} tensor.

	x	y	z	U(eq)
Pd(1)	5000	5000	5000	24(1)
P	4246(1)	3623(1)	5737(1)	22(1)
Cl(1)	3312(1)	6216(1)	6196(1)	46(1)
Cl(2)	1421(2)	8584(1)	8570(1)	91(1)
Cl(4)	315(2)	9152(1)	7020(1)	99(1)
Cl(3)	-945(2)	7866(1)	8363(2)	120(1)
C(1)	3119(3)	3393(2)	8164(2)	24(1)
C(2)	2031(3)	3934(2)	7642(2)	24(1)
C(3)	3314(3)	2338(2)	8335(2)	26(1)
C(4)	3811(3)	3968(2)	8571(2)	26(1)
C(5)	5778(3)	2779(2)	6175(2)	24(1)
C(6)	4243(3)	1874(2)	8874(2)	31(1)
C(7)	4740(3)	3456(2)	9094(2)	30(1)
C(8)	2505(4)	1706(2)	7966(2)	34(1)
C(9)	3466(4)	5140(2)	8506(2)	32(1)
C(10)	501(3)	4353(3)	8194(2)	36(1)
C(11)	4983(3)	2416(2)	9250(2)	30(1)
C(12)	6876(4)	1815(2)	5532(2)	36(1)
C(13)	6693(4)	3434(2)	6405(2)	36(1)
C(14)	5996(4)	1894(3)	9833(2)	39(1)
C(15)	2404(3)	4069(2)	6679(2)	23(1)
C(16)	1215(3)	4657(2)	6347(2)	31(1)
C(17)	3163(4)	3279(2)	4219(2)	38(1)
C(18)	-279(4)	5055(3)	6907(2)	39(1)
C(19)	4843(4)	5531(3)	8404(2)	41(1)
C(20)	3962(3)	2745(2)	4918(2)	27(1)

C(21)	-648(4)	4898(3)	7845(2)	41(1)
C(22)	3323(4)	1123(3)	4658(2)	43(1)
C(23)	3203(4)	1945(2)	5391(2)	33(1)
C(24)	8045(4)	1182(3)	5990(3)	48(1)
C(25)	1112(5)	1606(3)	8743(3)	59(1)
C(26)	3363(4)	2447(3)	3467(2)	44(1)
C(27)	7866(4)	2801(3)	6857(3)	44(1)
C(28)	3575(4)	631(3)	7519(2)	45(1)
C(29)	2677(4)	1611(3)	3892(3)	48(1)
C(30)	8944(4)	1829(3)	6234(3)	47(1)
C(31)	2152(4)	5716(3)	9374(3)	48(1)
C(32)	693(5)	8169(3)	7773(3)	60(1)
C(33)	5023(5)	1681(4)	10771(3)	57(1)
C(34)	7247(5)	905(3)	9322(3)	64(1)

Table 9. Bond lengths [Å] and angles [°].

Pd(1)-Cl(1)#1	2.2972(8)
Pd(1)-Cl(1)	2.2972(8)
Pd(1)-P#1	2.3457(7)
Pd(1)-P	2.3457(7)
P-C(15)	1.837(3)
P-C(20)	1.856(3)
P-C(5)	1.863(3)
Cl(2)-C(32)	1.737(4)
Cl(4)-C(32)	1.764(5)
Cl(3)-C(32)	1.725(5)
C(1)-C(3)	1.411(4)
C(1)-C(4)	1.413(4)
C(1)-C(2)	1.508(4)
C(2)-C(10)	1.395(4)
C(2)-C(15)	1.412(4)
C(3)-C(6)	1.393(4)
C(3)-C(8)	1.523(4)
C(4)-C(7)	1.394(4)
C(4)-C(9)	1.524(4)
C(5)-C(13)	1.530(4)
C(5)-C(12)	1.526(4)
C(6)-C(11)	1.392(4)
C(7)-C(11)	1.382(4)
C(8)-C(28)	1.524(5)
C(8)-C(25)	1.531(5)
C(9)-C(31)	1.532(5)
C(9)-C(19)	1.535(4)
C(10)-C(21)	1.377(5)
C(11)-C(14)	1.520(4)
C(12)-C(24)	1.532(5)
C(13)-C(27)	1.529(5)
C(14)-C(33)	1.522(5)
C(14)-C(34)	1.522(5)
C(15)-C(16)	1.407(4)

C(16)-C(18)	1.371(4)
C(17)-C(20)	1.537(4)
C(17)-C(26)	1.535(4)
C(18)-C(21)	1.381(5)
C(20)-C(23)	1.534(4)
C(22)-C(23)	1.531(4)
C(22)-C(29)	1.526(5)
C(24)-C(30)	1.519(5)
C(26)-C(29)	1.517(5)
C(27)-C(30)	1.516(5)

Cl(1)#1-Pd(1)-Cl(1)	180.000(1)
Cl(1)#1-Pd(1)-P#1	92.94(3)
Cl(1)-Pd(1)-P#1	87.06(3)
Cl(1)#1-Pd(1)-P	87.06(3)
Cl(1)-Pd(1)-P	92.94(3)
P#1-Pd(1)-P	180.000(17)
C(15)-P-C(20)	105.10(13)
C(15)-P-C(5)	110.75(12)
C(20)-P-C(5)	105.19(13)
C(15)-P-Pd(1)	112.91(9)
C(20)-P-Pd(1)	112.02(9)
C(5)-P-Pd(1)	110.49(9)
C(3)-C(1)-C(4)	119.7(3)
C(3)-C(1)-C(2)	119.9(2)
C(4)-C(1)-C(2)	120.0(2)
C(10)-C(2)-C(15)	118.0(3)
C(10)-C(2)-C(1)	114.8(2)
C(15)-C(2)-C(1)	127.1(2)
C(6)-C(3)-C(1)	118.9(3)
C(6)-C(3)-C(8)	119.5(3)
C(1)-C(3)-C(8)	121.6(3)
C(7)-C(4)-C(1)	118.6(3)
C(7)-C(4)-C(9)	119.9(3)
C(1)-C(4)-C(9)	121.3(3)
C(13)-C(5)-C(12)	109.7(2)

C(13)-C(5)-P	109.34(19)
C(12)-C(5)-P	115.7(2)
C(11)-C(6)-C(3)	122.2(3)
C(11)-C(7)-C(4)	122.7(3)
C(28)-C(8)-C(3)	112.6(3)
C(28)-C(8)-C(25)	110.3(3)
C(3)-C(8)-C(25)	110.6(3)
C(4)-C(9)-C(31)	109.3(2)
C(4)-C(9)-C(19)	114.4(3)
C(31)-C(9)-C(19)	109.0(3)
C(21)-C(10)-C(2)	123.1(3)
C(7)-C(11)-C(6)	117.7(3)
C(7)-C(11)-C(14)	120.9(3)
C(6)-C(11)-C(14)	121.4(3)
C(24)-C(12)-C(5)	110.1(3)
C(5)-C(13)-C(27)	111.4(3)
C(11)-C(14)-C(33)	110.4(3)
C(11)-C(14)-C(34)	112.1(3)
C(33)-C(14)-C(34)	111.4(3)
C(16)-C(15)-C(2)	117.6(3)
C(16)-C(15)-P	111.4(2)
C(2)-C(15)-P	130.9(2)
C(18)-C(16)-C(15)	122.8(3)
C(20)-C(17)-C(26)	108.6(3)
C(16)-C(18)-C(21)	119.4(3)
C(23)-C(20)-C(17)	109.6(2)
C(23)-C(20)-P	114.2(2)
C(17)-C(20)-P	116.1(2)
C(10)-C(21)-C(18)	119.0(3)
C(23)-C(22)-C(29)	112.2(3)
C(22)-C(23)-C(20)	110.1(3)
C(30)-C(24)-C(12)	111.8(3)
C(29)-C(26)-C(17)	111.2(3)
C(30)-C(27)-C(13)	110.9(3)
C(26)-C(29)-C(22)	111.9(3)
C(27)-C(30)-C(24)	110.6(3)

Cl(3)-C(32)-Cl(2)	109.5(3)
Cl(3)-C(32)-Cl(4)	111.3(2)
Cl(2)-C(32)-Cl(4)	109.5(2)

Symmetry transformations used to generate equivalent atoms:
#1 -x+1,-y+1,-z+1

Table 10. Anisotropic displacement parameters ($Å^2 x\ 10^3$). The anisotropic displacement factor exponent takes the form: $-2p^2[\ h^2\ a^{*2}U^{11} + ... + 2\ h\ k\ a^*\ b^*\ U^{12}\ ]$

	U^{11}	U^{22}	U^{33}	U^{23}	U^{13}	U^{12}
Pd(1)	32(1)	18(1)	18(1)	3(1)	-2(1)	-7(1)
P	27(1)	19(1)	18(1)	3(1)	-5(1)	-6(1)
Cl(1)	60(1)	25(1)	32(1)	-4(1)	14(1)	-13(1)
Cl(2)	117(1)	88(1)	123(1)	46(1)	-88(1)	-61(1)
Cl(4)	120(1)	98(1)	67(1)	5(1)	-45(1)	-1(1)
Cl(3)	78(1)	111(1)	186(2)	2(1)	-41(1)	-52(1)
C(1)	22(1)	30(2)	16(1)	4(1)	-2(1)	-9(1)
C(2)	25(2)	25(2)	24(2)	3(1)	-8(1)	-11(1)
C(3)	27(2)	31(2)	21(2)	4(1)	-5(1)	-12(1)
C(4)	25(2)	34(2)	17(1)	3(1)	-3(1)	-11(1)
C(5)	25(2)	23(1)	23(2)	6(1)	-6(1)	-8(1)
C(6)	36(2)	29(2)	28(2)	9(1)	-10(1)	-11(1)
C(7)	34(2)	37(2)	24(2)	4(1)	-12(1)	-16(1)
C(8)	42(2)	35(2)	33(2)	9(1)	-16(1)	-19(2)
C(9)	39(2)	30(2)	28(2)	4(1)	-13(1)	-12(1)
C(10)	29(2)	48(2)	28(2)	4(1)	-5(1)	-12(2)
C(11)	30(2)	37(2)	24(2)	6(1)	-9(1)	-11(1)
C(12)	31(2)	31(2)	41(2)	-5(1)	-11(1)	-4(1)
C(13)	41(2)	31(2)	39(2)	1(1)	-16(2)	-12(1)
C(14)	42(2)	43(2)	42(2)	14(2)	-25(2)	-18(2)
C(15)	26(2)	21(1)	24(2)	2(1)	-8(1)	-8(1)
C(16)	36(2)	30(2)	26(2)	3(1)	-14(1)	-5(1)
C(17)	53(2)	34(2)	30(2)	4(1)	-21(2)	-10(2)
C(18)	29(2)	41(2)	44(2)	3(2)	-17(2)	-1(1)

C(19)	53(2)	37(2)	37(2)	-1(1)	-12(2)	-23(2)
C(20)	33(2)	24(2)	23(2)	2(1)	-9(1)	-7(1)
C(21)	21(2)	51(2)	43(2)	-1(2)	-6(1)	-4(1)
C(22)	54(2)	35(2)	46(2)	-1(2)	-18(2)	-19(2)
C(23)	38(2)	31(2)	31(2)	3(1)	-12(1)	-13(1)
C(24)	34(2)	35(2)	67(2)	-5(2)	-20(2)	3(2)
C(25)	56(2)	72(3)	60(2)	5(2)	-10(2)	-43(2)
C(26)	57(2)	44(2)	30(2)	-2(2)	-23(2)	-8(2)
C(27)	43(2)	48(2)	53(2)	6(2)	-26(2)	-19(2)
C(28)	67(2)	34(2)	43(2)	10(2)	-26(2)	-22(2)
C(29)	55(2)	50(2)	44(2)	-10(2)	-23(2)	-16(2)
C(30)	29(2)	57(2)	55(2)	9(2)	-15(2)	-12(2)
C(31)	49(2)	37(2)	48(2)	-4(2)	-6(2)	-8(2)
C(32)	49(2)	51(2)	67(3)	-16(2)	-18(2)	5(2)
C(33)	61(2)	79(3)	45(2)	30(2)	-31(2)	-30(2)
C(34)	50(2)	61(3)	79(3)	2(2)	-37(2)	0(2)

Table 11. Hydrogen coordinates (x 10^4) and isotropic displacement parameters ($Å^2$x 10^3).

	x	y	z	U(eq)
H(5)	5257	2530	6773	29
H(6)	4375	1163	8987	37
H(7)	5227	3838	9355	36
H(8)	2122	2096	7475	41
H(9)	3114	5320	7949	38
H(10)	240	4257	8841	43
H(12A)	6286	1378	5403	43
H(12B)	7420	2031	4932	43
H(13A)	5978	4048	6835	43
H(13B)	7233	3688	5825	43
H(14)	6514	2393	9956	46
H(16)	1459	4785	5706	37
H(17A)	3623	3814	3928	45
H(17B)	2057	3625	4545	45
H(18)	-1054	5434	6653	47
H(19A)	4571	6269	8283	61
H(19B)	5718	5124	7882	61
H(19C)	5119	5451	8980	61
H(20)	5020	2325	4528	32
H(21)	-1679	5163	8242	50
H(22A)	2756	647	4967	52
H(22B)	4414	704	4374	52
H(23A)	3716	1603	5842	39
H(23B)	2109	2304	5737	39
H(24A)	7499	922	6564	57
H(24B)	8767	571	5558	57
H(25A)	603	1202	8492	88
H(25B)	391	2302	8989	88
H(25C)	1451	1249	9246	88
H(26A)	2857	2781	3010	52
H(26B)	4470	2122	3130	52

H(27A)	8467	3236	6973	53
H(27B)	7322	2599	7465	53
H(28A)	4498	703	7055	67
H(28B)	3048	297	7213	67
H(28C)	3870	202	8001	67
H(29A)	2894	1060	3397	57
H(29B)	1548	1921	4156	57
H(30A)	9645	1407	6558	56
H(30B)	9575	2031	5655	56
H(31A)	2455	5526	9933	72
H(31B)	1236	5522	9411	72
H(31C)	1927	6470	9334	72
H(32)	1478	7529	7395	72
H(33A)	4217	2328	11076	85
H(33B)	5675	1420	11166	85
H(33C)	4552	1159	10676	85
H(34A)	6777	374	9245	95
H(34B)	7952	644	9684	95
H(34C)	7815	1059	8707	95

References

(1) (a) Diederich, F.; Stang, P. J. *Metal-Catalyzed Cross-Coupling Reactions*; Wiley-VCH, New York, 1998. (b) de Meijere, A. *Metal-Catalyzed Cross-Coupling Reactions*; 2nd Ed; Wiley-VCH, Weinheim, 2004. (c) Tsuji, J. *Palladium Reagents and Catalysts, New Perspectives For The 21st Century*; Wiley, West Sussex, 2004. For other reviews on C-N and C-O bond forming reactions, see: (d) Muci, A. R.; Buchwald, S. L. *Top. Curr. Chem.* **2002**, *219*, 131. (e) Hartwig, J. F. In *Handbook of Organopalladium Chemistry for Organic Synthesis*; Negishi, E., Ed.; Wiley-Interscience: New York, 2002; p 1051. (f) Jiang, L.; Buchwald, S. L. *Palladium-Catalyzed Aromatic Carbon-Nitrogen Bond Formation. In Metal-Catalyzed Cross-Coupling Reactions*; 2nd Ed; de Meijere, A., Diederich, F., Eds.; Wiley-VCH; Weinheim, 2004; p 699. (g) Schlummer, B.; Scholz, U. *Adv. Synth. Catal.* **2004**, *346*, 1599.

(2) Amatore, C.; Jutand, A. *J. Organomet. Chem.* **1999**, *576*, 254.

(3) Littke, A. F.; Fu, G. C. *Angew. Chem. Int. Ed.* **2002**, *41*, 4176.

(4) For the initial proposal regarding the formation of $L_1Pd(0)$ complexes, see: (a) Paul, F.; Patt, J.; Hartwig, J. F. *J. Am. Chem. Soc.* **1994**, *116*, 5969. (b) Hartwig, J. F.; Paul, F. *J. Am. Chem. Soc.* **1995**, *117*, 5373.

(5) For reviews on highly active Pd-catalysts, see: (a) Farina, V. *Adv. Synth. Catal.* **2004**, *346*, 1553. (b) Christmann, U.; Vilar, R. *Angew. Chem. Int. Ed.* **2005**, *44*, 366.

(6) Huser, M.; Youinou, M.-T.; Osborn, J. A. *Angew. Chem. Int. Ed.* **1989**, *28*, 1386.

(7) Grushin, V. V.; Alper, H. *J. Chem. Soc., Chem. Commun.* **1992**, 611.

(8) (a) Ben-David, Y.; Portnoy, M.; Milstein, D. *J. Am. Chem. Soc.* **1989**, *111*, 8742. (b) Ben-David, Y.; Portnoy, M.; Milstein, D. *J. Chem. Soc., Chem. Commun.* **1989**, 1816. (c) Ben-David,

Y.; Gozin, M.; Portnoy, M.; Milstein, D. *J. Mol. Catal.* **1992**, *73*, 173. (d) Portnoy, M.; Milstein, D. *Organometallics* **1993**, *12*, 1655. (e) Portnoy, M.; Milstein, D. *Organometallics* **1993**, *12*, 1665.

(9) (a) Reddy, N. P.; Tanaka, M. *Tetrahedron Lett.* **1997**, *38*, 4807. (b) Shen, W. *Tetrahedron Lett.* **1997**, *38*, 5575.

(10) (a) Nishiyama, M.; Yamamoto, T.; Koie, Y. *Tetrahedron Lett.* **1998**, *39*, 617. (b) Yamamoto, T.; Nishiyama, M.; Koie, Y. *Tetrahedron Lett.* **1998**, *39*, 2367.

(11) (a) Littke, A. F.; Fu, G. C. *Angew. Chem. Int. Ed.* **1998**, *37*, 3387. (b) Littke, A. F.; Dai, C.; Fu, G. C. *J. Am. Chem. Soc.* **2000**, *122*, 4020.

(12) (a) Littke, A. F.; Fu, G. C. *Angew. Chem. Int. Ed.* **1999**, *38*, 2411. (b) Littke, A. F.; Schwarz, L.; Fu, G. C. *J. Am. Chem. Soc.* **2002**, *124*, 6343.

(13) (a) Littke, A. F.; Fu, G. C. *J. Org. Chem.* **1999**, *64*, 10. (b) Littke, A. F.; Fu, G. C. *J. Am. Chem. Soc.* **2001**, *123*, 6989.

(14) (a) Kawatsura, M.; Hartwig, J. F. *J. Am. Chem. Soc.* **1999**, *121*, 1473. (b) Beare, N. A.; Hartwig, J. F. *J. Org. Chem.* **2002**, *67*, 541. (c) Hama, T.; Liu, X.; Culkin, D. A.; Hartwig, J. F. *J. Am. Chem. Soc.* **2003**, *125*, 11176. (d) Liu, X.; Hartwig, J. F. *J. Am. Chem. Soc.* **2004**, *126*, 5182.

(15) (a) Hartwig, J. F.; Kawatsura, M.; Hauck, S. I.; Shaughnessy, K. H.; Alcazar-Roman, L. M. *J. Org. Chem.* **1999**, *64*, 5575. (b) Kuwano, R.; Utsunomiya, M.; Hartwig, J. F. *J. Org. Chem.* **2002**, *67*, 6479. (c) Hooper, M. W.; Hartwig, J. F. *Organometallics* **2003**, *22*, 3394. (d) Hooper, M. W.; Utsunomiya, M.; Hartwig, J. F. *J. Org. Chem.* **2003**, *68*, 2861.

(16) Alcazar-Roman, L. M.; Hartwig, J. F. *J. Am. Chem. Soc.* **2001**, *123*, 12905.

(17) Kataoka, N.; Shelby, Q.; Stambuli, J. P.; Hartwig, J. F. *J. Org. Chem.* **2002**, *67*, 5553.

(18) (a) Stauffer, S. R.; Lee, S.; Stambuli, J. P.; Hauck, S. I.; Hartwig, J. F. *Org. Lett.* **2000**, *2*, 1423. (b) Grasa, G. A.; Viciu, M. S.; Huang, J.; Nolan, S. P. *J. Org. Chem.* **2001**, *66*, 7729. (c) Viciu, M. S.; Kissling, R. M.; Stevens, E. D.; Nolan, S. P. *Org. Lett.* **2002**, *4*, 2229.

(19) (a) Urgaonkar, S.; Nagarajan, M.; Verkade, J. G. *Tetrahedron Lett.* **2002**, *43*, 8921. (b) Urgaonkar, S.; Nagarajan, M.; Verkade, J. G. *J. Org. Chem.* **2003**, *68*, 452. (c) Urgaonkar, S; Nagarajan, M.; Verkade, J. G. *Org. Lett.* **2003**, *5*, 815. (d) Urgaonkar, S.; Xu, J.-H.; Verkade, J. G. *J. Org. Chem.* **2003**, *68*, 8416.

(20) (a) Li, G. Y. *Angew. Chem. Int. Ed.* **2001**, *40*, 1513. (b) Li, G. Y.; Zheng, G.; Noonan, A. F. *J. Org. Chem.* **2001**, *66*, 8677. (c) Li, G. Y. *J. Organomet. Chem.* **2002**, *653*, 63. (d) Li, G. Y. *J. Org. Chem.* **2002**, *67*, 3643. (e) Wolf, C.; Lerebours, R. *J. Org. Chem.* **2003**, *68*, 7077. (f) Wolf, C. Lerebours, R. *J. Org. Chem.* **2003**, *68*, 7551. (g) Wolf, C.; Lerebours, R.; Tanzini, E. H. *Synthesis* **2003**, 2069. (h) Wolf, C.; Lerebours, R. *Org. Lett.* **2004**, *6*, 1147. (i) Wolf, C.; Lerebours, R. *Org. Biomol. Chem.* **2004**, *2*, 2161. (j) Khanapure, S. P.; Garvey, D. S. *Tetrahedron Lett.* **2004**, *45*, 5283.

(21) For applications of adamantylphosphines, see: (a) Aranyos, A.; Old, D. W.; Kiyomori, A.; Wolfe, J. P.; Sadighi, J. P.; Buchwald, S. L. *J. Am. Chem. Soc.* **1999**, *121*, 4369. (b) Ehrentraut, A.; Zapf, A.; Beller, M. *Synlett* **2000**, 1589. (c) Zapf, A.; Ehrentraut, A.; Beller, M. *Angew. Chem. Int. Ed.* **2000**, *39*, 4153. (d) Stambuli, J. P.; Stauffer, S. R.; Shaughnessy, K. H.; Hartwig, J. F. *J. Am. Chem. Soc.* **2001**, *123*, 2677. (e) Ehrentraut, A.; Zapf, A.; Beller, M. *J. Mol. Catal. A: Chem.* **2002**, *182-183*, 515. (f) Ehrentraut, A.; Zapf, A.; Beller, M. *Adv. Synth. Catal.* **2002**, *344*, 209. (g) Schnyder, A.; Indolese, A. F.; Studer, M.; Blaser, H.-U. *Angew. Chem. Int. Ed.* **2002**, *41*, 3668. (h) Schnyder, A.; Aemmer, T.; Indolese, A. F.; Pittelkow, U.; Studer, M. *Adv. Synth. Catal.* **2002**, *344*, 495. (i) Köllhofer, A.; Pullmann, T.; Plenio, H. *Angew. Chem. Int. Ed.*

2003, *42*, 1056. (j) Hillerich, J.; Plenio, H. *Chem. Commun.* **2003**, 3024. (k) Remmele, H.; Köllhofer, A.; Plenio, H. *Organometallics* **2003**, *22*, 4098. (l) Köllhofer, A.; Plenio, H. *Chem. Eur. J.* **2003**, *9*, 1416. (m) Tewari, A.; Hein, M.; Zapf, A.; Beller, M. *Synthesis* **2004**, 935. (n) Zapf, A.; Beller, M. *Chem. Commun.* **2005**, 431.

(22) Hamann, B. C.; Hartwig, J. F. *J. Am. Chem. Soc.* **1998**,*120*, 7369.

(23) Shen, Q.; Shekhar, S.; Stambuli, J. P.; Hartwig, J. F. *Angew. Chem. Int. Ed.* **2005**, *44*, 1371.

(24) Old, D. W.; Wolfe, J. P.; Buchwald, S. L. *J. Am. Chem. Soc.* **1998**, *120*, 9722.

(25) (a) Wolfe, J. P.; Buchwald, S. L. *Angew. Chem. Int. Ed.* **1999**, *38*, 2413. (b) Wolfe, J. P.; Singer, R. A.; Yang, B. H.; Buchwald, S. L. *J. Am. Chem. Soc.* **1999**, *121*, 9550. (c) Wolfe, J. P.; Tomori, H.; Sadighi, J. P.; Yin, J.; Buchwald, S. L. *J. Org. Chem.* **2000**, *65*, 1158. (d) Fox, J. M.; Huang, X.; Chieffi, A.; Buchwald, S. L. *J. Am. Chem. Soc.* **2000**, *122*, 1360. (e) Old, D. W.; Harris, M. C.; Buchwald, S. L. *Org. Lett.* **2000**, *2*, 1403. (f) Harris, M. C.; Buchwald, S. L. *J. Org. Chem.* **2000**, *65*, 5327. (g) Yin, J.; Buchwald, S. L. *J. Am. Chem. Soc.* **2000**, *122*, 12051. (h) Torraca, K. E.; Kuwabe, S.-I.; Buchwald, S. L. *J. Am. Chem. Soc.* **2000**, *122*, 12907. (i) Parrish, C. A.; Buchwald, S. L. *J. Org. Chem.* **2001**, *66*, 2498. (j) Parrish, C. A.; Buchwald, S. L. *J. Org. Chem.* **2001**, *66*, 3820. (k) Moradi, W.; Buchwald, S. L. *J. Am. Chem. Soc.* **2001**, *123*, 7996. (l) Torraca, K. E.; Huang, X.; Parrish, C. A.; Buchwald, S. L. *J. Am. Chem. Soc.* **2001**, *123*, 10770. (m) Vogl, E. M.; Buchwald, S. L. *J. Org. Chem.* **2002**, *67*, 106. (n) Gaertzen, O.; Buchwald, S. L. *J. Org. Chem.* **2002**, *67*, 465. (o) Yin, J.; Rainka, M. P.; Zhang, X.-X.; Buchwald, S. L. *J. Am. Chem. Soc.* **2002**, *124,* 1162. (p) Harris, M. C.; Huang, X.; Buchwald, S. L. *Org. Lett.* **2002**, *4*, 2885. (q) Rutherford, J. L.; Rainka, M. P.; Buchwald, S. L. *J. Am. Chem. Soc.* **2002**, *124*, 15168. (r) Hennessy, E. J.; Buchwald, S. L. *J. Am. Chem. Soc.* **2003**, *125*, 12084. (s) Anderson, K. W.; Mendez-Perez, M.; Priego, J.; Buchwald, S. L. *J. Org. Chem.* **2003**, *68*, 9563.

(26) For the synthesis of monophosphinobiaryl ligands, see: (a) Tomori, H.; Fox, J. M., Buchwald, S. L. *J. Org. Chem.* **2000**, *65*, 5334. (b) Kaye, S.; Fox, J. M.; Hicks, F. A.; Buchwald, S. L. *Adv. Synth. Catal.* **2001**, *343*, 789.

(27) (a) Walker, S. D.; Barder, T. E.; Martinelli, J. R.; Buchwald, S. L. *Angew. Chem. Int. Ed.* **2004**, *43*, 1871. (b) Barder, T. E.; Walker, S. D.; Martinelli, J. R. *J. Am. Chem. Soc.* **2005**, *127*, 4685.

(28) (a) Huang, X.; Anderson, K. W.; Zim, D.; Jiang, L.; Klapars, A.; Buchwald, S. L. *J. Am. Chem. Soc.* **2003**, *125*, 6653. (b) Nguyen, H. N.; Huang, X.; Buchwald, S. L. *J. Am. Chem. Soc.* **2003**, *125*, 11818. (c) Gelman, D.; Buchwald, S. L. *Angew. Chem. Int. Ed.* **2003**, *42*, 5993.

(29) Galardon, E.; Ramdeehul, S.; Brown, J. M.; Cowley, A.; Hii, K.-K.; Jutand, A. *Angew. Chem. Int. Ed.* **2002**, *41*, 1760.

(30) Jones, W. D.; Kuykendall, V. L. *Inorg. Chem.* **1991**, *30*, 2615.

(31) (a) Stambuli, J. P.; Bühl, M.; Hartwig, J. F. *J. Am. Chem. Soc.* **2002**, *124*, 9346. (b) Stambuli, J. P.; Incarvito, C. D.; Bühl, M.; Hartwig, J. F. *J. Am. Chem. Soc.* **2004**, *126*, 1184.

(32) Yamashita, M.; Hartwig, J. F. *J. Am. Chem. Soc.* **2004**, *126*, 5344.

(33) (a) Rosner, T.; Le Bars, J.; Pfaltz, A.; Blackmond, D. G. *J. Am. Chem. Soc.* **2001**, *123*, 1848. (b) Rosner, T.; Sears, P. J.; Nugent, W. A.; Blackmond, D. G. *Org. Lett.* **2000**, *2*, 2511. (c) Blackmond, D. G.; McMillan, C. R.; Ramdeehul, S.; Schorm, A.; Brown, J. M. *J. Am. Chem. Soc.* **2001**, *123*, 10103. (d) Singh, U. K.; Strieter, E. R.; Blackmond, D. G.; Buchwald, S. L. *J. Am. Chem. Soc.* **2002**, *124*, 14104.

(34) For studies examining the reduction of Pd(II) to Pd(0) with amines, see: (a) Amatore, C.; Carré, E.; Jutand, A.; M'Barki, M. A. *Organometallics*, **1995**, *14*, 1818. (b) McCrindle, R.;

Ferguson, G.; Arsenault, G. J.; McAllees, A. J.; Stephenson, D. K. *J. Chem. Res. Synop.* **1984**, 360.

(35) This trend is consistent with the A-values obtained for *i*-Pr (2.21), Me (1.74), and OMe (0.60), respectively: Carroll, F. A. *Perspectives On Structure And Mechanism In Organic Chemistry*; Brooks/Cole: Pacific Grove, CA, 1998; p 138.

(36) A similar mechanism has been proposed for the Pd-catalyzed aerobic alcohol oxidation: (a) Steinhoff, B. A.; Stahl, S. S. *Org. Lett.* **2002**, *4*, 4179. (b) Steinhoff, B. A.; Guzei, I. A.; Stahl, S. S. *J. Am. Chem. Soc.* **2004**, *126*, 11268.

(37) For examples of β-hydride elimination from Pd(II)-amido complexes, see: (a) Diamond, S.E.; Mares, F. *J. Organomet. Chem.* **1977**, *142*, C55. (b) Murahashi, S. I.; Yoshimura, T.; Tsumiyama, T.; Kojima, T. *J. Am. Chem. Soc.* **1983**, *105*, 5002. (c) Bryndza, H. E.; Tam, W. *Chem. Rev.* **1988**, *88*, 1163. (d) Hartwig, J. F.; Richards, S.; Barañano, D.; Paul, F. *J. Am. Chem. Soc.* **1996**, *118*, 3626. (e) Lu, C. C.; Peters, J. C. *J. Am. Chem. Soc.* **2004**, *126*, 15818.

(38) For the direct observation of imine formation from the coupling of *N*-methylbenzylamine with 3,5-Dimethylbromobenzene using $Pd(dba)_2$/2 P(*o*-tolyl)$_3$ as the catalyst and NaO*t*-Bu as the base, see: Guram, A. S.; Rennels, R. A.; Buchwald, S. L. *Angew. Chem., Int. Ed. Engl.* **1995**, *34*, 1348-1350.

(39) For reports on the magnitude of the KIE values in β-hydride elimination reactions from metal-alkyl, metal-alkoxide, and metal-amide complexes in the range between 1.3 and 2.5, see: (a) Mueller, J. A.; Sigman, M. S. *J. Am. Chem. Soc.* **2003**, *125*, 7005. (b) Mueller, J. A.; Jensen, D. R.; Sigman, M. S. *J. Am. Chem. Soc.* **2002**, *124*, 8202. (c) ten Brink, G.-J.; Arends, I. W. C. E.; Sheldon, R. A. *Adv. Synth. Catal.* **2002**, *344*, 355. (d) Zhao, J.; Hesslink, H.; Hartwig, J. F. *J. Am. Chem. Soc.* **2001**, *123*, 7220. (e) Noronha, G.; Henry, P. M. *J. Mol. Catal. A: Chem.* **1997**,

120, 75. (f) Romeo, R.; Alibrandi, G.; Scolaro, L.M. *Inorg. Chem.* **1993**, *32*, 4688. See also ref. 36.

(40) For reports on the magnitude of the KIE values in β-hydride elimination reactions from metal-alkyl, metal-alkoxide, and metal-amide complexes in the range between 5.9 and 7, see: (a) Lu, C. C.; Peters, J. C. *J. Am. Chem. Soc.* **2004**, *126*, 15818. (b) Mueller, J. A.; Goller, C. P.; Sigman, M. S. *J. Am. Chem. Soc.* **2004**, *126*, 9724. (c) Jensen, D. R.; Schultz, M. J.; Mueller, J. A.; Sigman, M. S. *Angew. Chem. Int. Ed.* **2003**, *42*, 3810. (d) Zhang, X.; Fried, A.; Knapp, S.; Goldman, A. S. *Chem. Commun.* **2003**, 2060.

(41) (a) Amatore, C.; Jutand, A.; M'Barki, M. A. *Organometallics* **1992**, *11*, 3009. (b) Amatore, C.; Carré, E.; Jutand, A.; M'Barki, M. A. *Organometallics* **1995**, *14*, 1818. (c) Amatore, C.; Carré, E.; Jutand, A.; M'Barki, M. A.; Meyer, G. *Organometallics* **1995**, *14*, 5605. (d) Amatore, C.; Jutand, A. *Acc. Chem. Res.* **2000**, *33*, 314. (e) Amatore, C.; Jutand, A.; Thuilliez, A. *Organometallics* **2001**, *20*, 3241.

(42) (a) Reid, S. M.; Boyle, R. C.; Mague, J. T.; Fink, M. J. *J. Am. Chem. Soc.* **2003**, *125*, 7816. (b) Krause, J.; Cestaric, G.; Haack, K.-J.; Seevogel, K.; Storm, W.; Pörschke, K.-R. *J. Am. Chem. Soc.* **1999**, *121*, 9807. (c) de Graaf, W.; Boersma, J.; Smeets, W. J. J.; Spek, A. L.; van Koten, G. *Organometallics* **1989**, *8*, 2907.

(43) For a review on the introduction of palladacyles into cross-coupling chemistry, see: Riermeier, T. H.; Zapf, A.; Beller, M. *Top. Catal.* **1997**, *4*, 301. See also ref. 5a.

(44) (a) Zim, D.; Buchwald, S. L. *Org. Lett.* **2003**, *5*, 2413. (b) Bedford, R. B.; Cazin, C. S. J.; Coles, S. J.; Gelbrich, T.; Horton, P. N.; Hursthouse, M. B.; Light, M. E. *Organometallics* **2003**, *22*, 987.

(45) Zhang, X.-X.; Buchwald, S. L. *unpublished results.*

(46) (a) Dyker, G. *Angew. Chem. Int. Ed.* **1999**, *38*, 1698. (b) Shilov, A. E.; Shul'pin, G. B. *Activation and Catalytic Reactions of Saturated Hydrocarbons in the Presence of Metal Complexes*; Kluwer Academic Publishers: Dordrecht, 2000. (c) Chatani, N.; Asaumi, T.; Ikeda, T.; Yorimitsu, S.; Ishii, Y.; Kakiuchi, F.; Murai, S. *J. Am. Chem. Soc.* **2000**, *122*, 12882. (d) Dangel, B. D.; Johnson, J. A.; Sames, D. *J. Am. Chem. Soc.* **2001**, *123*, 8149. (e) Johnson, J. A.; Li, N.; Sames, D. *J. Am. Chem. Soc.* **2002**,*124*, 6900. (f) Dangel, B. D.; Godula, K.; Youn, S. W.; Sezen, B.; Sames, D. *J. Am. Chem. Soc.* **2002**, *124*, 11856. (g) Sezen, B.; Franz, R.; Sames, D. *J. Am. Chem. Soc.* **2002**, *124*, 13372.

(47) Louie, J.; Hartwig, J. F. *Angew. Chem. Int. Ed.* **1996**, *35*, 2359.

(48) Values corrected for the amounts of natural abundance M + 1 and M + 2.

(49) Quin, L. D. *A Guide to Organophosphorus Chemistry*; Wiley-Interscience: New York, 2000; p 207.

(50) Andreu, M. G.; Zapf, A.; Beller, M. *Chem. Commun.* **2000**, 2475.

(51) Stambuli, J. P.; Kuwano, R.; Hartwig, J. F. *Angew. Chem. Int. Ed.* **2002**, *41*, 4746. For the initial preparation of Pd(I) dimers, see: Dura-Villa, V.; Mingos, D. M. P.; Vilar, R.; White, A. J. P.; Williams, D. J. *J. Organomet. Chem.* **2000**, *600*, 198.

(52) Ozawa, F.; Kubo, A.; Hayashi, T. *Chem. Lett.* **1992**, 2177.

Eric R. Strieter

Massachusetts Institute of Technology
Room 18-305
77 Massachusetts Ave
Cambridge, MA 02139

(617) 253-1852 (work)
(617) 515-3653 (home)
(617) 253-3297 (fax)
strieter@mit.edu

EDUCATION

Ph.D. 2005 *Massachusetts Institute of Technology.*
Research Advisor: Professor Stephen L. Buchwald.
Thesis Title: "Mechanistic Studies on the Metal-Catalyzed Carbon-Nitrogen Bond-Forming Reactions".

B.S. 2000 with Honors in Chemistry. *University of Wisconsin, Madison.*

AFFILIATIONS

American Chemical Society, Member.

AWARDS

ACS Division of Organic Chemistry Graduate Fellowship, 2003-2004.
Hilldale Fellowship, 1999.

PUBLICATIONS

"Mechanistic Investigations of the Copper-Catalyzed *N*-Arylation of Amides." Strieter, E. R.; Blackmond, D. G.; Buchwald, S. L. *manuscript in preparation.*

"On the Differences in Activity Between Catalysts Derived from Various Monophosphinobiaryl Ligands in the Pd-Catalyzed C-N Bond-Forming Reaction ." Strieter, E. R.; Blackmond, D. G.; Buchwald, S. L. *manuscript in preparation.*

"Identification of Pd Speciation During the Pd-Catalyzed C-N Bond-Forming Reaction Using Catalysts Based on Xantphos." Klingensmith, L. M.; Strieter, E. R.; Buchwald, S. L. *manuscript in preparation.*

"The Role of Chelating Diamine Ligands in the Goldberg Reaction: A Kinetic Study on the Cu-Catalyzed Amidation of Aryl Iodides." Strieter, E.R.; Blackmond, D.G.; Buchwald, S.L. *J. Am. Chem. Soc.* **2005**, *127*, 4120.

"Insights into the Origin of High Activity and Stability of Catalysts Derived from Bulky, Electron-Rich Monophosphinobiaryl Ligands in the Pd-Catalyzed C-N Bond Formation." Strieter, E.R.; Blackmond, D.G.; Buchwald, S.L. *J. Am. Chem. Soc.* **2003,***125*, 13978.

"Mechanistic Insights into the Pd(BINAP) – Catalyzed Amination of Aryl Bromides: Kinetic Studies under Synthetically Relevant Conditions." Singh, U.K.; Strieter, E.R.; Blackmond, D.G.; Buchwald, S.L. *J. Am. Chem. Soc.* **2002**, *124*, 14104.

"Dioxolane-to-Bridged Acetal-to-Spiroketal via Ring-Closing Metathesis and Rearrangement: A Novel Route to 1,7- Dioxaspiro[5.5]undecanes." Keller, V.A.; Martinelli, J.R.; Strieter, E.R.; Burke, S.D. *Org. Lett.* **2002**, *4*, 467.